Department of Imaging and Applied Physics

Rapid Response Monitoring of Transient Radio Emission Associated With Gamma-Ray Bursts And Circinus X-1

Aquib Moin

This thesis is presented for the Degree of

Doctor of Philosophy (PhD)

of

Curtin University

2011 August

Declaration

To the best of my knowledge and belief this thesis contains no material previously published by any other person except where acknowledgement has been made. This thesis contains no material which has been accepted for the award of any other degree or diploma in any university.

I hereby declare that the research work under the framework of this PhD project is conducted by the candidate and the contributions to any part of this work by others is outlined below. The papers produced during the course of this PhD have had due contributions from the co-authors.

Chapter 2: Members of the Australian Long Baseline Array (LBA) team provided extensive support and assistance in setting up the e-VLBI observations. Dr. Chris Phillips developed the e-VLBI monitoring system.

Chapter 3: Dr. James Miller-Jones helped in the analysis and publication of the results of e-VLBI observations of Circinus X-1.

Chapter 4: Dr. James Miller-Jones helped in extending the analysis of the Circinus X-1 ToO VLBI observations and contributed to produce key results related to the milliarcsecond jets associated with Circinus X-1. He also led the effort to transform the results into a paper. Dr. Cormac Reynolds and Dr. Hayley Bignall correlated the Circinus X-1 VLBI data.

Chapter 5: Dr. Mark Wieringa helped with the production of GRB 100621a images.

Chapter 6: Dr. Greg Taylor helped with GRB 100418a VLBI data processing.

Aquib Moin

August 10, 2011

Perth, Australia

Acknowledgements

Over the course of this PhD project, a number of people helped and supported me generously in various ways. I would like to take this opportunity to extend my heartiest gratitude to them all.

I am extremely grateful to my wife and family for always being there for me and finding immense happiness in what I wanted to do in my life.

I would like to sincerely thank my primary supervisor, Prof. Steven Tingay for his untiring and relentless support and guidance, and for all his help at every step of my PhD work. I am extremely thankful to him for taking me through the entire experience. It was his vision and insight that laid the foundation of this project and it was due to his persistent efforts that I was able to carry out this project from start to finish. I cannot thank him enough for how much he helped and supported me and for the extra miles he went to facilitate my efforts over the entire time period I spent doing my PhD work. I am also thankful to him for making me a part of world-class initiatives such as Curtin Institute of Radio Astronomy (CIRA) and International Centre for Radio Astronomy Research (ICRAR) and enabling me to enter the exciting domain of radio astronomy.

I would like to thank Dr. Chris Phillips, Dr. Cormac Reynolds, Dr. Hayley Bignall and Dr. James Miller-Jones for helping me learn various tools of the trade and teaching me various technical as well as scientific aspects of radio astronomy observations and data analysis. In the same vein, I also thank Adam Deller and Emil Lenc for being great mentors.

I would also like to thank a number of people at the Australia Telescope National Facility (ATNF) of CSIRO Astronomy and Space Science (CASS) Division who have always been there to support me for my observations and who always extended a helping hand whenever required. Special mention

amongst them are Dr. Phil Edwards, Dr. Tasso Tzioumis, Dr. Jamie Stevens and Dr. Robin Wark. In addition to them, I would also like to extend my gratitude to the administration and visitor services staff at ATNF CASS for their kindness and support. They have always made me feel home at the lodges at Marsfield, Parkes and Narrabri.

I would like to thank the collaborators in my research, Dr. Greg Taylor, Dr. Poonam Chandra, Dr. Dale Frail and Dr. Mark Wieringa, for all their help and useful contributions to the work carried out as part of my PhD.

For this PhD work, financial support was provided by the Curtin International Postgraduate Research Scholarship (CIPRS). In addition to this, I was also awarded the ATNF graduate scholarship, which supported me for my frequent visits to ATNF observatories over the course of my PhD.

I am also thankful to the administrative staff at the Department of Imaging and Applied Physics of Curtin University, at CIRA and at ICRAR, for the help and facilitation they provided me.

I express my heartiest gratitude to all of those who helped, supported and facilitated me in any way in achieving the milestone of obtaining my PhD. This work would not have been possible without their sincere support.

Abstract

This PhD project was aimed at carrying out comprehensive observational studies of radio sources associated with two types of transients: a) Gamma-Ray Bursts (GRBs) b) an X-ray binary system Circinus X-1, by exploring and utilising new technologies and the enhanced capabilities of radio astronomy facilities in Australia. The emergence of the electronic-Very Long Baseline Interferometry (e-VLBI) capability of the Australian Long Baseline Array (LBA) and the new broadband backend for the Australia Telescope Compact Array (ATCA) has opened up new observational possibilities. These new upgrades enabled the rapid-response, high sensitivity and high resolution observations of transient radio sources. As part of this project, the radio behaviour of the peculiar X-ray binary system, Circinus X-1, was studied by executing an unprecedented e-VLBI observation campaign aimed at tracking the system along its entire binary orbit. Following the e-VLBI campaign, Target-of-Opportunity VLBI observations of Circinus X-1 allowed for the first time the detection of milliarcsecond-scale jets associated with it. The second part of this project involved a coordinated and systematic GRB detection and monitoring program, leading to the detection of the radio afterglow of an unusual gamma-ray burst, GRB 100418a which was studied in detail in an attempt to understand the underlying physical processes associated with GRBs. This program also allowed us to build-up some observational statistics and maintain a record of southern GRBs.

Contents

List of Figures

List of Tables

LIST OF TABLES

Chapter 1

Introduction

1.1 Goals and Objectives

The primary objective of this PhD project was to utilise the capabilities of the existing radio telescopes situated in the Southern Hemisphere to conduct a well-coordinated and systematic observational study of transient radio sources associated with X-ray binary systems (e.g. Han & Hjellming 1992; Hjellming et al. 1998; Fomalont, Geldzahler, & Bradshaw 2001; Fender et al. 2004; Gallo et al. 2004) and Gamma-Ray Burst (GRB) afterglows (e.g. Frail et al. 1997; Kulkarni et al. 1998; Frail et al. 2003; van der Horst et al. 2008). The main activities under the framework of this PhD were to: a) study the radio behaviour of the peculiar X-ray binary system Circinus X-1 as a function of its orbital phase; and b) detect and follow the evolution of the radio afterglows of a number of GRBs as a function of time. As part of this PhD work, some previously unexplored operational capabilities of the radio astronomy instruments in Australia were also successfully utilised. Details of these observational programs appear in the chapters to follow.

The project was also aimed at providing some experience of transient detection and monitoring programs with existing telescopes and the ways in which rapid response, real-time radio astronomical observations involving multiple telescopes can be planned, coordinated and executed. An enhanced version of such observational campaigns will be a regular mode of operation for upcoming Square Kilometre Array (SKA) precursors, the Australian Square Kilometre Array Pathfinder (ASKAP), MWA (Murchison WIdefield Array) and MeerKAT (Karoo Array Telescope).

The two main facilities extensively used in the project were the Australia Telescope Compact Array (ATCA) near Narrabri, Australia, and the Australian Long Baseline Array (LBA), which comprises 6 radio telescopes in Australia, operated by the Australia Telescope National Facility (ATNF) of the Commonwealth Scientific and Industrial Research Organization (CSIRO) Astronomy and Space Science (CASS) Division, and by the University of Tasmania (UTas).

The ATCA[1] is a radio astronomy facility consisting of six individual radio antennas, which operate together as a connected-element interferometer in which all of the elements of the array get the time standard from the same clock (Thompson, Moran & Swenson 2002). Recently, the ATCA became four times more sensitive after the Compact Array Broadband Backend (CABB) upgrade replaced the old digital backend and various frontend elements with wideband systems. The bulk of the scheduled radio observations conducted within the framework of this PhD project occurred after CABB commenced operations in April 2009. Figure 1.1 is a photograph of the radio antennas that form the ATCA.

Figure 1.1: The ATCA - The Australia Telescope Compact Array, Narrabri, NSW, Australia. Image credit: ATNF CASS.

The second major facility used in this PhD was the Australian LBA[2], a Very Long Baseline Interferometry (VLBI) facility in Australia, which comprises the ATCA, Mopra, Parkes, Hobart, Ceduna and Tidbinbilla telescopes. Latest additions to the LBA are the Warkworth and ASKAP antennas. Like the ATCA, the LBA is also a radio interferometer in which all of the telescopes observe the same object simultaneously and the signals from pairs of telescopes are then combined and processed in a signal

[1] http://www.narrabri.atnf.csiro.au
[2] http://www.atnf.csiro.au/vlbi/

processor called a "correlator" to obtain data in the form of visibility products, which are produced by multiplying the signal from an antenna with the complex conjugate of the signal from the other antenna in the pair. The visibility data are then processed and analysed offline to produce a radio image of the source under investigation. The LBA is a longer baseline radio interferometer array, consisting of a number of telescopes including ATCA, which are situated at large distances from each other. Each telescope in the LBA is supplied with an independent clock signal and the greater distances between the stations provide baselines much longer (hundreds of kilometres) than ATCA (maximum baseline 6 km). The VLBI technique enables the study of astronomical objects with high angular resolution. Figure 1.2 shows the locations of Australian VLBI stations.

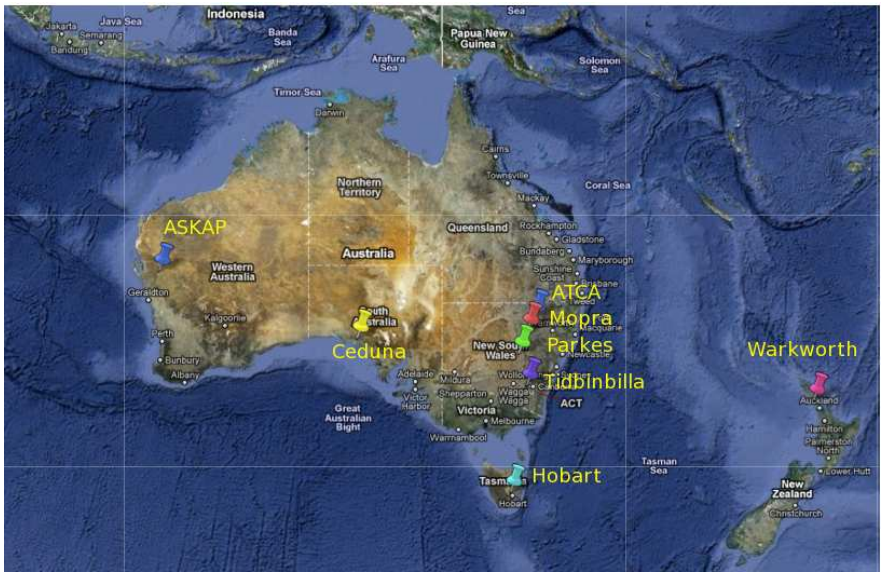

Figure 1.2: The LBA - The Long Baseline Array for VLBI in Australia. Image Credit: Google Maps.

In e-VLBI (electronic-VLBI) mode, the telescopes of the array are connected via fast data networks to transport data to the correlator and the observations are conducted in real time to obtain results immediately. In this project, the LBA was used in both VLBI and e-VLBI modes to conduct rapid response follow-up observations of a special class of astronomical objects called "transients", which unlike persistent sources appear on the sky for only a short period of time. Transient sources can broadly be categorized as slow transients (> 5 seconds) and fast transients (< 5 seconds), based on the duration

of prompt emission. The focus of this PhD project was the observation and monitoring of the evolution of slow radio transients over a time-scale of a few days, using the ATCA and e-VLBI/VLBI.

e-VLBI is particularly useful for the rapid response, target-of-opportunity observations of transient sources initially detected by space-borne X-ray (Swift XRT, RXTE ASM, MAXI GSC) or Gamma-ray (Swift BAT, Fermi LAT/GBM) instruments and then followed up by lower resolution radio telescopes such as the ATCA or the Expanded Very Large Array (EVLA). Transient radio sources associated with objects and/or phenomena like X-ray binaries or Gamma-Ray Bursts, when detected by the ATCA with a radio intensity higher than a certain threshold, can be immediately followed up by the e-VLBI capability of the LBA for high-resolution monitoring and imaging. An e-VLBI observation can be quickly set up at short notice, which makes it a very powerful tool to study the radio behaviour and possibly the morphology of interesting known and unknown transient sources in real time. e-VLBI is well suited to the observation of objects that require short lead-time attempts at detection and real-time feedback for decision making regarding continued monitoring with larger instruments or extended arrays.

An example of how an e-VLBI real-time instrument was critical in the study of an X-ray binary is the contribution the Parkes-Tidbinbilla Interferometer made to the observation of Galactic radio source, GRO 1655-40 (Tingay et al. 1995). This source was a 1 Jy object at VLBI resolution. With this experiment, the apparent superluminal (greater than the speed of light) motion of the radio components associated with GRO 1655-40 was detected.

As part of this PhD project, the ATCA observations of radio transients associated with GRBs and the X-ray binary Circinus X-1 provided the triggers to invoke the LBA based on pre-established criteria in order to carry out VLBI/e-VLBI observations. The enhancement of the ATCA bandwidth by a factor of 16 enabled very sensitive observations, the results of which were used as a trigger for LBA observations. The operation of the LBA in e-VLBI mode became possible after the development of the DiFX software correlator (Deller et al. 2007, Deller et al. 2011) which enabled the correlation of data streams from the telescopes over high speed network connections.

Over the course of this PhD research, separate and extensive observational programs on GRB afterglows and the peculiar Galactic X-ray binary Circinus X-1 were carried

out.

1.1.1 X-ray Binary Studies: e-VLBI/VLBI observations of Circinus X-1

A major component of this PhD project was an e-VLBI/VLBI observation and monitoring campaign in which the behaviour of the peculiar Southern Hemisphere neutron star X-ray binary Circinus X-1 (Figure 1.3) was studied in detail.

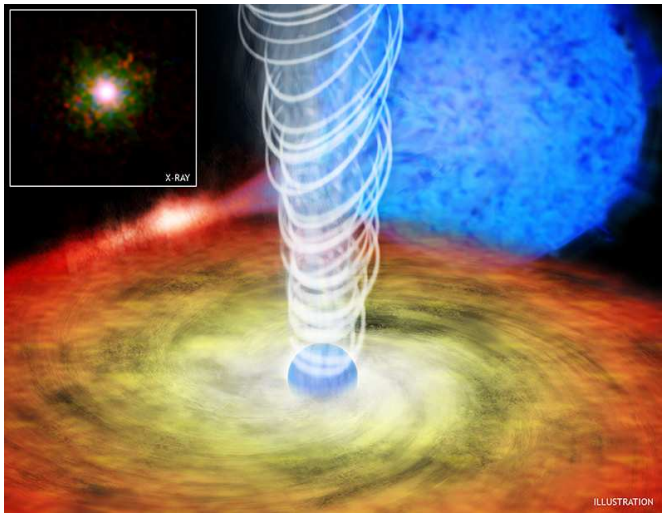

Figure 1.3: Artist's impression of the Circinus X-1 system - Inset: Chandra's X-ray image of Cir X-1; image scale: 3-arcmin across. This illustration shows the neutron star in the X-ray binary system, Circinus X-1, orbiting the giant companion and pulling material from it with its powerful gravitational force onto an accretion disk. As a result of their interaction at the closest approach, a relativistic jet of energetic particles is produced, which gives rise to multi-wavelength emission from the system which can be detected by space-borne and ground-based telescopes. Image credit: X-ray: NASA/CXC/Univ. of Wisconsin-Madison/S.Heinz et al.; Illustration: NASA/CXC/M.Weiss.

X-ray binary systems produce high-energy emission due to the regular or irregular accretion of material from a less-evolved star on to a compact object, either a neutron star or a black hole, which are in orbit around each other. The variations in the activity of a persistent or transient X-ray binary is believed to be due to the changes in the accretion rate, which are manifested as X-ray spectral state transitions. Bright outbursts are observed from these systems when they undergo a hard-to-soft transition. The decline in the luminosity then causes a transition from high/soft state to low/hard state

(e.g. Esin et al. 1997; Meyer, Liu & Meyer-Hofmeister 2000; Remillard & McClintock 2006). As the accretion settles onto a stable disc, relativistic jets can form, producing radio emission (e.g. Tingay et al. 1995; Mirabel & Rodriguez 1999; Fender, Belloni & Gallo 2004, Migliari & Fender et al. 2006; Miller-Jones et al. 2010). Coordinated observations allow the study of state transitions that occur in X-ray binary systems, the production and evolution of jets that are produced as a result, and the signatures of disc/jet coupling on timescales of days or weeks. As the X-ray binary systems are small analogues of Active Galactic Nuclei (AGN), the study of these systems can add to our knowledge and understanding of relativistic jet production.

In 2007, Circinus X-1 was successfully detected by the LBA at the 10 mJy level (Phillips et al. 2007) verifying the e-VLBI mode of LBA operation. The natural follow-up of that work was to do more frequent sampling of the Circinus X-1 orbit so as to study its radio behavior along the entire orbit on VLBI scales. This provided the motivation for the X-ray binary work conducted as part of this PhD work.

Thus the Australian e-VLBI array was utilised with the ATCA, Mopra, Parkes and Hobart telescopes to observe Circinus X-1 in real time (Moin et al. 2011). More recently, target of opportunity (ToO) VLBI observations of Circinus X-1 were also conducted in response to X-ray satellite and ground-based single dish detections providing the trigger for VLBI (Miller-Jones et al. 2012). The Circinus X-1 work is described in detail in chapters 3 and 4.

This project demonstrates the possibility and potential of carrying out X-ray binary observations with a next generation instrument such as ASKAP. It helped the e-VLBI team understand the requirements, constraints, advantages and bottle-necks in organizing transient detection observations using a real-time instrument for a long-term monitoring campaign. The VLBI observations with the LBA usually take place during the pre-scheduled VLBI week 3-4 times a year. The Cir X-1 e-VLBI campaign was unprecedented in a sense that it was the first time that such an extended e-VLBI observational campaign was scheduled outside the fixed VLBI week to exclusively track the transient activity of the XRB as a function of its orbital phase. Therefore coordination between the VLBI stations for real-time sessions to be conducted every second day, resource and personnel allocation on short notices, establishment of optimized network routes and evolution of visibility monitoring software were the main highlights of the campaign in operational terms, which helped gain the understanding and gave the idea

what it would take to execute a continuous real-time transient monitoring project. It allowed the e-VLBI team to build experience in conducting rapid follow-up observations to monitor the X-ray binary system, Circinus X-1, in real time. It therefore, enabled the team to better understand the practical operational aspects of such an extended rapid-response monitoring program. This experience will prove useful in the planning of experiments in the ASKAP era.

Being a fast, real-time instrument with an efficient scheduling system and automated data-processing pipelines, ASKAP will be able to quickly respond to X-ray binary transient alerts from space-borne instruments and produce results to detect and monitor the real-time radio evolution of X-ray binary systems over time scales of days. In addition to this, ASKAP is also expected to detect radio transient sources independently while carrying out sky surveys. In response to a strong ASKAP detection, e-VLBI/VLBI observations of the source could be invoked, which holds the potential to map structural changes such as motion of components, acceleration or deceleration of jets, as they occur. As a new addition to the LBA, ASKAP will greatly improve the resolution of the array with the introduction of new, long east-west baselines allowing the study of source morphology with even finer detail. With a large field-of-view, multiple beams and fast surveying speed, ASKAP will have the capability to detect a large number of radio sources, possibly associated with X-ray binaries, that otherwise remain undetected due to observational limitations. Such long-term campaigns with ASKAP and subsequent follow-up with an extended VLBI array will unveil new facts about the associated physical processes, structure and behaviour of X-ray binary systems.

1.1.2 The GRB afterglow program

As a part of this PhD work, a comprehensive and systematic Southern Hemisphere GRB detection and monitoring program with the ATCA was carried out from May 2008 to July 2010. The primary goal was to detect the radio afterglows of the GRBs not visible from the Northern Hemisphere and to track their flux density variability, to build up and maintain a statistical record of GRBs from the Southern Hemisphere. Within the framework of this campaign, selected samples of GRBs were observed during multiple sessions in an attempt to identify very bright afterglows which could then be followed up with higher resolution using VLBI/e-VLBI.

During the course of the project, radio monitoring campaigns were carried out and data acquired for particularly bright GRBs, having relatively long-lasting afterglows in an attempt to test the connection between GRBs (Figure 1.4) and Type I supernovae (Galama et al. 1998; Campana et al. 2006; Waxman, Meszaros & Campana 2007; Kulkarni et al. 1998 and many references therein) and one of the hypothesized energy injection models which attempts to explain the long lasting GRB afterglows (Rees & Meszaros 1998; Zhang et al. 2006). However, none of the detected GRB radio afterglows were found to be associated with a supernova, therefore only the previously-established cases of GRB-supernova connection were studied within this context. A test of an energy injection model against the observed results was conducted the details of which are presented in Chapter 6. In addition to the long-duration GRBs, a few short-duration GRBs were also observed in an attempt to detect the associated radio afterglows. The short-duration GRBs are rare and their possible progenitors are less clearly understood (Barthelmy et al. 2005; Dermer & Atoyan 2006; Jin et al. 2007 and references therein) than those of the long-duration GRBs.

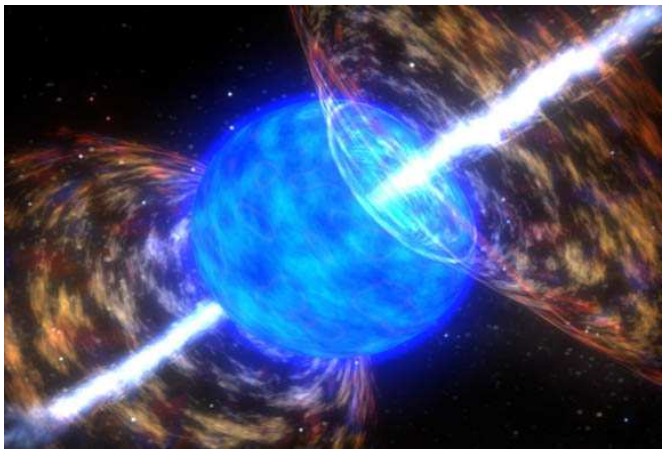

Figure 1.4: Artist's impression of a Gamma-Ray Burst - The illustration depicts the "core-collapse" model of GRB events. This model suggests the collapse of the core of a massive star and the explosion of the outer layers of the star, which triggers the highly energetic gamma-ray emission and the formation of a supernova. The late interaction of ejected material and the surrounding material then produces longer-lived "afteglow" which can be detected and observed in different frequency bands. Image credit: NASA GSFC.

One of the purposes of this Southern Hemisphere GRB detection and monitoring program was to gain some preliminary understanding as to what strategy could be

implemented to conduct such experiments with existing instruments, and what lessons can be learned for future transient detection programs. The GRB afterglow detection and monitoring programs that were carried out during this PhD project allowed us to learn about the triggering mechanisms that can be put in place for rapid response observations, the step-by-step systematic procedure which can be implemented to follow a radio transient and operational requirements, advantages and constraints attached to a large-scale instrument.

The aforementioned aspects of radio transient work have indeed provided some experience which could prove to be relevant for the planning and execution of future transient detection and monitoring projects with the upcoming SKA precursors such as ASKAP. ASKAP is being designed to be a very fast and sensitive full-sky survey instrument at radio wavelengths, and could be the only facility in the region capable of detecting the predicted large percentage of GRBs that are not detected with gamma-ray satellites due to possible beaming effects (so-called orphan afterglows). Some evidence has shown that there are relativistic jets and outflows associated with GRBs (Sari, Piran & Halpern 1999; Frail et al. 2001), which evolve over timescales of days and gamma/X-ray emission is detected by space-borne instruments only if the jet associated with the GRB is beamed towards the Earth. This effect prevents the high-energy satellites from seeing all possible GRB events. ASKAP, being an all-sky instrument with multiple beams, could search for the radio afterglows of GRBs without the bias of a gamma-ray detection as a selection criterion. The execution of a major Southern Hemisphere GRB project with the ATCA and e-VLBI demonstrated here, could be continued and extended using ASKAP to explore some interesting possibilities in transient science in the near future. A detailed description of the GRB project is given in chapters 5 and 6.

1.2 Motivation

At the time when this project was conceived and discussed, a number of activities were initiated in the context of Square Kilometre Array (SKA) science and technology research. The SKA-related projects such as the SKA science case studies, SKA design studies and SKA site selection studies were commenced. A number of SKA Precursor projects, ASKAP, MeerKAT, MWA, also emerged and took shape as instruments that

could demonstrate SKA readiness and capability. The study of the variable Universe, i.e. transient science, was identified as one of the key areas in which the aforementioned instruments can play a vital role in answering questions such as:

- What could be the possible origins of these transients?
- What are the underlying astrophysical processes and mechanisms?
- What is the time scale for the persistence of compact features?
- What is the incidence of jets in these objects?
- How do the jets evolve with time and frequency?
- How is the source morphology related to the multi-wavelength emission behavior of the source?

Therefore, before the next generation telescopes come online, the exploration of transient detection and follow-up VLBI programs in the Southern Hemisphere was conceived as a project and as a component of ASKAP science programs such as VAST (Variables And Slow Transients). This PhD project was motivated by this exploratory idea.

1.3 Statement of Originality

The study of transient radio sources has become important in radio astronomy over the past few years, but until recently it was relatively an under-explored area of research because of scientific and technical challenges. Although it has picked up pace, the proportion of transient science projects is limited compared to other areas of observational astronomy.

The emergence of new capabilities in radio astronomy instruments, a few groundbreaking discoveries such as the Lorimer burst (Lorimer et al. 2007) and the need to study and test the anticipated capabilities of the next generation of instruments paved the way for a number of projects related to transient science.

With the recent innovative technical upgrades to the LBA such as the sensitivity enhancement and replacement of the old LBA hardware correlator with the DiFX

software correlator, e-VLBI has now become a stable and mainstream science operations mode with LBA.

After some work on e-VLBI operations that verified the capability for the LBA, this PhD project was formulated to conduct new radio astronomical experiments with e-VLBI on the LBA. The e-VLBI/VLBI campaign on Circinus X-1 formed the major component of this PhD, which was an unprecedented and original observational campaign pushing the LBA operations to their limits. Such a campaign was never attempted before with the LBA and it resulted in important new results which helped understand a peculiar astronomical system.

The other part of this PhD, a major systematic and long-term GRB detection and monitoring program was also planned and executed for the first time in the Southern Hemisphere. There had been some individual infrequent GRB observations with the ATCA in the past but such a large sample of Southern Hemisphere GRBs has never been systematically observed. This program and the use of CABB to pursue it is also unprecedented and original. The outcome of this program was a statistical database of GRB observations and a record of relationships between various parameters such as GRB durations, evolution timescales, energies etc.

At the time of project conclusion, the original results produced as an outcome of this PhD work have opened up numerous avenues and possibilities for extension into large radio transient science projects, forming the basis for the planning and execution of long-term observational programs to study transients with upcoming radio astronomy facilities in the near future.

1.4 Thesis Outline

Chapter 2 outlines the emergence of e-VLBI and CABB as new tools for radio astronomy in Australia, with an account of the observational setup and the operational details for the experiments conducted as part of this PhD project.

Chapter 3 describes the e-VLBI and VLBI observations and monitoring of the neutron star X-ray binary Circinus X-1. It starts off by giving a brief background on X-ray binary systems followed by a description of the observations and the details of the observation sessions. The discussion section then highlights the analysis and interpretation of data and the outcome of the e-VLBI work done.

Chapter 4 describes the VLBI ToO observations that were conducted in response to triggers from X-ray satellites and the single-dish radio follow-up. The results of the high-resolution imaging of Circinus X-1 are then presented. The final section summarizes the entire e-VLBI and VLBI campaign on Circinus X-1.

Chapter 5 gives an overview of the Southern Hemisphere GRB radio detection and monitoring program with the ATCA. After a brief theoretical background of GRBs, the observations of GRBs and the outcome are described. In the subsequent section, some statistics and analysis from the GRB program are presented.

Chapter 6 provides the details of multi-instrument monitoring of GRB100418a. Some brief introduction of the GRB is given, then the ATCA, EVLA and VLBA observations are described in the following sections. The last section gives some analysis of the observed results and conclusions from the monitoring of the GRB.

Chapter 7 draws some key conclusions as an outcome of the work done under the framework of this PhD.

Chapter 2

New tools for radio astronomy in Australia: e-VLBI and the Australia Telescope Compact Array Broadband Backend

2.1 Introduction

In recent years, the premium radio astronomy instruments in Australia have undergone major upgrades, which have greatly enhanced their capabilities. The upgrades have not only improved the performance and efficiency of the instruments but they have also enabled new modes of operation and innovative experiments. This chapter discusses the Long Baseline Array (LBA) with emphasis on its new capabilities, and the Australia Telescope Compact Array (ATCA) Broadband Backend, and outlines the way they have proven to be useful for this PhD project.

The standard derivation of the interferometry equations will not be presented here since this chapter serves as a description of the instruments and the modes of operation used in this project and the mathematical treatment of radio interferometry is beyond the scope of this chapter. Relevant references for the detailed account of fundamentals of radio interferometry will be provided where and when required.

2.2 e-VLBI in Australia and beyond

Since the time it was first performed in the late 1960s, Very Long Baseline Interferometry (VLBI) has been producing key scientific results and has enabled ground-breaking results in the field of radio astronomy (Jones, Terzian & Sramek 1981, Jauncey et al. 1995, Stirling et al. 2001, Lobanov et al. 2006 and many references therein). In 1969, the first trans-pacific VLBI fringes were obtained between a NASA Deep Space Network (DSN) telescope in California and the DSN telescope at Tidbinbilla near Canberra, laying the foundation for global VLBI (Cohen et al. 1969). A ground-breaking VLBI experiment was conducted in 1976, the array consisting of two radio antennas in the US, one in Russia and another one at Tidbinbilla, Australia. The experiment formed the first global VLBI array used for very high angular resolution observations of an astronomical source (Batchelor et al. 1976). VLBI observations since then have been providing increasingly high angular resolution, which has allowed astronomers to study the small-scale structure of cosmic radio sources and to image the central regions of numerous large-scale astronomical systems so as to directly observe underlying astrophysical processes, such as the production and evolution of relativistic jets (e.g. Tingay et al. 1998; Ly, Walker & Junor 2007; Homan et al. 2009).

The global VLBI network has grown over the last four decades, with radio telescopes in Australia, the Americas, Europe, Asia and South Africa regularly used for VLBI. A significantly prominent achievement of the VLBI community was "Space-VLBI" which was a global effort called the VLBI Space Observatory Program (VSOP), made possible by putting a radio antenna in space. The 8-m VSOP radio antenna was installed on board a satellite called HALCA and it was launched by Japan's Institute of Space and Astronautical Science (ISAS). The global VLBI array with the VSOP antenna formed a telescope having a maximum diameter of about three times the diameter of Earth (See e.g. Hirabayashi et al. 2000)

In the Southern Hemisphere, VLBI operations started as the Southern Hemisphere VLBI Experiment (SHEVE) in the 1980s (Preston et al. 1984). The primary goal of the initiative was to make use of the radio antennas in the Southern Hemisphere to carry out VLBI experiments on various interesting southern sky radio sources (Preston et al. 1993, Jauncey et al. 1994, Tzioumis et al. 2002). Most of the antennas included in the SHEVE array are still being used as components of the Australian Long Baseline

Array (LBA), with the addition of a few new antennas to carry out radio interferometry experiments with even higher resolution and sensitivity (Tzioumis 1997, Tzioumis et al. 2010, Petrov et al. 2010).

The LBA is a result of continuous upgrades over a twenty-year period. Recently, there have been significant upgrades in the LBA hardware and software, which have greatly enhanced the operational capabilities of the array. The most notable upgrades are the increase in the recorded bandwidth due to the replacement of the tape-based recording system with a disk-based recording system, and the development of the DiFX software correlator (Deller et al. 2007, Deller et al. 2011), which has replaced the S2 hardware correlation system and is now used to correlate LBA observations.

Presently, the LBA includes the ATCA (6 $\times$ 22m) Mopra (22m), Parkes (64m), Tidbinbilla (70m) (CSIRO), Hobart (26m), and Ceduna (30m) (University of Tasmania) telescopes in Australia, and international telescopes such as the Hartebeesthoek radio telescope in South Africa. A number of radio telescopes in the US, China, Japan, India and South America are also used occasionally to reach certain scientific goals. Newest additions to the LBA are one of the ASKAP antennas (12m) in Western Australia and the Warkworth telescope (12m) in New Zealand. Tables 2.1, 2.2 and 2.3 present some basic specifications of ATCA, LBA and the enhanced LBA with the ASKAP and Warkworth antennas at 8.4, 4.8 and 1.4 GHz.

Curtin University serves as the official correlation centre for the LBA. The Curtin University radio astronomy group operates and maintains a 20-node (160-core) high-performance computer cluster called the "Curtin University Parallel Processor for Astronomy (CUPPA)" which runs the DiFX correlator and is used for all LBA correlation. DiFX has enabled more sensitive observations, introduced much more flexibility, robustness and ease of operation in the LBA system and a new capability, so-called "electronic-Very Long Baseline Interferometry" (e-VLBI).

e-VLBI is a mode of doing long baseline interferometry in real time. Instead of recording the sampled, digitized data on disks and transporting the data disks to some central location (e.g. Curtin University) to perform the correlation operation, the data coming from the telescopes are directly streamed over high-speed network links and the data streams are correlated in real time with the correlator operating in e-VLBI mode.

e-VLBI has now become a regular mode of VLBI operation for other VLBI networks as well. The Shanghai Astronomical Observatory (SHAO) operates the Chinese VLBI

Network (CVN) comprising the Sheshan (25m), Nanshan (25m), Miyun (50m) and Kunming (40m) radio telescopes, which are all connected via networks to conduct e-VLBI for astronomy, geodesy and spacecraft tracking. SHAO has plans to extend their e-VLBI operations by upgrading to faster network links and the inclusion of the upcoming Shanghai (65m) and FAST (500m) telescopes (Zheng, Zhang & Shu 2005). The CVN telescopes regularly participate in European VLBI Network (EVN) and International VLBI Service (IVS) experiments.

In Japan, the Japanese Space Agency (JAXA), National Institute of Information & Communication Technologies (NICT) and Geospatial Information Authority (GSI) are involved in real-time data transfers and e-VLBI experiments between the Kashima (34m), Tsukuba (32m), UDSC (64m), and USC (34m) dishes, and the telescopes in Australia, Europe, China and the USA, via fast network links (Koyama et al. 2002; Sekido et al. 2008). Their primary use of e-VLBI/VLBI is for tracking and orbit determination of JAXA's IKAROS (Interplanetary Kite-craft Accelerated by Radiation Of Sun) satellite (Mori et al, 2009).

MIT Haystack Observatory in the United States has also been working to perform e-VLBI operations (Whitney et al. 2003; Whitney, Lapsley & Doeleman 2003; Lapsley & Whitney 2004). They have conducted a number of successful e-VLBI tests with telescopes in the US (Aricebo, Westford), in Japan (Kashima) and in Europe (Wettzell, Westerbork, Onsala). They primarily use the e-VLBI facility for data transfer and they also emphasise the standardisation of transport protocols and the production of hardware [1].

The most developed e-VLBI network is the European VLBI Network (EVN) which now regularly conducts e-VLBI observations for science experiments and has produced a number of high-impact results (Paragi et al. 2005, Tudose et al. 2007, Perez-Torres et al. 2009, Giroletti et al. 2011). The EVN is a network of 18 telescopes spread across Europe, Asia and Southern Africa, with more to become a part of the EVN soon. The EVN is operated in e-VLBI mode as the "e-EVN" by the Joint Institute for VLBI in Europe (JIVE), which is an entity in the Netherlands that hosts the EVN correlator, i.e. data from all of the participating VLBI telescopes in Europe, Asia and Southern Africa are shipped/transported to JIVE for correlation. Under the framework of a project called NEXPReS (Novel EXplorations Pushing Robust e-VLBI Services), JIVE

[1] http://www.haystack.mit.edu/tech/vlbi/evlbi/index.html

utilises its Mark IV DataProcessor correlator for e-VLBI operations, which is equipped with custom software to fetch the data from the interconnected European networks in real time, and to run and monitor the correlation jobs. The e-EVN[2] now regularly conducts Target-of-Opportunity observations to observe interesting transient sources.

In order to make efforts to better cordinate the VLBI operations with an increased number of telescopes in the Asia-Pacific region, an initiative called the APT (Asia Pacific Telescope) was undertaken in 1991. This initiative has now been extended as "e-APT" which is a network of radio telescopes in Australia, Japan, China and Europe to collaborate and coordinate for e-VLBI operations. A number of successful e-VLBI tests have been conducted over high speed networks connecting telescopes continents apart[3].

The primary advantage of e-VLBI operations is the immediate availability of correlated data, which are ready to be processed and analyzed with standard radio astronomy software such as AIPS (Astronomical Image Processing System; Greisen 2003) and DIFMAP (Shepherd, Pearson & Taylor 1994). Another advantage of doing e-VLBI is the reduced costs of disk shipping (in case of the availability of subsidized network access), which is involved in disk-based VLBI. e-VLBI allows the investigators to produce results quickly and the entire VLBI operation to be carried out on a much shorter time scale. This is particularly critical in the case of rapid response and Target-of-Opportunity (ToO) experiments in which a time-critical decision is to be made regarding a potentially interesting source. Based on some form of event trigger, an e-VLBI observation can be quickly set up to observe and monitor a transient source, without missing interesting source activity. Instant results can be produced to check the source behaviour over a short time scale. An extensive and rapid monitoring of the radio transient associated with the neutron star X-ray binary Circinus X-1 was possible with the e-VLBI capability of the LBA. The details of this work will appear in Chapter 3. In addition to this, an attempt at e-VLBI observations of a GRB afterglow is described in Chapter 5.

[2]http://www.evlbi.org/evlbi/evlbi.html
[3]http://www.expres-eu.org/evlbi.html

Table 2.1: Array specifications for ATCA, LBA (phased ATCA, Mopra, Parkes, Ceduna, Hobart, Tid70) and enhanced LBA (LBA(e): phased ATCA, Mopra, Parkes, Ceduna, Hobart, Tid70, ASKAP, Warkworth) at X-band. The spatial resolution is computed for a source at a distance of 1Mpc. Observation parameters assumed for the calculations: integration time = 12h, time on calibrator (ATCA) = 30%, time on calibrator (VLBI) = 50%, dual polarisation, weighting scheme: natural, $1/\sigma^2$.

Array	Max. Baseline (km)	Freq. (GHz)	B.width (MHz)	Max. Angular Resolution (θ)	Max. spatial Resolution (L) (parsec)	Image Sensitivity (μJy/beam)
ATCA	6	8.5	2048	1.5 (arcsec)	7.272	8
LBA	1704	8.4	32	5.3 (mas)	0.025	23
LBA(e)	5321	8.4	32	1.7 (mas)	0.008	22

Table 2.2: Array specifications for ATCA and LBA (phased ATCA, Mopra, Parkes, Ceduna, Hobart) at C-Band. ASKAP, Warkworth and Tid70 do not currently operate at 4.8 GHz. The spatial resolution is computed for a source at a distance of 1Mpc. Observation parameters assumed for the calculations: integration time = 12h, time on calibrator (ATCA) = 30%, time on calibrator (VLBI) = 50%, dual polarisation, weighting scheme: natural, $1/\sigma^2$.

Array	Max. Baseline (km)	Freq. (GHz)	B.width (MHz)	Max. Angular Resolution (θ)	Max. spatial Resolution (L) (parsec)	Image Sensitivity (μJy/beam)
ATCA	6	5.1	2048	2.3 (arcsec)	11.6	13
LBA	1704	4.8	32	9.2 (mas)	0.044	60
LBA(e)	-	-	-	-	-	-

Table 2.3: Array specifications for ATCA, LBA (phased ATCA, Mopra, Parkes, Hobart) and enhanced LBA (LBA(e): phased ATCA, Mopra, Parkes, Hobart, ASKAP, Warkworth) at L-Band. Ceduna and Tid70 do not operate at 1.4 GHz. The spatial resolution is computed for a source at a distance of 1Mpc. Observation parameters assumed for the calculations: integration time = 12h, time on calibrator (ATCA) = 30%, time on calibrator (VLBI) = 50%, dual polarisation, weighting scheme: natural, $1/\sigma^2$. .

Array	Max. Baseline (km)	Freq. (GHz)	B.width (MHz)	Max. Angular Resolution (θ)	Max. spatial Resolution (L) (parsec)	Image Sensitivity (μJy/beam)
ATCA	6	1.7	2048	8.3 (arcsec)	43.633	14
LBA	1400	1.4	32	38.5 (mas)	0.186	45
LBA(e)	5321	1.4	32	10.1 (mas)	0.048	44

2.2.1 The LBA e-VLBI Network

The Southern Hemisphere e-VLBI network has evolved since inception such that a number of tests and experiments have been conducted using high speed network connections in Australia and beyond. Successful 1 Gbps e-VLBI tests between ATNF telescopes and Curtin University and telescopes in China[4], Japan and New Zealand[5] have already been undertaken.

The e-VLBI facility in the Southern Hemisphere mainly utilises Australia's Academic and Research Network (AARNet) which provides dedicated links between the telescopes, the correlator and the ATNF headquarters in Marsfield, Sydney, NSW, Australia. Three ATNF CASS telescopes, the ATCA, Mopra and Parkes are connected with dedicated 1 Gbps links and there are dedicated 1 Gbps links connecting the ATCA and Parkes with Marsfield as well. The network link to Hobart has recently been upgraded to a 1 Gbps link. The ATNF telescopes and the ATNF headquarters in Marsfield are also connected via a 1 Gbps link with Curtin University and the VLBI data are now regularly transferred over the network instead of shipping disks for regular VLBI observations.

Fig. 2.1 is an example of the CSIRO ATNF network "weather" map which shows

[4]http://www.csiro.au/news/AstronomyWithoutBorders.html

[5]http://www.aarnet.edu.au/News/2011/02/09/AARNet-Trans-Tasman-virtual-e-telescope-trial.aspx

the network connections as incoming and outgoing datastreams between observatories, ATNF headquarters, Curtin University and the network hubs involved in the e-VLBI operation. Also shown is the data transfer rate and the traffic volume for each link.

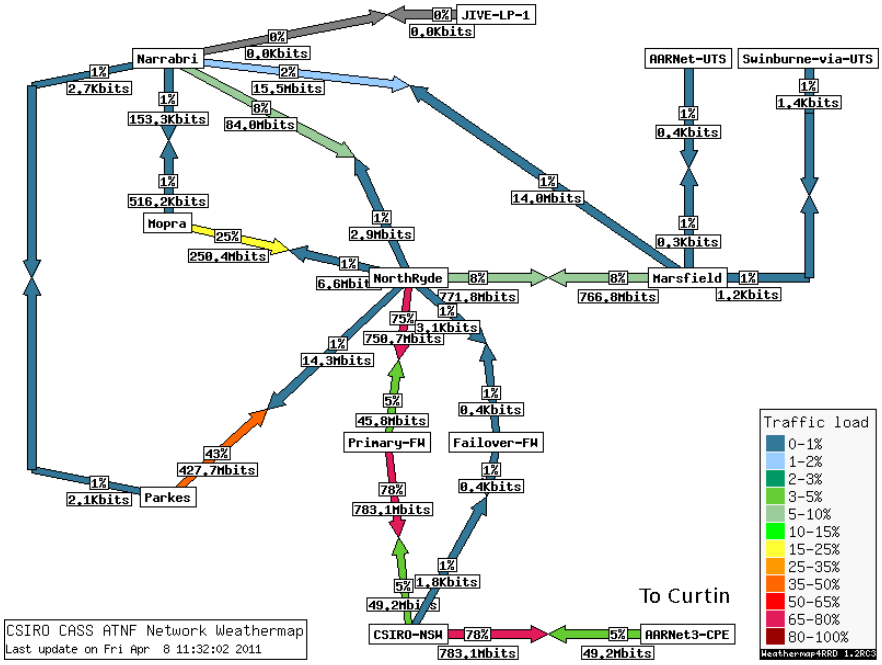

Figure 2.1: The e-VLBI network - The LBA network weather map showing the e-VLBI network connections in Australia.

2.2.2 The Telescopes

Currently, the Southern Hemisphere e-VLBI array comprises the ATCA, Mopra, Parkes and Hobart telescopes. The Ceduna and Tidbinbilla telescopes have no fast network connections as yet.

2.2.2.1 The Australia Telescope Compact Array (ATCA)

The Australia Telescope Compact Array[6] (Figure 2.2) is Australia's premium interferometer telescope for radio astronomy. It is situated at the Paul Wild Observatory near the town of Narrabri in New South Wales, about 550 km northwest of Sydney. It is

[6] http://www.narrabri.atnf.csiro.au/

operated and maintained by the Australia Telescope National Facility (ATNF) which is a part of CSIRO Astronomy and Space Science Division (CASS).

The ATCA comprises six 22-metre radio antennas installed on east-west rail tracks, with an extent of 6 km. In 1998, a 214-m north-south spur was also constructed to create hybrid arrays. Five out of six antennas are movable while antenna 6 is standing fixed at the distance of 6 km giving the longest baseline. The five movable antennas can be driven on a 3-km rail track and a number of array configurations can be achieved by positioning the antennas at 44 different station posts. There are 17 standard array configurations starting from a very compact one to the longest one with a maximum baseline length of 6km. The frequency range in which the array can be used to make observations is 1.1 - 105 GHz. In order to obtain the best possible uv-coverage, a 12-hour observing run must be carried out since ATCA is an east-west earth-rotation aperture synthesis interferometer. The ATCA is a central component of the Southern Hemisphere VLBI array.

Recently, the ATCA has been upgraded with a new Compact Array Broadband Backend (CABB) hardware correlator, which has increased the total bandwidth from 128 MHz to 2 GHz, thereby increasing the sensitivity by a factor of 4. This upgrade is allowing observers to detect much weaker sources and providing the facility to cover a much wider range of frequencies simultaneously. CABB is described further within the context of observations for this PhD project in section 2.3

Figure 2.2: The ATCA - The Australia Telescope Compact Array near Narrabri. Image credit: ATNF CASS.

2.2.2.2 Mopra

The Mopra telescope[7] (Figure 2.3) is located near Coonabarabran in NSW, which is about 450 km northwest of Sydney. Operated by the ATNF, it is a single 22-metre antenna similar to the ATCA antennas primarily used for mm-spectroscopy but it is also an integral part of the LBA. For VLBI observations, Mopra can be used within a frequency range from 1.4 to 22 GHz and it is fully remotely operated. ATCA-Mopra forms the shortest baseline in the LBA network, approximately 113 km.

Figure 2.3: Mopra - The Mopra telescope near Coonabarabran. Image credit: ATNF CASS.

2.2.2.3 Parkes

The Parkes 64-metre telescope[8] (Figure 2.4) is one of the world's largest fully steerable radio astronomy instruments and it is one of the two most sensitive elements of the LBA. The Parkes Observatory is situated 20 km North of the town of Parkes in NSW, about 380 km west of Sydney. The Parkes telescope is equipped with a suite of receivers and it operates in the frequency range of 0.44 - 43 GHz. The Parkes telescope is also operated and maintained by ATNF.

[7] http://www.narrabri.atnf.csiro.au/mopra/
[8] http://www.parkes.atnf.csiro.au/

Figure 2.4: "The Dish" (Parkes) - The Parkes telescope near the town of Parkes. Image credit: ATNF CASS.

2.2.2.4 Hobart

The Hobart[9] (Figure 2.5) telescope is located at the Mt. Pleasant Observatory which is 20 km east of Hobart in Tasmania. The facility is run by the University of Tasmania. It is also a dish antenna with a diameter of 26 meters. The telescope can be operated over a frequency range of 0.66 to 22 GHz. The Hobart telescope is used for a number of purposes such as the International VLBI Service for geodesy and spectral line observations. It is regularly used as an element of the Australian LBA network due to being the Southern-most antenna and therefore involved in long north-south baselines.

2.2.3 e-VLBI Hardware

Although the driving engine of the Australian e-VLBI network is the DiFX software correlator (Deller et al. 2007, Deller et al. 2011), the e-VLBI operation requires various hardware components to work in coordination.

The signal from the antenna feed is fed to samplers and digitisers and the output

[9] http://www-ra.phys.utas.edu.au/observatories/26m-intro.html

Figure 2.5: Mt. Pleasant telescope - The University of Tasmania telescope near Hobart. Image credit: Mt. Pleasant Observatory.

signal from each antenna is then acquired by the VLBI Data Acquisition System (DAS). The next hardware element in the system is the recorder computer at each observatory. The recorder computers record the LBA format datastreams, which in the case of e-VLBI, are transported to the computer cluster running the DiFX correlator via network connections. There are three computer clusters that can alternatively be used for e-VLBI correlation: a) The PAM (Parkes ATCA Mopra) cluster installed at Parkes Observatory; b) Curtin University's 14-node Curtin ATNF VLBI Experiment (CAVE) cluster installed at the Paul Wild Observatory (ATCA) and c) The CUPPA cluster installed at the Curtin University.

The e-VLBI software fetches the datastreams from the recorder computers over the network and the high-performance parallel-processor clusters are used to run the DiFX correlator to correlate data in real time. The correlated data are stored on the storage device attached to the cluster running the correlator, from where they can be copied to another location for calibration and imaging.

2.2.4 e-VLBI Software

2.2.4.1 The Correlator

In radio interferometry, the cross-correlation operation is performed to combine the radio signals that arrive with a certain delay at each radio telescope in the array . The signal received at each telescope is converted into digital datastreams and the datastreams from every possible telescope pair are then correlated to produce the visibility products. The visibility product is the final output of a radio interferometer and is a component of the Fourier transform of the sky brightness distribution. All possible visibility products, when combined and Fourier-transformed, produce the radio image of the field the telescopes have observed. So the correlation of datastreams is the central function of radio interferometry which produces the output of an interferometer. The tool that is used to perform the correlation operation is called a correlator (Thompson, Moran & Swenson 2002).

Traditionally, correlators have been implemented in hardware by designing and deploying special-purpose electronic circuitry to perform the correlation operation. The correlation of recorded signals involves a Fourier Transform (F) and a cross-multiplication (X). Either of the two operations can be performed first and based on the order of these operations the correlator can either be an "FX" or an "XF" implementation (Thompson, Moran & Swenson 2002, Romney 1999).

The hardware correlators used for arrays like the Very Long Baseline Array (VLBA) in the US and the LBA in Australia have always been specialized computers, custom-designed and developed for the sole purpose of correlation for VLBI. The main drawbacks of hardware correlators are that they can only offer a very limited flexibility, they are expensive and their production is quite a complicated and specialized task.

In order to explore the possibility to perform the correlation operation using a software implementation of a correlator running on a commercially-available high-performance computer system, an initiative was taken in 2005 to develop a "software correlator" to support the disk-based VLBI recording system for the LBA. As an outcome of this effort the FX-style "Distributed FX" (DiFX) correlator emerged and it replaced the S2 hardware correlation system for the LBA.

DiFX provided a much higher level of flexibility, ease of operation and the possibility of distributing the correlation tasks over parallel nodes of a high-performance computer

cluster. Written entirely in C++, it offers all the benefits, control and power of a high-level object-oriented programming languague, making it an inexpensive, efficient and flexible solution for correlation. It has also provided ease of operation, maintenance and the provision to add functionality without having to re-build the entire system (Deller et al. 2007; Deller et al. 2011).

The DiFX code in C++ utilises the "Intel Performance Primitive" (IPP)[10] library, which provides specialized routines for vector processing which enhances the processor performance in a parallel computing environment. DiFX makes use of the "Message Passing Interface" (MPI)[11] to handle the data transfer within the cluster environment.

DiFX is installed and executed on an off-the-shelf multi-node or multi-processor computer cluster, which can offer the facility of distributed or parallel computing. In DiFX, one of the nodes is designated as the master node called the "FX-manager" and a number of nodes are designated as data management nodes. The FX-manager node controls the correlation operation and instructs the data management nodes to read the data from the defined location or network. It then assigns the correlation tasks to the specified number of processing nodes in a distributed manner. Once the correlation is finished the correlated VLBI data are available at a specified location on the master node.

DiFX is a software suite that also includes auxiliary programs that generate various interferometry parameters such as the delays and station positions necessary for correlation. DiFX can be configured by using an input file, which specifies the VLBI experiment details, path to the data, parameters to perform the Fast Fourier Transform, number of processing and data management nodes to be used, etc.

The feature of DiFX that enables e-VLBI is that its operation doesn't depend on the origin of the datastreams. Whether they are coming from a storage location or a network, the system treats them in a similar way once they are loaded in the datastream buffer. Therefore, in case of an e-VLBI operation, the telescope datastreams are supplied to DiFX from the network, which doesn't affect the correlation operation, and correlated data become available right after the correlator finishes its job.

For LBA e-VLBI operations, the DiFX correlator is installed on the CAVE cluster in Narrabri and the PAM cluster in Parkes.

[10] software.intel.com/en-us/intel-ipp/

[11] http://www.mcs.anl.gov/research/projects/mpi/

2.2.4.2 The Recorder Servers

In addition to the correlator, there are software routines installed on the cluster which initiate the recorder servers. The recorder server program fetches the datastreams from the telescopes. Written in Perl, the server programs are installed on the data recording computers at Parkes, ATCA, Mopra and Hobart. The program needs to be provided with the experiment name and the duration of the experiment as its inputs. When launched, the recorder servers start to send the datastreams from the recording computers via network links between the observatories and the cluster using TCP or UDP communication protocols. Until interrupted, the servers keep on transmitting data.

During an e-VLBI operation with the LBA, the recorder server programs are automatically launched at each observatory by a startup script running on the cluster. Just before the start of correlation, the recorder servers start to send in the datastreams and the correlation operation keeps going until the recorder servers or the correlator itself is interrupted. Figure 2.6 shows recorder server programs running at the recorder computers at the observatories (ATCA, Mopra, Parkes, Hobart) participating in the e-VLBI experiment.

Figure 2.6: The recorder servers - The recorder server program used to fetch the telescope data from the recording computer.

2.2.4.3 The Monitoring Programs

When the DiFX correlator is launched for the real-time correlation operation to perform e-VLBI, the correlator starts to produce the visibility products for all the telescope pairs in the array and keeps on writing the data to a FITS (Flexible Image Transport System) file. This occurs in the background and the correlator output is not directly visible to the operator. In order to monitor the correlation operation during an e-VLBI session and get first-hand information on the quality of visibility data, a set of monitoring programs were developed at ATNF, enabling the correlated visibility data to be viewed in real time.

The monitoring programs are C++ programs which can be launched in parallel with the correlator during an e-VLBI session. It is a client/server setup in which the monitor client requests specific data from the server. When launched, the monitor server opens up a network socket which waits for a response from the correlator. Once the correlator starts up, a socket connection is established over the network and the visibility output of the correlator can be read by the monitoring program over the socket. The monitor server establishes the connection and waits for the monitor client to be launched, which is a program that requests the monitor server to send specific products selected on the basis of baseline, frequency, polarization product etc. The monitor server then fetches the requested data and the PGPLOT library[12] is then used to display correlation coefficient, correlation amplitude and phase for the selected products.

When everything in the e-VLBI system starts to run properly, a fringe can be seen on the monitoring display as all telescopes observe a strong calibrator source. The detection of fringes between various telescopes in the array verifies that the e-VLBI observation is working, all of the parameters are correctly set and the expected visibility data are being produced by the correlator. Otherwise, a number of parameters such as the frequency settings at the observatories, the polarization, inputs to the correlator and/or the telescope schedule files can be checked for trouble-shooting.

The monitoring setup is a very effective way of checking and monitoring the e-VLBI performance in real time, identifying problems and fixing them on the fly rather than going until the end of the session without knowing anything about the quality of the

[12] http://www.astro.caltech.edu/~tjp/pgplot/

output data produced as an outcome of the e-VLBI operation. Figure 2.7 shows the e-VLBI setup on the CAVE cluster.

Figure 2.7: e-VLBI Software - The e-VLBI correlator and monitoring programs running during an e-VLBI experiment.

2.2.5 e-VLBI Operation

In order to conduct an LBA experiment in the e-VLBI mode, the telescopes are set up just as they are in the usual VLBI mode. The observation schedules are written in SCHED[13] (Craig Walker) which produces the "VEX" (VLBI EXperiment) files, which contain information on the frequency of observation, source positions, antenna positions, time schedule and various other parameters that define a VLBI experiment. Once generated, the VEX file is then converted for every telescope to a format readable by its local scheduling system. The respective schedule files are then copied to the computers driving the telescopes and they feed the telescopes with a schedule to launch an e-VLBI session to observe the desired sources at specified frequencies at various locations in the sky.

The e-VLBI operation is then set up on one of the processing clusters (CAVE, PAM or CUPPA). As a first step all the required files, i.e. the input file and other associated files which contain the delay and station information for the experiment are created in or copied to the experiment directory. The DiFX setup files are also copied into the

[13] http://www.aoc.nrao.edu/∼cwalker/sched/sched/

same directory. All of these files are required to set various DiFX parameters for the experiment to be correlated.

After getting all four telescopes ready for the e-VLBI experiment, the schedules are started simultaneously at all telescopes at the specified time. As soon as all of the telescopes are tracking the desired source, the data are ready to be taken. Each observatory is equipped with the VLBI data acquisition system (DAS), which are data acquisition boards connected to the recorder machines. The CSIRO telescopes have two DAS so a maximum for 4 x 64 MHz IFs with an aggregate data rate of 1024 Mbps is achievable while the Hobart telescope has a single DAS allowing a maximum of 2 x 64 IFs and a data rate of 512 Mbps. The frequencies of observation, number of IFs, and polarization products can be set through the VLBI schedule file. The DAS at each telescope then starts to produce the baseband data in the LBA format.

The next step is to start the e-VLBI software on the CAVE or PAM cluster which launches the DiFX correlator and the recorder servers. In addition to this, the monitor server and the monitor client are also initialized, which will wait for the correlator to start producing the correlated data. The DiFX correlator also waits for the data to come in. The recorder server at each site then starts to transmit data over the network to the cluster. The correlator software then starts to manage the datastreams and the correlation process subsequently begins.

The monitor software receives the requested visibilities and plots them in real time, which can readily verify the e-VLBI performance. If there are no fringes, the correlation is stopped for trouble shooting and resumed when the problem (which could be wrong frequency, wrong schedule, error in the schedule etc.) is identified and rectified. The correlator opens up a time-tagged FITS file in the current directory and writes the visibilities to it.

At the end of the e-VLBI session, the FITS data files produced at the output of the correlator are then transported from the cluster to another location where they can be loaded in AIPS (Greisen 2003) for data reduction and analysis.

2.2.6 e-VLBI Post Processing

In the case of the e-VLBI observations conducted for this thesis, the correlated data were copied from the CAVE or PAM cluster to the CUPPA cluster at Curtin University. The first-stage analysis and automated verification of the data was done using

a custom made AIPS-based pipeline (C. Reynolds, private communication) written in ParselTongue (a Python interface to AIPS; Kettenis et al. 2006), which allows a quick check of the data quality.

The LBA data analysis pipeline runs on the CUPPA cluster and it requires an input file to set parameters such as the experiment, input and output location of the data, the AIPS tasks to be performed and the plots to be generated. After start-up, the pipeline loads the data into AIPS, corrects the data for phase errors, flags the bad data based on online monitoring, and calibrates the data on the strong calibrators in the dataset. The pipeline then plots the power spectra for each baseline in the array and anything peculiar can be easily noted in the bandpass. It also plots the visibility amplitudes and phases as a function of time and frequency showing the entire dataset.

After the initial verification of e-VLBI data using the pipeline, the bad data points due to RFI or instrumental errors in the data can be manually identified in AIPS and removed using tasks UVFLG or TVFLG. The data can then be plotted as a function of frequency using the task POSSM and as a function of time using the task VPLOT. The next step is to fringe-fit the data by running the task FRING which uses a phase calibrator to determine the solutions to correct the phases so as to ensure that they are constant as a function of frequency. The amplitude corrections can then be determined using VLBI amplitude calibrators and running the tasks SETJY and CALIB. Another level of amplitude calibration can be achieved by doing the T_{sys} (system temperature) calibration using the task ANTAB. The task ANTAB requires a text file that contains the T_{sys} information for all of telescopes in the array. The ANTAB T_{sys} data can be obtained from each observatory and an ANTAB text file can be generated to be used by the ANTAB task. All of the amplitude and phase corrections are applied to the entire dataset using the task CLCAL. The calibrated data can be viewed using tasks POSSM and VPLOT again. The data are then split into individual sources using the task SPLIT so as to study and image each source of interest separately. The single-source dataset is then written as a FITS file using the task FITTP and exported out of AIPS to be loaded, analysed and imaged using the DIFMAP software (Shepherd, Pearson & Taylor 1994).

In DIFMAP the FITS data file can be loaded using the command *obs* and can be plotted using commands *radplot* and *projplot*. Here, RFI peaks can be flagged out using the flagging functions of *radplot* or *projplot*. As a first step toward imaging,

the image and cell sizes are set (e.g. image size: 1024 x 1024 pixels and cell size: 1.07 x 1.07 milliarcseconds) using the command *mapsize*. The data are then Fourier transformed using the command *mapplot* to make a dirty image. Standard radio interferometry procedures such as deconvolution (Thompson, Moran & Swenson 2002) and self-calibration are then carried out using the CLEAN algorithm (Högbom 1974; Clark 1980; Schwab 1984b),which can be applied using the command *clean* with, for example, 100 iterations, and self-calibration of the source can then be performed using cthe ommand *selfcal*, until all of the believable emission components are cleaned, an adequate residual RMS (root mean square) level is attained and a final clean radio image of the field is produced using the command *mapplot cln*. The contour levels in the image can be set using the command *loglevs*. As part of the analysis, source structure, short- and long-term variability of the source as a function of time can be studied.

2.2.7 Future directions for e-VLBI: New Zealand and ASKAP

The newest additions to the Southern Hemisphere VLBI array are the ASKAP[14] (Johnston et al. 2007; Petrov et al. 2010) telescope near Boolardy in Western Australia and the Warkworth radio telescope (Gulyaev & Natusch 2008) operated by Auckland University of Technology in New Zealand. The inclusion of these two telescopes to the LBA has improved the uv-coverage and enhanced the east-west angular resolution by a factor of 4.

Recently, the first LBA + ASKAP + NZ science experiment was carried out and the parsec-scale structure of the calibrator source PKS 1934-638 was examined at a frequency of 1.4 GHz (Tzioumis et al. 2010). For this experiment, a data recording system developed at Curtin University was used for both the ASKAP and Warkworth telescopes and the data were correlated using the DiFX correlator at Curtin University.

The correlated data were initially processed in AIPS and then the calibrated single source file was exported to DIFMAP for imaging. The source was detected with higher resolution than previously studied and the frequency dependent structure effects were examined.

The inclusion of the ASKAP and Warkworth antennas in the LBA network has opened up the possibility to add more uv-coverage and resolution to LBA observations and it would only get better with a system supporting higher frequencies also. This

[14]http://www.atnf.csiro.au/projects/askap/

kind of enhancement is critical in trying to study and resolve the morphology of sources which are associated with, for example, relativistic jets, and it will allow the study of finer details of some interesting southern sources like Circinus X-1, relevant to the work presented in this thesis.

More recently, the first successful Trans-Tasman e-VLBI test has been conducted between the Warkworth telescope and the LBA telescopes, which is another milestone towards an expanded Southern Hemisphere e-VLBI network. In July 2011, the first e-VLBI experiment, with an ASKAP antenna, was carried out at the eve of SKA Forum in Banff, Canada, demonstrating the capability to readily make the next generation instrument a part of the existing Australian e-VLBI network so as to be able to conduct high-resolution, rapid-response observations.

2.3 CABB: Compact Array Broadband Backend

2.3.1 Introduction

Since the time of its inception in 1988, the Australia Telescope Compact Array (ATCA) has been a world-class radio interferometer in the Southern Hemisphere. It has produced a number of ground breaking results and added significantly to our knowledge of the Universe (e.g. Norris et al. 1993; Kulkarni et al. 1998; Kim et al. 1998; Corbel et al. 2002; Staveley-Smith et al. 2002; Burgay et al. 2003; Camilo et al. 2008; Massardi et al. 2011 and many references therein). The observational bandwidth of ATCA was 128 MHz until April 2009 when the old ATCA backend and some of the frontend components were replaced by the "Compact Array Broadband Backend" (CABB) so as to realise a major bandwidth and in turn, sensitivity upgrade.

Wilson et al. (2011) provide a comprehensive account of various components of CABB and this section draws heavily from that paper and can be taken as a summary of the detailed CABB description. After giving an introduction to the CABB upgrade, Wilson et al. (2011) present the main technical and scientific enhancements that the CABB system offers, followed by the description of various stages and subsystems of the CABB project. After that, the associated software and the relevant upgrades in the data reduction software package are covered and then some scientific projects demonstrating the capabilities of CABB are briefly outlined.

The CABB upgrade has provided a number of significant enhancements to the ATCA. The total recorded bandwidth for each IF (Intermediate Frequency) band has increased from 128 MHz to 2.048 GHz with dual polarization, which is a factor of 16 improvement, thereby increasing the continuum sensitivity by a factor of 4. The 2.048 GHz spectrum provides 2048 independent channels with a channel-width of 1 MHz in the continuum mode. The use of 10-bit digitisation (previously 2-bit) has helped achieve a lower T_{sys}, higher dynamic range and improved correlator efficiency. The CABB project also served as a technology demonstrator for the Square Kilometre Array, as a number of innovative and state-of-the-art equipment and techniques such as wide-band subsystems, fast data transfer on fibre optics, multi-bit digitisation, versatile digital filterbank etc. developed under the framework of CABB are relevant to the SKA.

2.3.2 The CABB System

The ATCA has undergone major hardware changes for the realisation and implementation of the CABB System. Various stages and processing units have been replaced by new systems and a full replacement of equipment has taken place.

The new wide-band system at ATCA consists of following stages:

- IF (Intermediate Frequency) conversion system;
- Digitisation and data transmission system;
- CABB correlator.

In the new CABB system, the conversion to a suitable frequency, sampling and digitisation of the baseband signal and conversion of the electrical signals to optical signals for transmission over fibre optics, are all done at the antenna side.

The ATCA can be tuned to two frequencies simultaneously and two orthogonal linear polarisation products are available at the output of the receiving system for each frequency. These two baseband signals from the receiver systems (two polarisations each) are then supplied to the IF conversion system as inputs. In the IF conversion system, primary band-filtering and amplification is performed on the signals and they are then up-/down-converted to a frequency appropriate for the sampler/digitiser stage.

Four 2 GHz IF bands produced at the output of the IF conversion system become the input of the sampler/digitiser stage of the CABB system. A wide-band high-sampling

rate (4 GS/s) Analogue-to-Digital Converter (ADC) was developed at ATNF to be used for the digitisation of the baseband signals coming from the IF conversion system. 10-bit sampling of the four IF bands is carried out at the Nyquist rate and then the sampled signals are quantised to complete the digitisation operation.

After digitisation, the four IF bands are required to be transported to the correlator room in the control building of the ATCA, and an optical transmission system is in place to serve this purpose. The same module which performs the analogue-to-digital conversion is equipped with an optical data transmission system. The 40 Gb/s digital data is converted into four 10 Gb/s serial data streams which are then converted to optical frequencies using laser chips. The four optical signals are then multiplexed and transported to the correlator room on a single optical fibre cable. The interface between the optical transmission system and the correlator is the Rear Transition Module (RTM). In addition to performing other functions such as receiving clock and control signals, providing data storage and ethernet connections, the RTM utilises the Receive Optical Sub-Assembly (ROSA), which receives the four optical signals from the data transmitter in the antenna building transmitted over optical fibre and converts the serial optical data streams back to parallel electrical data streams to be processed by the correlator.

The ATCA backend consists of a digital filterbank FX-style correlator module for each of the two observing frequencies, specially designed and developed at ATNF for CABB to make it a wide-band, high-dynamic range system. The correlator system consists of 16 CABB signal processing cards called “Front Boards” and 16 RTMs. The Front Boards and the RTMs are mounted on an “Advance Telecom Computer Architecture” (AdvTCA) chassis, a commercially available item used for telecommunication applications. Using the AdvTCA chassis all of the Front Boards and RTMs can be appropriately interconnected to function together as a signal processing system.

The CABB correlator cards are fed with four IF bands, which are received and converted to electrical signals by the RTMs for each observing frequency. The 2 GHz wide bands are then subdivided into desired number of channels, with channel widths of 1, 4, 16 or 64 MHz, using the polyphase digital filter banks, providing the facility to have up to 16 “zoom” windows within the IF bands. The availability of the zoom modes primarily facilitates spectral line studies and is therefore irrelevant to this work. After the channel selection and some initial processing, the signals are supplied to the

"Correlation Cell Array" which is an array of logic devices employed to perform the correlation operation i.e. the multiplication of signals from every antenna with the conjugate of the corresponding signal of every other antenna to obtain the complex visibility products. At the output of the correlator, correlated data with a bandwidth of 2 GHz comprising up to 2048 channels become available. The ATCA antennas with this new broadband system can be tied together and beams can be formed to use ATCA for VLBI.

The ATCA still uses the "CAOBS" software system to prepare and setup the ATCA systems to launch an observation. The new functions have been integrated in the ATCA control environment and the amplitude, phase and delay calibration is now manually done as opposed to the previously used automated calibration routine. Another significant change is the use of a java-based "CABB Scheduler" to create an ATCA observation schedule, in place of the old terminal-based program called "atcasched". The CABB Scheduler accommodates the new features of CABB and it also offers a number of new functionalities for observers such as the availability of the ATCA calibrator database and a velocity calculator within the CABB Scheduler interface.

2.3.3 CABB observations

A major part of the work done under the framework of this PhD project was the ATCA observations and monitoring of GRB afterglows. The GRB observation program began in the pre-CABB era when the available observing bandwidth was only 128 MHz. With the sensitivity obtained with this bandwidth the chances to significantly detect the radio afterglow of a typical GRB were low, since the radio sources associated with GRBs are weak and they fade away over a timescale of a few days. The observations conducted after the full deployment of CABB in April 2009 enjoyed a factor of 4 increase in the ATCA sensitivity, which comes by virtue of the bandwidth increment by a factor of 16, greatly enhancing the possibility to detect weak GRB radio afterglows.

The CABB update hugely benefited the GRB observation program and allowed the detection and monitoring of radio afterglows in four GRBs. The observations were conducted at the frequencies of 5.5 and 9.0 GHz and the new system gave us the frequency ranges of 4.5 - 6.5 GHz and 8.0 - 10 GHz, respectively, which provided much larger frequency coverage and improved the chances of detection.

In addition to this, CABB observations of the X-ray binary Circinus X-1 also proved to be critical in determining its radio behaviour, providing the trigger for e-VLBI/VLBI observations. Wide-band dual-frequency CABB observations of Circinus X-1 ensured that the radio flaring activity of the source was not missed due to poor frequency coverage and the flux density trend over a range of frequencies was mapped with higher sensitivity.

With the backdrop of recent developments and advancements in radio astronomy, CABB has proved to be a technical milestone which has not only enhanced the capabilities, efficiency and performance of an existing radio telescope in the Southern Hemisphere, but also serves as a key correlator technology demonstrator with a potential to pave the way for the design and development of next generation correlators for the upcoming telescopes like ASKAP, MWA and eventually SKA.

2.4 Conclusions

In the past two decades, the tools and techniques for radio astronomy have made new strides. These new ways and advancements became possible because of the rapid development of technology and extension of possibilities in the software domain. The availability of high performance and cost-effective computing and processing equipment and innovations in software development have introduced features and functionalities that have revolutionized the way radio astronomy is done.

As in various other parts of the world, there has been a rapid rise in the technology upgrades for radio astronomy in Australia. Almost every major instrument underwent a major capability upgrade; for instance, a receiver upgrade at Parkes Observatory and the deployment of the wide-band Mopra Spectrometer (MOPS) at the Mopra telescope. Within the scope of this PhD project, the e-VLBI capability of the Long Baseline Array and the wide-bandwidth enhancement (CABB) at ATCA were utilised to carry out radio astronomy experiments.

The operation of the LBA in e-VLBI mode allowed rapid follow-up and monitoring of a nearby X-ray binary system, Circinus X-1, along its entire orbit. As it now takes a much shorter time to set up, not having to put sets of storage devices at every telescope, e-VLBI is a much more feasible, efficient and quick way to monitor the short-term, time-critical behaviour of a radio source, as the telescopes in an e-VLBI

array are connected via fast network links. Real-time data transfer and correlation of the datastreams takes place to produce immediate results. Such an arrangement is ideal for the study of radio transients with Target-of-Opportunity (ToO) observations, which require a rapid response. The possibility of doing e-VLBI on Circinus X-1 enabled unprecedented observations to be made. In the future, the use of an extended e-VLBI network with more telescopes and longer observations holds the potential to reveal many more interesting details of the sources under investigation in a short span of time.

After producing ground-breaking results over the past two decades, the ATCA has taken a major leap in terms of capability and performance with the development and deployment of the CABB. This PhD project greatly benefited from the CABB upgrade as it improved the chances of detection and monitoring the weak radio afterglows associated with Gamma-Ray Bursts and wide-bandwidth, high sensitivity CABB observations provided the trigger for Target-of-Opportunity e-VLBI/VLBI observations.

These new tools of radio astronomy have not only provided astronomers with better performance and much improved results, the pathway towards their development, deployment and operation has provided useful insights on the potential requirements, constraints, bottlenecks and solutions relevant to many upcoming telescopes and systems associated with them. They are building background knowledge and helping develop the expertise which will prove to be useful in realising new equipment, new software and new techniques for radio astronomy in the future, for example, as part of the SKA project.

Chapter 3

e-VLBI Observations and monitoring of Circinus X-1

The work presented in this chapter formed the basis of a paper published in Monthly Notices of Royal Astronomical Society (MNRAS):

e-VLBI observations of Circinus X-1 on AU scales: e-VLBI observations of Circinus X-1: monitoring of the quiescent and flaring radio emission on AU scale.

A. Moin, C. Reynolds, J. C. A. Miller-Jones, S. J. Tingay, C. J. Phillips, A. K. Tzioumis, G. D. Nicolson, R. P. Fender, 2011, MNRAS, 414, Issue 4, 3551-3556.

3.1 Introduction

Circinus X-1 (Cir X-1) is a Galactic X-ray binary (XRB) system consisting of a confirmed low-magnetic field neutron star (Linares et al. 2010) accreting matter from a less evolved companion believed to be a supergiant of spectral type B5–A0 (Jonker, Nelemans & Bassa 2007). At a distance of 3.8–10.5 kpc (Jonker & Nelemans 2004; Iaria et al. 2005), the binary system has an eccentric orbit with an orbital period of 16.6 d (Kaluzienski et al. 1976), although the exact eccentricity is not well constrained, with estimates ranging from $e \sim 0.45$ (Jonker et al. 2007) to $e \sim 0.8$ (Murdin et al. 1980). The enhanced mass accretion rate onto the neutron star close to periastron is believed to explain the X-ray, infrared and radio flares seen following orbital phase 0 (Haynes, Lerche & Murdin 1980; Murdin et al. 1980). During these flares, Cir X-1 can

become the brightest confirmed neutron star system at radio wavelengths, with flux densities > 1 Jy.

According to their mass accretion rates, accreting low-magnetic field neutron stars show different sets of X-ray spectral and timing characteristics, according to which they are classified as either atoll sources or Z-sources (Homan et al. 2010). Cir X-1 can show the properties of both Z sources (Shirey et al. 1997) and atoll sources (Oosterbroek et al. 1995), and prior to periastron passage, shows behaviour that is characteristic of neither class (Soleri et al. 2009b). The source thus defies simple classification.

Cir X-1 is surrounded by a synchrotron nebula, which is believed to have been inflated by jets launched from the inner regions of the accretion flow (Tudose et al. 2006). The jets have been resolved on arcsecond scales in both the radio (Stewart et al. 1993; Tudose et al. 2006) and X-ray (Heinz et al. 2007; Soleri et al. 2009a) bands. The time delay between the successive brightening of different radio components was interpreted as evidence for the relativistic nature of the outflow ($\Gamma > 15.0$ for a distance of 6.5 kpc; Fender et al. 2004; Tudose et al. 2008).

The intensity of the radio flares close to periastron has varied significantly over time. In the period 1975–1985, peak intensities in excess of 2 Jy were observed at radio wavelengths (e.g. Haynes et al. 1978). After 1985, the flares became significantly weaker, peaking at < 50 mJy in the period 1996–2006 (Tudose et al. 2008). More recently, the source has shown episodes of brighter flaring events (Nicolson 2007; Calvelo et al. 2010), following which electronic very long baseline interferometry (e-VLBI) observations with the Long Baseline Array (LBA) detected compact radio emission from Cir X-1 on milliarcsecond scales (Phillips et al. 2007) for the first time since the high-activity phase of 1975–1985 (Preston et al. 1983).

The appearance of the compact radio source associated with Cir X-1 in 2007, as revealed with e-VLBI, was suggested to be the quiescent, non-variable emission from the binary system that is persistent during at least part of the 16.6 day orbit, and was not associated with a high flaring state of the system. This conclusion was based on a comparison of the data from Phillips et al. (2007) and Preston et al. (1983), in particular the estimated sizes of the radio-emitting structures.

In order to determine the evolution of the radio emission as a function of the binary orbital phase, Phillips et al. (2007) suggested an extended campaign of sensitive e-VLBI observations could be used to distinguish constant quiescent radio emission from

the flaring radio emission seen near periastron. This chapter reports on the results of such an extended campaign.

3.2 Observations and Results

An e-VLBI observing campaign was conducted with multiple observing sessions, to follow the evolution of the compact radio emission associated with Cir X-1 around its 16.6 day orbit. Further e-VLBI/VLBI observations with a larger array and a longer observing time were conducted in 2010 July to monitor the system as it came back to a high flaring state in 2010 May, the details of which are presented in Chapter 4. The e-VLBI observations helped improve the sampling of the compact radio emission as a function of orbital phase. The Cir X-1 orbital phases corresponding to all of the observation sessions mentioned in this chapter were calculated using the ephemeris of Nicolson (2007). Table 3.1 summarizes the data obtained during the multiple observing sessions.

The All Sky Monitor (ASM) onboard the Rossi X-ray Timing Explorer (RXTE) satellite indicated that the 1-d-averaged 2–10 keV X-ray count rate over the period of our observations was always <5 counts s^{-1}, with an average below 1 counts s^{-1}. This is over an order of magnitude lower than that observed in the period 1996 – 2003 (see Fig. 1 of Tudose et al. 2008), when the flaring activity was already significantly weaker than that observed prior to 1985. The radio flares at periastron were consequently significantly weaker during our observing campaign than during the only previous orbital phase-resolved VLBI monitoring campaign of Preston et al. (1983).

The telescopes used in the e-VLBI array were the Parkes radio telescope (64m), Australia Telescope Compact Array (ATCA) in Narrabri (5 x 22m) and the Mopra radio telescope (22m), all operated by Australia's Commonwealth Scientific and Industrial Research Organisation (CSIRO) Astronomy and Space Science division. The Hobart 26-m telescope, operated by The University of Tasmania, was used for two sessions conducted on 2009 December 9 and 16. The three CSIRO telescopes were connected via a 1 Gbps network and data were transported from the telescopes to a Beowulf cluster at the ATCA. Data were streamed from the ATNF telescopes at a sustained rate of 512 Mbps from the telescopes to the processing cluster and the data from Hobart were streamed at 128 Mbps. The cluster at the ATCA ran the DiFX software correlator

Table 3.1: e-VLBI observations of Cir X-1. S is the flux density/3σ upper limit.

Date	Time UT	Orbital Phase	Beam size (mas × mas)	RMS (mJy)	S (mJy)	Freq. (GHz)
26/02/2009	17:30-21:30	0.768-0.779	141×75	0.14	< 0.42	1.4
01/03/2009	13:30-20:00	0.940-0.956	163×77	0.20	< 0.60	1.4
15/07/2009	04:00-07:00	0.150-0.157	727×50	0.60	5.7 ± 0.6	1.7
30/11/2009	19:00-22:00	0.541-0.548	403×63	0.10	< 0.30	1.4
02/12/2009	19:00-22:00	0.661-0.669	753×61	0.12	< 0.36	1.4
04/12/2009	19:00-22:00	0.782-0.790	452×62	0.25	< 0.75	1.4
06/12/2009	19:00-22:00	0.903-0.911	1060×61	0.13	< 0.39	1.4
09/12/2009	19:00-22:00	0.086-0.094	164×20	0.54	3.7 ± 0.5	1.4
11/12/2009	19:00-22:00	0.207-0.215	1360×62	0.31	2.4 ± 0.3	1.4
16/12/2009	19:00-22:00	0.509-0.517	306×20	0.37	< 1.11	1.4

(Deller et al. 2007), which was used to correlate the data streams coming from the telescopes in real time. The observing sessions in 2009 February, March and December were conducted at a frequency of 1.4 GHz, while the frequency of observations in 2009 July was 1.7 GHz. The total bandwidth for each of the observing sessions was 64 MHz in each of two orthogonal circular polarizations recorded as 4×16 MHz bands.

Figure 3.1 shows the typical *uv*-coverage obtained for a 3-hour observing session. The telescope data streams were correlated with an integration time of 1s and 256 spectral channels across each 16 MHz band. The DiFX correlator output files were analysed with an AIPS-based LBA-pipeline written in ParselTongue (Kettenis et al. 2006) to obtain preliminary results, following which a more detailed analysis was carried out in AIPS (Greisen 2003) and DIFMAP (Shepherd, Pearson & Taylor 1994) using standard data analysis techniques. Amplitude calibration was carried out in AIPS using the primary flux calibrator J1924-2914 to set the flux density scale. We estimate a systematic uncertainty of about 10 per cent in the overall amplitude scale.

Radio emission associated with Cir X-1 was clearly detected at frequencies of 1.4 and 1.7 GHz during the observing epochs corresponding to the orbital phases following periastron (orbital phase = 0.0), but no compact radio emission was observed at any other phase along the orbit. Figures 3.2, 3.3 and 3.4 show the LBA images for the three

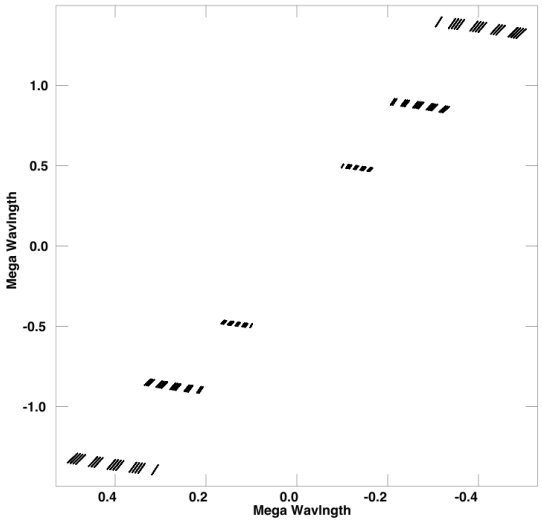

Figure 3.1: *uv* **coverage for Cir X-1 observation session** - The figure shows the *uv*-coverage for a single 3-hr Cir X-1 e-VLBI session.

epochs in which the source was detected. In all cases, the source was unresolved down to the beamsize of the array. Our best resolution during the epochs when Cir X-1 was detected was $164 \times 20\,\mathrm{mas}^2$ in position angle 58.8° east of north. This provides a lower limit on the brightness temperature of $T_\mathrm{b} > 10^6\,\mathrm{K}$. While this does not completely rule out thermal emission, the resolved jets previously detected in this system (Stewart et al. 1993; Heinz et al. 2007) lead us to interpret the emission as synchrotron radiation from the jets.

While simultaneous ATCA data were taken during the e-VLBI observations, the array was in its compact EW352 configuration for all epochs except 2009 July 15, in which it was in an even more compact H75 configuration. At the low frequency of 1.4 GHz, the corresponding useful resolutions ($2'$ and $7.5'$ respectively) would have been insufficient to distinguish emission from the radio jets from persistent diffuse emission from the surrounding radio nebula (Tudose et al. 2006). Thus it was not possible to determine whether the long baselines of the LBA were resolving out extended emission on scales of $\sim 1''$.

Figure 3.5 shows the Cir X-1 orbit and the points along the orbit where the recent e-VLBI observations and the VLBI observations of Phillips et al. (2007) and Preston et al. (1983) were made. The compact radio emission appears to turn on around orbital

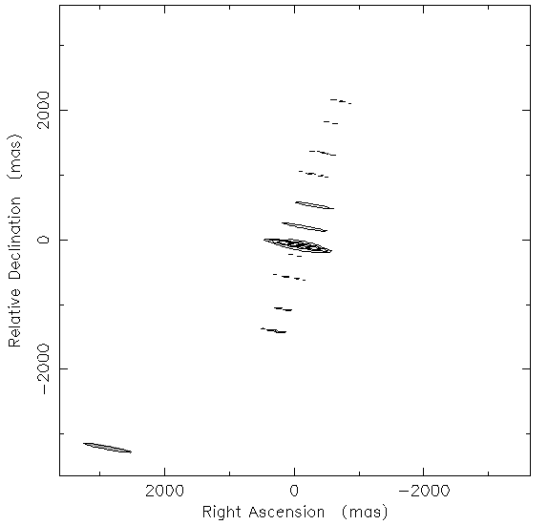

Figure 3.2: e-VLBI detection of Cir X-1, epoch 1 - July 15, 2009 at 1.7 GHz. Peak flux density: 5.7 ± 0.6 mJy. Contour levels: -20 20 28.28 39.98 56.54 79.95 % of the peak intensity.

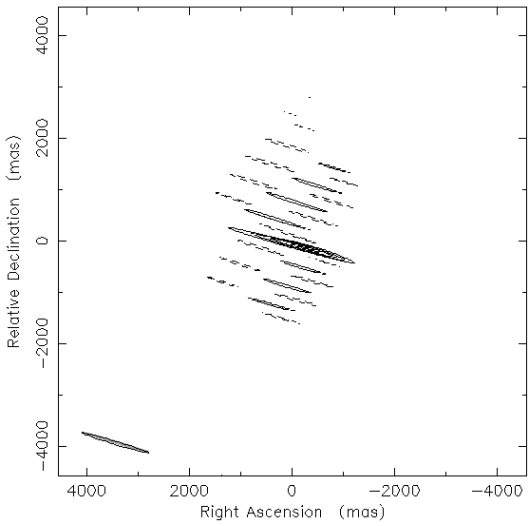

Figure 3.3: e-VLBI detection of Cir X-1, epoch 2 - December 9, 2009 at 1.4 GHz. Peak flux density: 3.7 ± 0.5 mJy. Contour levels: -20 20 28.28 39.98 56.54 79.95 % of the peak intensity.

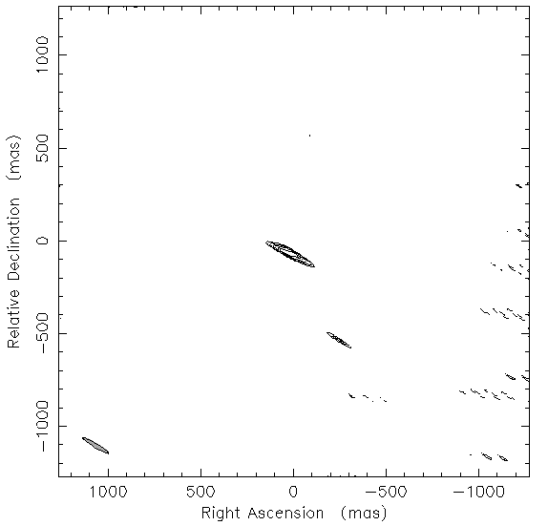

Figure 3.4: e-VLBI detection of Cir X-1, epoch 3 - December 11, 2009 at 1.4 GHz. Peak flux density: 2.4 ± 0.3 mJy. Contour levels: -20 20 28.28 39.98 56.54 79.95 % of the peak intensity.

phase 0.0, but fades away following the flaring event at periastron, and there is no bright, compact radio emission around the rest of the orbit.

To search for radio flaring in the downstream lobes, we made wide-field images of all 10 data sets from our e-VLBI campaign, going out to 5 arcsec from the phase centre in each case. This corresponds to the maximum angular separation between the core and the downstream lobes measured by Tudose et al. (2008). By retaining the maximum time resolution and a frequency resolution of 32 kHz, we were unaffected by either time or bandwidth smearing. No radio emission brighter than 5σ was detected away from the phase centre (see Table 3.1 for the rms noise level in each image). Therefore, we rule out any flaring of compact components downstream in the lobes (as seen on larger scales by Fender et al. 2004) brighter than 2.8 mJy. This implies that either the core flare at periastron did not result in a dark flow propagating downstream at ultrarelativistic speeds to energize the lobes, that the lobe flares are sufficiently faint that they were below our sensitivity limit, or that the lobes are sufficiently diffuse or extended to be resolved out by our LBA observations.

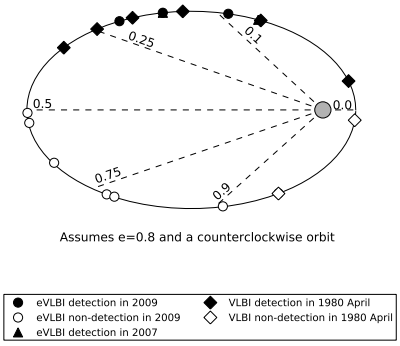

Figure 3.5: Cir X-1 orbit - All VLBI observations of Circinus X-1 plotted as a function of position in the orbit. The Cir X-1 orbital phases were determined using the ephemeris of Nicolson (2007). Filled symbols denote detections and open markers non-detections. Circles represent the results from our 2009 e-VLBI campaign. Triangles represent the e-VLBI detections of Phillips et al. (2007). Diamonds represent the VLBI detections made by Preston et al. (1983) while Cir X-1 was in a high flaring state. There is no evidence for a bright quiescent component that persists throughout the orbit.

3.3 Discussion

3.3.1 The absence of a quiescent compact component

Our sampling of the entire orbit of Cir X-1 with high angular resolution e-VLBI observations shows no evidence for compact radio emission outside the flaring event associated with periastron passage (Figure 3.6). Thus there is no evidence for the compact, non-variable, quiescent component proposed by Phillips et al. (2007). Compact radio emission is detected only at orbital phases following periastron passage when the enhanced mass accretion is believed to power a synchrotron-emitting relativistic jet, as directly resolved on larger scales by Tudose et al. (2006), Tudose et al. (2008).

Our findings are consistent with all previously-reported VLBI observations of Cir X-1. Preston et al. (1983) observed a large flare in 1980 April (Figure 3.7). Prior to the beginning of the radio flare at orbital phase 0.002, they did not detect any quiescent emission on the 275-km baseline between Parkes and Tidbinbilla, to a 5σ upper limit of $\sim 20\,\mathrm{mJy}$. All subsequent detections in their monitoring campaign were consistent with the decay of a single large flaring event initiated at or close to orbital phase zero.

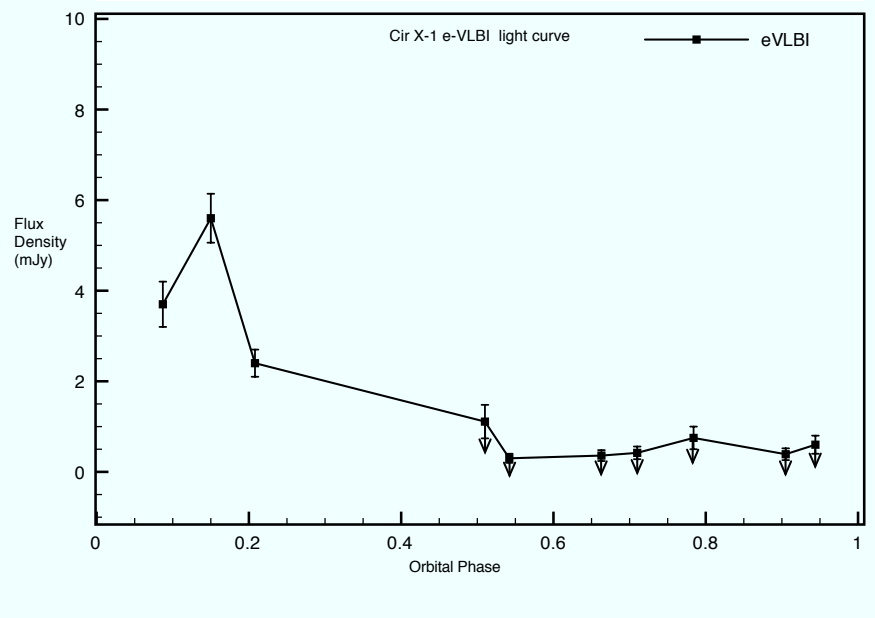

Figure 3.6: Cir X-1 e-VLBI light curve (2009) - Radio light curve from our 2009 e-VLBI campaign.

The only other reported VLBI detection of Cir X-1, by Phillips et al. (2007), was again made in the few days following periastron passage. Their 1.6-GHz observations were made from orbital phase 0.03–0.11, and their 8.4-GHz observations a day later, from orbital phase 0.14–0.17, in both cases consistent with the results of our observing campaign.

The compact quiescent component postulated by Phillips et al. (2007) was suggested in response to an apparent discrepancy in the angular size of the source between the observations of Preston et al. (1983) in 1980 and those of Phillips et al. (2007) in 2007. However, as noted by the authors, the flares being compared were separated by $\sim 30\,\mathrm{y}$ in time and had peak flux densities which differed by almost 2 orders of magnitude. Therefore, it may not be valid to compare these two very different flares at face value.

The second motivation for the hypothesized compact quiescent component was to explain the absence of resolved jet-like structures in the 1.6-GHz image of Phillips et al. (2007). If the proper motion of the ejecta from the flaring events in Cir X-1 is indeed as high as $400\,\mathrm{mas\,d^{-1}}$, as postulated by Fender et al. (2004) and suggested by Tudose et al. (2008) from a re-analysis of the same data, then any ejecta should have been resolved

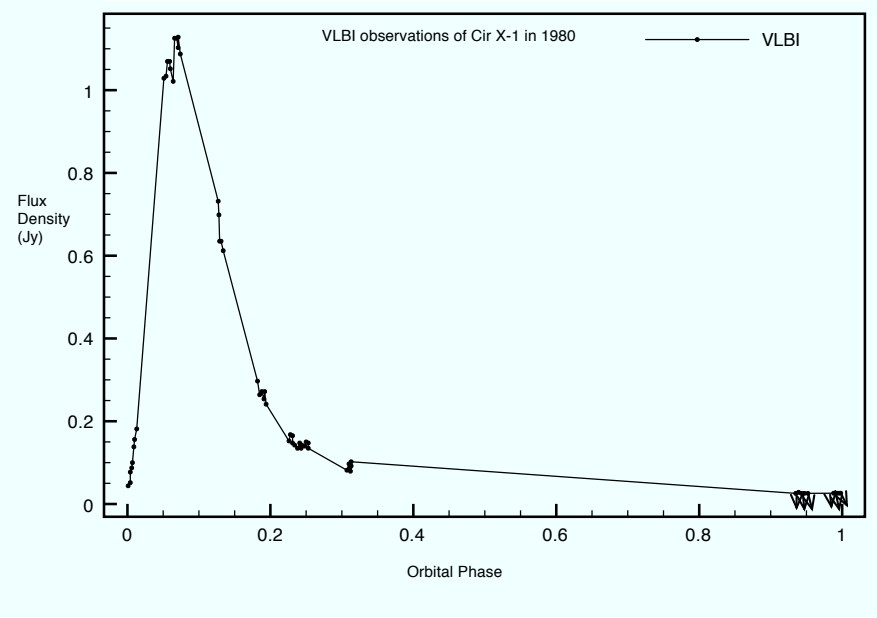

Figure 3.7: Cir X-1 VLBI light curve (1980) - Correlated flux density on the Parkes-Tidbinbilla baseline during VLBI observations made in 1980 (data taken from Preston et al. (1983).

beyond the beam size in both the observations of Phillips et al. (2007) and in our e-VLBI runs on 2009 July 15 and December 11, assuming that the proper motion of the ejecta does not vary between outbursts, and that the ejection event occurred at orbital phase 0.0 in each case. However, we note that this proper motion is based on ATCA observations of correlated radio flaring events seen in the unresolved binary core and downstream jet lobes, and depends on the correct association of a given core flare with the downstream lobe flare. In no case has a proper motion been definitively measured by fitting the trajectory of moving components. The most comprehensive analysis of the core-lobe flaring delay was performed by Tudose et al. (2008), who considered all possible associations of core and lobe flares at two different frequencies, in three separate outbursts, and concluded a minimum apparent velocity $\beta_{\rm app}c \sim 3(d/{\rm kpc})$ where c is the speed of light and d is the source distance, believed to be in the range 3.8–10.5 kpc (Jonker & Nelemans 2004; Iaria et al. 2005). However, we note that since the radio flaring in Circinus X-1 appears to be periodic on the orbital period, this may introduce an ambiguity of some multiple of 16.6 d into the core-lobe flaring delay, and hence into the assumed proper motion of the ejecta. Finally, since no moving components

were observed in the ATCA images in which the core-lobe delay was detected, the jet responsible for injecting energy into the downstream lobes could be a dark, unseen flow, as suggested to be present in Sco X-1 (Fomalont, Geldzahler & Bradshaw 2001). In that case, we would not expect our VLBI observations to resolve discrete ejecta moving from the core to the lobes. The non-detection of lobe emission in any of our VLBI observations suggests that if such a dark flow exists, the working surface where it impacts on the surroundings must be either too diffuse or too faint for us to detect with our observational set-up.

In summary, since neither of the original motivations for the existence of a compact, quiescent component can be definitively validated, and in the absence of any observational evidence for non-variable emission of this nature, we can rule out the presence of quiescent radio emission on milliarcsecond scales, to a 3σ level of $0.3\,\mathrm{mJy\,beam^{-1}}$ in our most sensitive observations (2009 November 30).

3.3.2 The absence of secondary flares at apastron

From the analysis of 10 years worth of ATCA monitoring data, Tudose et al. (2008) found evidence for radio flaring events not just close to periastron, but also at phase 0.5 ± 0.1, attributed to enhanced wind accretion at a local minimum in the relative velocity between the neutron star and the stellar wind of the companion, close to apastron. It seems unlikely that the apastron flares were caused by blobs > 5 arcsec away from the core. If there were any such blobs present, it should have been possible to see them in the images produced in Tudose et al. (2008), given the spatial resolution of the data used by Tudose et al. (2008), the fractional amplitude variation ($\sim$100%) and duration of the apastron flares. The amplitude of these day-time-scale flares was in the range 4–15 mJy. Fig. 5 of Tudose et al. (2008) also shows shorter time-scale flaring events around orbital phase 0.5, lasting only 2–3 h. These are most obvious at 8.6 GHz, being both smoothed out and reduced in amplitude on moving to the lower frequency of 4.8 GHz. Figures 3.8 and 3.9 show the daily averaged data of Tudose et al. (2008), with radio flux density plotted as a function of orbital phase, with clear evidence for emission at positions in the orbit away from periastron. The flares are most evident in the data from 1996 and 2000. A comparison with the e-VLBI monitoring data in Figure 3.6 shows that there is no evidence for similar flaring events at milliarcsecond angular scales in either of the observations within this range of orbital phase (2009 November 30

and December 16). This implies that these flaring events are either sporadic such that we missed them in two separate orbital cycles, that their peak brightness is sufficiently variable for us not to detect them at our e-VLBI sensitivity limit or that they arise from sufficiently diffuse emission that they are resolved out on VLBI scales. The absence of compact emission in our e-VLBI data also rules out the presence of shorter flaring events on time-scales of hours, although we note that our observations were carried out at 1.4 and 1.7 GHz. Given the smoothing of the short-time-scale flares seen with the ATCA at 4.8 GHz, this is unsurprising. If these rapid flaring events arise from a compact jet (from which we see emission from the surface of optical depth unity, e.g. Blandford & Konigl 1979), it is likely that any rapid variations would be sufficiently smoothed out by the time they reached the 1.4-GHz photosphere that they would not be significantly detected.

Figures 3.8 and 3.9 are based on the ATCA observations of Circinus X-1 conducted over a decade (1996-2006), showing radio flux densities as a function of orbital phase (data taken from Tudose et al. (2008)). Figure 3.8 shows the 4.8-GHz observations and Figure 3.9 the 8.6-GHz observations. As can be seen from these figures, there is some evidence for secondary flares at orbital phases ~ 0.5.

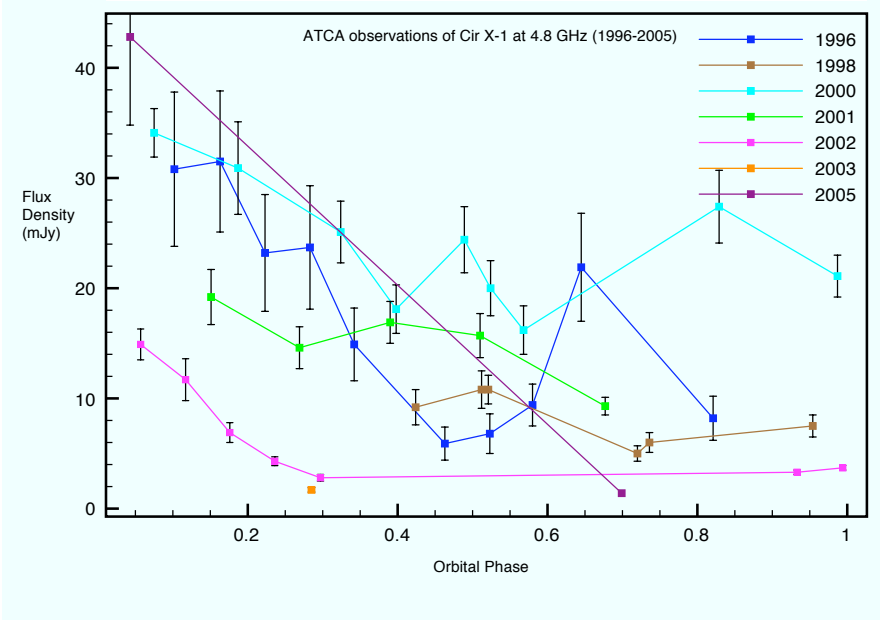

Figure 3.8: ATCA light curve at 4.8 GHz - ATCA observations of Circinus X-1 (Tudose et al. 2008).

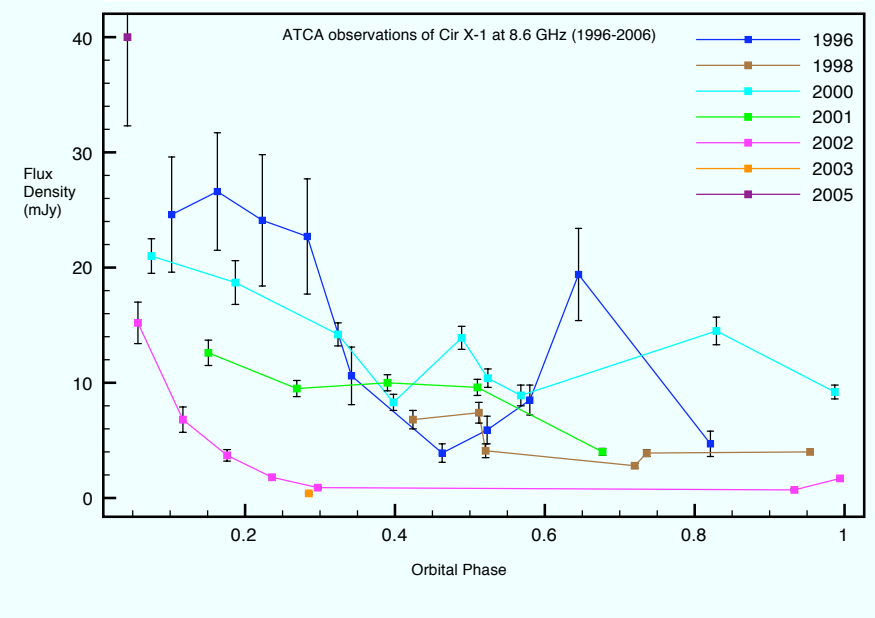

Figure 3.9: ATCA light curve at 8.6 GHz - ATCA observations of Circinus X-1 (Tudose et al. 2008).

3.3.3 The size scale of the emission

The largest angular scale probed by our VLBI observations corresponds to the length of the shortest baseline (between Mopra and ATCA; 113 km). At an observing frequency of 1.4 GHz, this corresponds to a largest angular size of 412 mas, or $3300(d/8\mathrm{kpc})$ AU, where d is the distance to Cir X-1. With infinite signal-to-noise, the non-detection of emission away from periastron would therefore limit the size scale of the emission to being greater than this. If this were solely responsible for the non-detection at orbital phase 0.51 on 2009 December 16, then linear expansion following the detected onset of the flare at orbital phase 0.09 on 2009 December 9 would imply an expansion speed of $> 2.7c$. However, the expansion of the emitting region would reduce the surface brightness, and since the upper limit on the source brightness on 2009 December 16 is only a factor of 2.1 less than the detected source brightness five days earlier, a significantly smaller expansion velocity would be sufficient to render the emission undetectable. The flux density of a simple adiabatically expanding synchrotron bubble (van der Laan 1966) scales as R^{-3} in the optically thick phase and R^{-2p} in the optically thin phase, where p is the index of the electron energy spectrum, with a canonical value

of 2.2. Thus expansion by only a small factor (1.2–1.3) would be sufficient to cause the observed decrease in source brightness to below the detection limit. Since the source was unresolved during the flaring event itself, we have no constraints on the original source size, so cannot therefore constrain the expansion velocity.

3.4 Cir X-1 e-VLBI in summary

We have used the LBA in e-VLBI mode to monitor the compact radio emission from Circinus X-1 as a function of orbital phase. The only milliarcsecond-scale detections of the source were made close to periastron, at orbital phases between 0.09 and 0.21. There is no evidence for compact radio emission during the majority of the orbit, to a 3σ upper limit of between 0.3 and 1.1 $\mathrm{mJy\,beam^{-1}}$, consistent with previous VLBI observations. We therefore rule out the hypothesis of Phillips et al. (2007), who postulated a non-variable, compact, quiescent component of radio emission with an intrinsic angular size of ~ 35 mas. We find that any flaring events at orbital phase 0.5 must be either too sporadic, faint or diffuse for us not to detect them with our e-VLBI observations. The lack of any resolved jet components moving away from the central binary system suggests that either the ultrarelativistic proper motions reported in the literature are in error, or that the ultrarelativistic flow is dark.

In the near future, higher-frequency 8.4-GHz VLBI observations including the ASKAP antenna(s) in Western Australia and the Warkworth Telescope in New Zealand will increase the available angular resolution by at least a factor of 20 and will enable us to study the morphology of the source and the evolution, dynamics and energetics of a possible relativistic jet associated to Cir X-1 and other such peculiar transient sources.

Chapter 4

High Resolution Imaging of Circinus X-1

The work presented in this chapter formed the basis of a paper published in Monthly Notices of Royal Astronomical Society (MNRAS):

The first resolved imaging of the milliarcsecond-scale jets in Circinus X-1.

J. C. A. Miller-Jones, A. Moin, S. J. Tingay, C. Reynolds, C. J. Phillips, A. K. Tzioumis, R. P. Fender, J. N. McCallum, G. D. Nicolson, V. Tudose, 2012, MNRAS, 419, Issue 1, L49-L53.

4.1 Introduction

Circinus X-1 is a unique and unusual X-ray binary system in our own Galaxy, which has been exhibiting puzzling characteristics over the past 30 years. Consistent radio observations have shown strong radio flares coupled with X-ray emission close to orbital phase 0.0. Present in this chapter, are the results from high-resolution ToO VLBI observations of Circinus X-1 in a high flaring state, conducted with the Australian Long Baseline Array. The VLBI observations were conducted close to the periastron passage of the 16.6 day orbit of the system revealing for the first time a resolved milliarcsecond scale jet associated with Circinus X-1.

4.2 Background

Circinus X-1 (Cir X-1) is one of the few confirmed Galactic neutron star X-ray binaries with resolved relativistic jets, which have been studied from arcsecond scales (Fender et al. 1998; Tudose et al. 2008) out to arcminute scales (Stewart et al. 1993; Tudose et al. 2006) where they have inflated a synchrotron-emitting radio nebula. The system comprises a neutron star primary (Linares et al. 2010) accreting from a less-evolved companion whose nature is less well constrained. The binary has an eccentric 16.6 day orbit (Kaluzienski et al. 1976), with enhanced accretion close to periastron (Murdin et al. 1980; Haynes et al. 1980) leading to radio flaring events. The distance to Cir X-1 is not well-constrained. From the peak luminosity of its Type I X-ray bursts, Jonker & Nelemans (2004) determined a distance in the range 7.8–10.5 kpc, although Iaria et al. (2005) derived a much lower value of 4.1 kpc from model-fitting of spectra that suggested a low hydrogen column towards the source.

In addition to the well-known radio jets, Cir X-1 is the only confirmed neutron star system with extended X-ray jets (Heinz et al. 2007; Soleri et al. 2009). The extended X-ray emission is oriented along the same position angle as the radio jets, and its diffuse, extended morphology is suggestive of a terminal shock where the jets run into the surrounding interstellar medium (Sell et al. 2010). Assuming a synchrotron origin for the X-ray emission, the inferred time-averaged jet power could be as high as 15% of the Eddington luminosity for the neutron star.

The orientation of the system remains controversial. The presence of X-ray dips (Shirey et al. 1999) and the spectral changes on egress (Brandt et al. 1996), as well as the P-Cygni profiles of detected X-ray lines (Brandt & Schulz 2000), argue for an edge-on accretion disc. However, the extremely high Lorentz factor ($\Gamma > 15$) inferred from the time delay between a brightening of the radio core and subsequent downstream flaring in the jets requires that the radio jets are inclined very close to the line of sight (Fender et al. 2004). Reconciling these two sets of observations would require bends in the jet or a severe misalignment between the jet axis and the orbital plane.

The ultra-relativistic flow inferred by (Fender et al. 2004) depends on the assumption of a causal relation between flaring events in the core and those subsequently observed downstream in the southeastern jet. However, the sparse time coverage of

the existing radio observations has thus far prevented this result from being independently confirmed. With the high angular resolution available using very long baseline interferometry (VLBI), we can track the motion of individual jet components, directly measuring their proper motions and hence constraining the Lorentz factor and inclination angle of the jets. However, compact radio emission is seen only during the radio flares immediately following periastron passage (Moin et al. 2011), and the low surface brightness sensitivity of VLBI arrays constrains the observations to periods of strong radio flaring in the system.

The radio flares regularly reached levels in excess of 1 Jy over the period 1975–1985, during which time Preston et al. (1983) constrained the angular size of the flaring component to lie between 1.5 and 15 mas at 2.3 GHz. The source then entered a more quiescent phase with flares peaking at mJy levels, and further activity was not seen again until 2006 (Nicolson 2007). This triggered further VLBI observations of Cir X-1, and in the first southern hemisphere electronic VLBI experiment, Phillips et al. (2007) detected a single, scatter-broadened component of size 60 ± 15 mas at 1.6 GHz. The source was also unresolved in the 1.4- and 1.7-GHz e-VLBI observations of Moin et al. (2011).

4.3 VLBI Target of Opportunity observation of Circinus X-1

The Circinus X-1 e-VLBI observing campaigns in 2009 (Moin et al. 2011) helped study the radio emission pattern of Circinus X-1 as a function of its orbital phase. At the time when those campaigns were conducted, Circinus X-1 was in a quiescent state since many years. In 2010, the peculiar X-ray binary system came back to a high flaring state. As part of the transient detection program carried out under the scope of this PhD, Target-of-Opportunity (ToO) VLBI observations of Circinus X-1 were then carried out, in response to strong detections with Hartebeesthoek Radio Astronomy Observatory (HartRAO; Nicolson, priv. comm.) and ATCA telescopes, to detect and monitor its activity in the high flaring state with higher resolution in an attempt to determine the milliarcsecond-scale morphology of the source.

4.4 Observations and data reduction

In response to the enhanced radio activity detected in 2010 May and June, we conducted a target-of-opportunity observation of Cir X-1 using the Australian Long Baseline Array (LBA) from 02:21–16:41 UT on 2010 July 28 (orbital phase 0.028–0.064, using the ephemeris of Nicolson 2007). The observations were conducted at a frequency of 8.4 GHz, using the relatively high observing frequency to reduce the angular broadening caused by interstellar scattering, hence increasing our effective angular resolution. The array comprised the ATCA, Ceduna, Hobart, Mopra and Tidbinbilla telescopes. The ATCA was used in tied-array mode, phasing together the four antennas CA01, CA02, CA03 and CA05 (CA04 had a hardware fault and was not used). No fringes were detected from Tidbinbilla, reducing our effective array to four antennas. The resulting *uv*-coverage is shown in Figure 4.1. The observations were conducted in dual-polarization format with two separate 32 MHz bands comprising a total bandwidth of 64 MHz. The ATCA was in its hybrid H168 configuration, with a maximum baseline of 4.47 km.

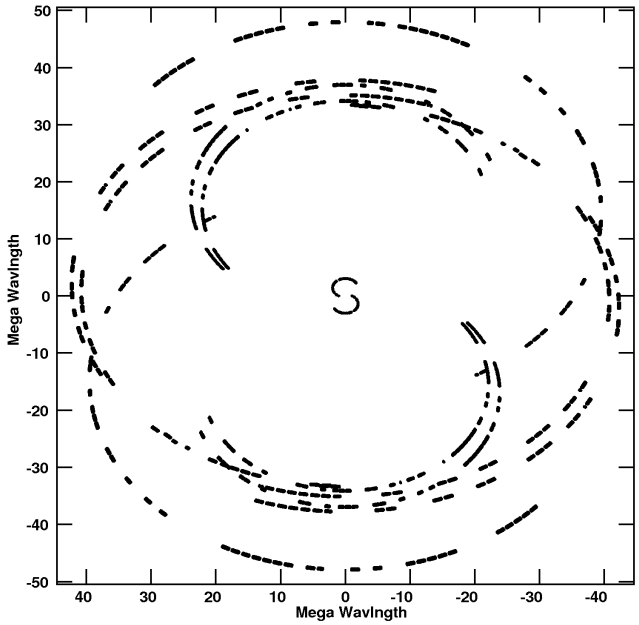

Figure 4.1: *uv*-coverage of Cir X-1 VLBI observation on July 28, 2010 - The short baseline is between the ATCA and Mopra stations. Note the large gaps at intermediate baseline lengths.

Correlation was performed using the DiFX software correlator (Deller et al. 2007, Deller et al. 2011), followed by preliminary analysis and verification of the data using a ParselTongue (Kettenis et al. 2006) pipeline. This revealed an error in the position of the target source arising from an error in the phase referencing calibrator coordinates. This error was corrected before a full data reduction was carried out in aips (Greisen 2003). The source amplitudes were determined using the primary VLBI flux calibrator 1921-293, assuming a flux density of 8 Jy. Since Cir X-1 was sufficiently bright, fringe fitting was performed on the target source. Imaging and self-calibration were then carried out in Difmap (Shepherd, Pearson & Taylor 1994)

4.5 Results

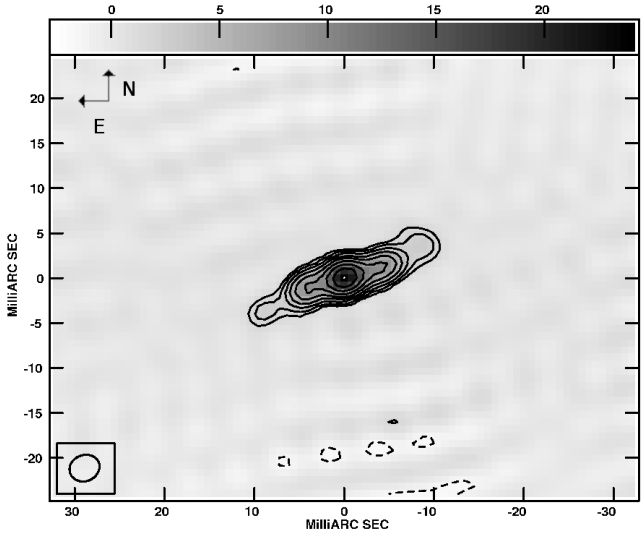

Figure 4.2: LBA image of Cir X-1 on 2010 July 28 - Contours are at $\pm(\sqrt{2})^n$ times the lowest contour level of 1.5 mJy beam^{-1}, where $n = -2, -1, 1, 2, 3....$ Greyscale shows the radio brightness in units of mJy beam^{-1}. Image noise level is 0.55 mJy beam^{-1}. North is up and East is to the left in the image. The source is resolved into a continuous jet of length $\sim$ 20 mas. It is not certain whether the zero point in RA and Dec coincides with the core of Cir X-1 or not.

Cir X-1 was resolved by the LBA into a jet-like structure with an extent of $\sim$ 20 mas (Figure 4.2) and a total flux density of 54 ± 7 mJy. Although our minimum and maximum baselines were 113 and 1702 km, respectively, the failure at Tidbinbilla

deprived us of intermediate baselines of order a few hundred kilometres. This created a large hole in the *uv*-plane (Figure 4.1), such that we were only sensitive to structures on scales of 4–9 and 67–250 mas. Our single short baseline (between ATCA and Mopra) was consistent with a point source whose flux density decayed from 90 to 35 mJy beam^{-1} over the course of the observations. This is relatively consistent with the analysis of the correlated data from the ATCA, which showed a marginally resolved source (with a beam size of 0.97×0.86 arcsec^2) with a flux density that decayed smoothly from 210 to 80 mJy over the course of the observing run. However, the LBA resolved out ~ 55 per cent of the radio emission detected by the ATCA, which must therefore be on size scales between 250 and 970 mas.

The changing source flux density over the 14.3 h observation violates one of the fundamental assumptions of aperture synthesis. In the absence of morphological variations, this would create amplitude errors during the imaging process. However, since our *uv*-coverage is already so sparse, we cannot compensate by only imaging short snapshots of data in which the amplitudes are relatively stable. Tests indicated that the data could not be binned more finely than into two separate halves without severely compromising the imaging fidelity. A comparison of the data from the first and second halves of the observation showed a fading core, as well as marginal ($\sim 5\sigma$) evidence for outward motion of the components (Figure 4.3). The inferred positional shift is 6.2 mas over the 7.15 h between the midpoints of the two data sets, implying a proper motion of 21 mas d^{-1}. This is significantly different from the 400 mas d^{-1} inferred by Fender et al. (2004) from the time delay between flaring in the core and subsequent flaring in downstream lobes.

To evaluate the effects of the changing source flux density and morphology combined with our relatively sparse *uv*-coverage, we performed some simulations within AIPS. We subtracted the clean components from our best image (Figure 4.2) in the *uv*-plane, and then added various source models back in to the *uv*-data. The decaying point source at the phase centre seen in the ATCA light curve could not reproduce the symmetric extended structure along the observed position angle. From this, we conclude that our observed structure is real, and is not an artifact caused by amplitude errors combined with limited *uv*-coverage. Adding a second, non-varying component along the position angle of our observed jet showed that we could not reproduce the observed symmetric

structure with an asymmetric, one-sided jet model. Finally, adding in a single, ballistically moving jet component created a one-sided, smooth jet, with a reduced surface brightness owing to the smoothing of the emission along the component trajectory. In this case, the jet locus appeared slightly curved, and artifacts appeared as stripes parallel to the jet trajectory, very similar to those seen in Figure 4.2. From these simulations, we conclude that the symmetric profile we observe is real, as it cannot be reproduced using any one-sided source model. We caution that the relatively smooth appearance of the jet in Figure 4.2 could be created by discrete, moving components on each side of the peak emission, especially given the structure in the observed residuals.

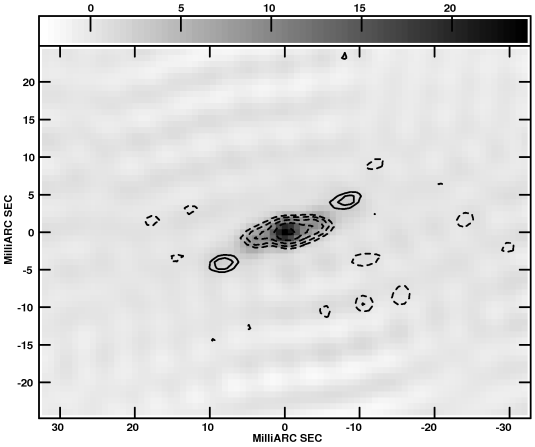

Figure 4.3: Difference image between the two halves of the LBA observing run on July 28, 2010 - Contours are at $\pm(\sqrt{2})^n$ times the lowest contour level of $1.5\,\mathrm{mJy\,beam^{-1}}$, where $n = -3, -2, -1, 1, 2, 3....$ Positive contours indicate that the emission was brighter in the second half of the observing run. Greyscale shows the radio brightness of the full data set (i.e. as shown in Figure 4.2) for comparison, in units of $\mathrm{mJy\,beam^{-1}}$. While the core fades between the first and second half of the observation, there is marginal evidence for the brightening of the outer parts of the jet.

The observed jets are elongated along a position angle 113° E of N, in good agreement with the position angle of the arcsecond-scale jets detected in both the radio and X-ray bands. Fender et al. (1998) derived a position angle of $110 \pm 10°$ for the extended arcsecond-scale radio emission, although Tudose et al. (2008) found this position angle to vary between epochs, with a mean of $129 \pm 13°$, although no unequivocal evidence for precession was detected. The deepest available X-ray images (Sell et al. 2010) show unresolved X-ray emission at a position angle 140° E of N, and extended diffuse

emission from 95–155° at a distance of 20–50″ from the central source.

We find no evidence for angular broadening of the radio emission, as reported by Phillips et al. (2007) at the lower frequency of 1.6 GHz. Their measured angular size of 60 ± 15 mas, scaled by the expected $\lambda^{2.2}$ dependence corresponds to 1.6 ± 0.4 mas at our observing frequency of 8.4 GHz, well below our beam size of 3.4×2.9 mas^2.

4.6 Discussion

4.6.1 Morphology

The emission appears fairly smooth and symmetric on either side of the peak. While initially reminiscent of the compact jets observed in the hard state of the black hole system GRS 1915+105 (Dhawan, Mirabel & Rodriguez 2000), we note several caveats to this interpretation. The proper motion of 21 mas d^{-1} inferred from Figure 4.3 would imply that discrete components would move by 3.7 beamwidths during our observation. This would be sufficient to create the observed smooth structure. Second, we have no spectral information, although previous multi-frequency ATCA observations have shown both optically thick and optically thin spectra during flaring events (Fender et al. 2005; Calvelo et al. 2010). Thus we cannot rule out the observed emission being caused by the outwards motion of discrete, optically-thin ejecta, as seen during outbursts of black hole X-ray binaries (e.g. Mirabel & Rodriguez 1994).

Should the emission arise from a steady, compact jet however, our image bears more resemblance to the symmetric compact jets observed in GRS 1915+105 (Dhawan et al. 2000) than to the asymmetric ones seen in Cygnus X-1 (Stirling et al. 2001). The low inclination angle of the jets to the line of sight in Cygnus X-1 ($\sim 27°$) implies that the counterjet in that system is Doppler-deboosted below the sensitivity level of the observations, such that only the approaching jet is seen. However, even with its higher inclination angle (66–70°), the symmetry of the compact jets in GRS 1915+105 was difficult to explain. Three possible explanations were put forward (Dhawan, Mirabel & Rodriguez 2000); an intrinsically slow jet such that the Doppler factors of approaching and receding jets were comparable, a highly relativistic velocity such that the approaching jet was also Doppler-deboosted in a similar way to the receding jet, or a counterjet being hidden by free-free absorption within a few hundred au of the core.

Since we did not phase-reference the observations of Cir X-1, all absolute positional information has been lost. For this reason, and because the astrometric parameters of Cir X-1 are not known, we cannot definitively identify the location of the binary system on the image. It is therefore uncertain whether the symmetric structure is due to approaching and receding ejecta of equal brightness, or whether we see only the brightness profile of the approaching jet that peaks well downstream of the core (as seen in the brightness profiles predicted by Hjellming & Johnston 1988). However, of the three explanations of Dhawan, Mirabel & Rodriguez (2000), we do not favour the fast jet and hidden counterjet scenarios. A highly-relativistic approaching jet would still need to be inclined close to the plane of the sky to be Doppler-deboosted close to the level of the receding jet, whereas the ultrarelativistic flow postulated by Fender et al. (2004) requires the jets to be within 5° of the line of sight. For free-free absorption to hide the counterjet, a dense equatorial disc wind would need to cause increased opacity out to several hundred AU from the binary system. The apparently symmetric motion in Figure 4.3 also tends to argue against this scenario. We therefore find the explanation of intrinsically slow jets to be most plausible. In that case, the jets are only mildly relativistic and inclined close to the plane of the sky. Thus there is minimal Doppler boosting, leading to the observed symmetry. From the extent of the jets and the time since the onset of the radio flare, we can attempt to verify this picture.

4.6.2 Jet speed

In chapter 3 (Moin et al. 2011) we showed that the compact radio emission from Cir X-1 is only present at and shortly after periastron passage. We can therefore assume that the observed jet was ejected close to orbital phase zero, and does not correspond to a steady, compact jet that persists throughout the orbit. According to the ephemeris of Nicolson (2007), orbital phase zero corresponds to the onset of the radio flare, and hence the latest time at which ejection could have taken place. We can use the predicted ejection date to constrain the apparent jet speed, assuming that the jet has reached the observed size of $\sim 20\,\mathrm{mas}$ in the $0.76\,\mathrm{d}$ between the predicted onset of the flare and the mid-time of our observing run (orbital phase 0.046). This gives a combined proper motion of approaching and receding jets of $\sim 26\,\mathrm{mas\,d^{-1}}$, similar to the value inferred from the difference imaging in Figure 4.3, and corresponding to an apparent combined speed of $1.2c\,(d/7.8\,\mathrm{kpc})$. While this constraint does not allow us to uniquely determine

the jet speed and inclination angle, for a given distance we can determine the jet speed as a function of inclination angle, as shown in Figure 4.4. Unless the inclination angle is extremely close to the line of sight, the intrinsic jet speed would appear to be only mildly relativistic.

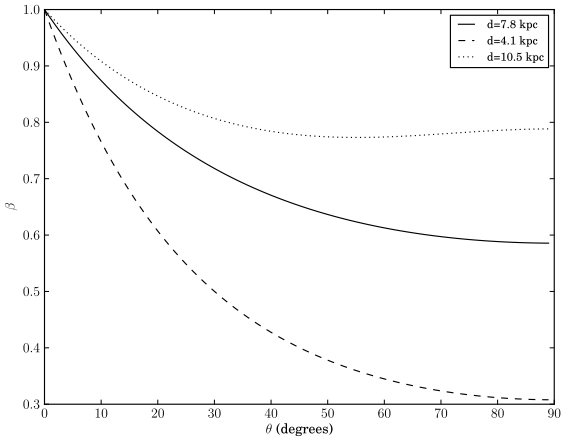

Figure 4.4: Cir X-1 jet speeds - Intrinsic jet speed as a function of inclination angle, given the proper motion constraint of $\mu_{\rm app} + \mu_{\rm rec} \approx 26\,{\rm mas\,d^{-1}}$. Curves are plotted for the assumed distance, as well as for the lower and upper bounds of the commonly accepted distance range for the source. Our proper motion constraint is compatible with a mildly relativistic jet velocity at any moderate inclination angle.

An ultrarelativistic flow with a proper motion of $400\,{\rm mas\,d^{-1}}$ would be smeared over 68 beams over the course of our 14.3 h observation. Unless the ejecta were intrinsically extremely bright ($> 112\,{\rm mJy}$), this would reduce the surface brightness below our 3σ detection threshold. However, accommodating this flow with the mildly-relativistic material assumed above to be responsible for the observed jets would require some form of spine-sheath structure, where the fast inner flow is surrounded by slower-moving material (e.g. Sol, Pelletier & Asseo 1989). Such a stratification is relatively well established for jets from active galactic nuclei (e.g. Laing 1996), and Meier (2003) offers some observational evidence for a two-flow structure in jets from stellar-mass compact objects, so this is certainly plausible. However, a spine-sheath jet would still require the jet to be oriented within 5° of the line of sight, to allow for the highly-relativistic motion observed by Fender et al. (2004). While reconciling this requirement with the

symmetric morphology discussed in Section 4.6.1 is difficult, the uncertainties in our interpretation are sufficient that we cannot definitively rule out this scenario.

4.6.3 Opening angle

The jets are not significantly resolved transverse to the jet axis. From the length of the jets and the beam size of $3.4 \times 2.9\,\mathrm{mas}^2$ in PA -69.1°, we find an upper limit on the opening angle of the jets of $< 18°$. This allows us to rule out poor collimation as an explanation for the half-opening angles of 35° found for the X-ray caps observed by Sell et al. (2010). The remaining options put forward by the authors are precessing jets or a jet axis aligned very close to the line of sight. The variation in the position angle of the extended radio emission (see Section 4.5) would seem to support the precession scenario, although the time sampling is currently too sparse to attempt to determine a precession period. However, we note that the standard deviation of the position angles (13°) is significantly smaller than the half-opening angle of the X-ray caps. To test the precession scenario, we would require multiple VLBI measurements of the position angle of the milliarcsecond-scale jets.

4.7 Summary

We have resolved the milliarcsecond-scale jets in Circinus X-1 for the first time. The jet morphology is symmetric, extended on a scale of $\sim 20\,\mathrm{mas}$ along a position angle 113° east of north, in good agreement with the position angle seen in ATCA observations of the arcsecond-scale jets. We do not resolve the jets along the minor axis, implying an opening angle of $< 18°$. The source brightness decayed over the course of the observing run, and we see marginal evidence for outward motion of the components between the first and second halves of the observation, implying a proper motion of $21\,\mathrm{mas\,d}^{-1}$. This is relatively consistent with the proper motion estimate derived assuming that the jets were launched at the onset of the radio flare at orbital phase zero, and implies a mildly relativistic jet. While the ultra-relativistic flow inferred by Fender et al. (2004) cannot be definitively ruled out, the symmetry of the observed jets would appear to cast further doubt on this scenario.

Chapter 5

Monitoring of Gamma-Ray Burst Afterglows At Radio Wavelengths

5.1 Introduction

Gamma-Ray Bursts (GRBs) are extremely energetic and short-lived transient events that can outshine the entire host galaxy for a brief period of time. A GRB is thought to be high-energy gamma-ray emission from very energetic relativistic particles which are propelled in an outflow from an astronomical system (Piran 2004). From the time when GRBs were first discovered by Vela satellites in 1967 (Klebesadel et al. 1973), a number of theories and models have been proposed to explain their observed characteristics and suggest their possible association with astronomical events such as: supernovae (Galama et al. 1998; Woosley & Bloom 2006); the merger of compact objects (Paczynski 1991; Narayan, Paczynski & Piran 1992); objects such as Comets (Mitrofanov 1990); X-ray binary systems (Livio & Waxman 2000; Chevalier & Li 1999); and pulsars (Usov 1992), but the true origin of GRBs is still not definitely known and the underlying processes are still only vaguely understood.

Since high energy emission from cosmic sources is absorbed by the Earth's atmosphere, GRBs are primarily detected by space-borne satellite observatories. Initially detected in gamma-rays, GRBs also exhibit longer-wavelength and longer-duration emission covering the entire electromagnetic spectrum from X-rays to radio waves. This electromagnetic radiation that follows a GRB event is called an "afterglow" (Waxman 1997a; Wijers, Rees, & Meszaros 1997; Frail et al. 2003; van der Horst, Wijers

& Rol 2005). The GRB afterglows in various wave bands typically persist for durations between 1 to 100 days. Ground-based telescopes and telescopes in Earth orbit take triggers to observe from the initial gamma-ray detections in an attempt to detect and monitor the GRB afterglows. The X-ray afterglows are detected and monitored by space-borne X-ray telescopes, while the optical, infrared and radio afterglows are monitored by ground-based telescopes.

In the past two decades, the launch of gamma-ray satellite observatories such as the Compton Gamma Ray Observatory (CGRO), having an all sky monitoring instrument called Burst And Transient Source Experiment (BATSE) onboard, helped astronomers detect and monitor GRB events with reasonable sensitivity and frequency and advanced the understanding of GRBs such as their origin, energetics, flux evolution characteristics etc (Piran 1992; Paczynski 1995; Briggs 1995). Another mission that played a key role in GRB science was the BeppoSAX satellite (Piro, Scarsi, & Butler 1995). Launched in 1997, it had an X-ray detector onboard, which for the first time detected the X-ray afterglow of a GRB (Costa et al. 1997). The X-ray detection of GRBs allowed accurate localisation ($<$ 5 arcsec) more quickly, enabling rapid response observations by instruments with small fields-of-view at other wavelengths. The X-ray spectroscopy also provided hints on the fact that GRBs are extragalactic and better localisations indicated that their distribution on the sky is isotropic (Paczynski 1991; Meegan et al. 1992).

The detection of the optical afterglow of GRB 970508 enabled astronomers to determine its redshift (z = 0.835) and allowed to definitively establish for the first time that GRBs lie at cosmological distances (Reichart 1998). The detection of the optical counterpart to a GRB is critical to study key properties of the explosion. The optical light-curve features a jet-break if the associated jet is in Earth's line of sight. The jet-break allows to compute the jet opening angle which in turn enables to estimate to true energy associated with the GRB event. The monitoring and study of the optical afterglow also allows to track the early evolution of the expanding shell. The redshift for the GRB can be estimated by optical spectroscopy, which helps to determine the distance and possibly establish a GRB's connection with its host galaxy.

The radio afterglow of a GRB remains for longest period of time due to the deceleration of the expanding ejecta that gives rise to the afterglow (Waxman 1997b). Unlike the X-ray or optical afterglow, the radio afterglow can be monitored over long periods,

allowing the study of different phases and transitions in the afterglow. Parameters such as the size, expansion rates and energetics of the emission region can be estimated, and models to explain the underlying emission mechanisms and the properties of the possible progenitor can be tested (Waxman 1997a; Chevalier & Li 1999; Bloom et al. 1999; Price et al. 2002; Berger et al. 2003; Toma et al. 2007 and many reference therein). Radio monitoring of GRB afterglows allow the study of their long-term evolution as a function of time and frequency (e.g. Frail et al. 1997; Waxman, Kulkarni & Frail 1998; Frail, Waxman & Kulkarni 2000).

Over the past 15 years, a large campaign to study GRB radio afterglows has been running in the Northern Hemisphere using the Very Large Array (VLA) in New Mexico, USA, and managed by a large collaboration between various astronomy institutes around the world (e.g. Kulkarni et al, 1998, Frail et al. 2000). There have been some Target-of-Opportunity (ToO) observations of southern GRBs conducted by the group in collaboration with astronomers at the ATNF in Australia, to complement the campaign in the Northern Hemisphere. Kulkarni et al. (1998) highlighted the connection between the southern GRB 980425 and SN1998bw, strengthening the GRB-Supernova association and Frail et al. (2003) produced a catalogue of GRB radio afterglows detected between 1997 and 2001. The ATCA observations of GRB 990510 provided plausible evidence for a jet associated with the GRB (Harrison et al. 1999) and Price et al. (2002) advocated a wind model for the GRB afterglow detected with ATCA observations of GRB 011121.

Long-term investigations of the GRB surroundings by observations to probe the afterglows have also provided support for the notion of collimated outflows associated with the GRBs (Sari, Piran & Halpern 1999; Panaitescu & Kumar 2002). Space-borne instruments such as Swift, Fermi, IPN etc., detect a GRB if the associated relativistic jet, having an opening angle θ_j, is beamed along Earth's line of sight (Harrison et al. 1999; Frail et al. 2001). As the relativistic blastwave sweeps the circumburst medium, the opening angle starts becoming larger as the collimated outflow loses its speed due to deceleration, resulting in the decline of observed flux density. Due to this beaming effect, it is possible that a number of GRBs that are not beamed along our line-of-sight or are off-axis, remain undetected. An all-sky survey radio instrument which keeps scanning the sky with multiple beams (e.g. ASKAP, Johnston et al. 2007) will potentially detect a number of such unbeamed GRBs afterglows at radio wavelengths.

Recently, the Swift (Barthelmy et al. 2005; Roming et al. 2005; Burrows et al. 2005 and many references therein) and Fermi (Atwood et al. 2009; Meegan et al. 2009) satellites have taken over from their predecessors and are equipped with much more sensitive and wide field-of-view instruments that enable the detection of a large number of interesting GRBs and their afterglows, increasing the detection rate to about 10–15 GRB events every month. These new missions are capable of determining GRB positions very accurately (< 2 arcsec) and can detect GRBs with very high energies. The positions and energetics of all the GRBs detected by space-borne missions are instantaneously disseminated via a web-based service called the GRB Coordination Network (GCN)[1]; the information is supplied in the form of short circulars. Follow-up observations of the GRB afterglows can then be immediately undertaken by ground-based telescopes in the optical, infrared and radio bands.

The ATCA observations of GRB afterglows before 2008 were mostly ToO observations carried out with ad hoc arrangements. The first dedicated and long-term Southern Hemisphere GRB afterglow detection and monitoring program was initiated as part of this PhD project, aiming for a systematic and coordinated long-term radio follow-up and to search for bright and particularly persistent GRB radio afterglows.

This chapter describes this Southern Hemisphere GRB radio afterglow detection and monitoring program, the primary goal of which was to search for peculiar GRB radio afterglow candidates that persist for longer periods of time, so that they could be observed and monitored continuously to study the behaviour of the radio afterglow in detail and to test afterglow models. The secondary objectives were to complement the Northern Hemisphere (EVLA) observation program, so as to cover the southern sky, build and maintain a record of observations of Southern Hemisphere GRBs for statistical purposes. As a result of this search, a persistent GRB afterglow associated with GRB 100418A was found. A comprehensive study of this GRB is presented in Chapter 6.

5.2 GRB Nomenclature and Types

Every GRB that is detected by a space-borne gamma-ray telescope is named as three letters 'G R B' followed by a 6-digit number that represents the year, month and day

[1] http://gcn.gsfc.nasa.gov

of detection in two digits each. That is, a GRB detected on February 1st, 2011 will be denoted as GRB 110201. If there is more than one detection on the same day, a suffix of the alphabet a, b, c.....z is added to the GRB name. In case of three GRB detections on February 1st, 2011, the GRBs will be named GRB 110201a, GRB 110201b and GRB 110201c.

GRB events can be subdivided into two distinct types, based on the duration of the burst. The events that last for more than 2 seconds are referred to as long-duration GRBs while those lasting less than 2 seconds are called short-duration GRBs. A GRB can last anywhere between a few milliseconds to a few minutes but the typical duration ranges from 1-100 seconds. The detection rate of long duration GRBs is much higher than that of short duration GRBs due to the rarity of short GRBs. While most of the theoretical explanations and observational interpretations predominantly address the long-duration GRBs, the mechanisms related to the short-duration GRBs are much less well understood (Barthelmy et al. 2005; Dermer & Atoyan 2006).

5.3 GRB Theory

Since the time GRBs were accidentally discovered, a variety of theories have been advanced to explain the possible GRB progenitors and the physical processes associated with the GRBs and their afterglows. Some early work on the origin of GRBs had established that GRBs are produced at cosmological distances (Paczynski 1986; Goodman 1986) and this notion formed the basis of most of the models that accounted for the energy levels, duration and intensities that were observed. Discussed below are the primary plausible theories and models attempting to answer key questions related to GRBs.

5.3.1 Merging Compact Objects

Due to their extraordinary nature, GRBs have always been associated with extreme events that involve the release of enormous amounts of energy. One such scenario is the merger of compact objects (Piran 2004).

When massive stars reach the end of their lives, they undergo a collapse into very small, dense and gravitationally powerful objects. As a result of this collapse, a star can become either a neutron star or a black hole (Shapiro & Teukolsky 1983).

5. MONITORING OF GAMMA-RAY BURST AFTERGLOWS AT RADIO WAVELENGTHS

Stellar compact objects often exist as part of a gravitationally bound binary system in which they are in orbit with another star (Lamb, Pethick & Pines 1973; McClintock & Remillard 2003). The interaction of the compact object with its companion results in strong X-ray emission, thus the binary systems are commonly called "X-ray binaries".

Neutron star or black hole X-ray binary systems can ultimately end up in a merger scenario, in which the companion star eventually explodes into a supernova, leaving behind either a neutron star or a black hole. In the case of a neutron star X-ray binary, what is left after the supernova explosion is a neutron star-neutron star (NS-NS), a neutron star-black hole (NS-BH) or possibly a neutron star-white dwarf (NS-WD) binary system. It is suggested that the radiation of gravitational waves from the binary system eventually leads to orbital decay that after a certain time brings the two objects so close together that they merge, with an enormous energy release. The conditions of the merger scenario i.e. very high energy release in a very short period of time from a region of small radius, leads to the inference that this event might be associated with a GRB (Paczynski 1986; Narayan, Piran & Shemi 1991; Paczynski 1991; Narayan, Paczynski & Piran 1992; Woosley 1993; Fryer et al. 1999 and many references therein).

Recently, a number of observational and analytical studies have led to clues supporting the hypotheses that associate the merger of compact objects with short-duration GRBs ($<$ 2 seconds) (Petrillo & Dietz 2012; Troja, Rosswog & Gehrels 2010; Lazzati & Perna 2009; Troja et al. 2008; Belczynski et al. 2005 and many references therein). The direct observational evidence for the orbital decay in pulsars due to the gravitational radiation damping (e.g. Taylor & Weisberg 1989), the discovery of NS-NS radio pulsars and the astrophysical processes associated with the merger of compact objects makes it the most plausible scenario for short GRBs. The merger model advanced to explain the short-hard GRBs proposes that when two compact objects in a tight binary orbit reach the stage of merging, thermal energy of order $\sim 10^{52}$ ergs is released in the form of neutrinos and antineutrinos which is then converted into electromagnetic energy (Goodman, Dar & Nussinov 1987; Eichler et al. 1989). This enormous amount of energy is released in $\sim$1 ms from a region having a radius $\sim$100 km then triggers what is observed as a short GRB. Narayan, Paczynski & Piran (1992) proposed another mechanism involving magnetic flares to explain the GRBs with more complex profiles. This model states that the post-merger magnetic fields reaching $\sim 10^{16}$ G achieves equipartition with the rotation. The magnetic fields then float above the disk and the major

reconnection events (magnetic flares) in the magnetic fields produce burst of energetic photons observed as a GRB. (For details: Paczynski 1986; Goodman 1986; Shemi & Piran 1990; Paczynski 1990).

Further to this, population synthesis studies have also been carried out to test the merger scenario-short GRB connection (e.g. Portegies Zwart & Yungelson 1998; Bloom et al. 1999; Belczynski et al. 2002c). For instance, Belczynski et al. (2006) employed population synthesis techniques to determine the formation and merger rates, merger times and merger locations (types of galaxies and region) for NS-NS and NS-BH binaries. Based on these calculations, the likelihood of the association of short-duration GRBs with compact object merger has been emphasized. Relating the results with the Swift detections and the identification of short-duration GRBs with their host galaxies by optical follow-up, it was shown that the identification of a number of short-duration GRBs with their respective host galaxies is in agreement with the outcome of the population synthesis studies presenting the redshift distribution, likely merger location, merger times, which is indicative of the fact that NS-NS and/or NS-BH mergers are the progenitors of short-duration GRBs.

Fryer et al. (1999) discussed the interesting scenario of a black hole-white dwarf merger. The massive star in the system undergoes a supernova explosion and turns into a neutron star in the first stage. While the companion starts to expand to a red giant, the neutron star starts to accrete very rapidly and collapses to become a black hole. The secondary star, which is now a red giant, eventually turns into a white dwarf. After becoming a BH-WD binary, this system could produce a GRB. With its extreme gravitational potential, the black hole starts to accrete from the white dwarf, which eventually transforms into an accretion disc around the black hole. This process involves release of a large amount of energy, which could potentially power a GRB. The comparatively lower energy (10^{48} - 10^{51} ergs) produced by the proposed BH-WD binary GRB suggests that the description better suits the long duration GRBs. Figure 5.1 is a representation of the merger scenario.

5.3.2 Pulsar Model

Another model with a neutron star as the central engine proposes that highly magnetised rapidly rotating neutron stars, or *pulsars*, can also be progenitors of GRBs (Usov 1992; Dai & Lu 1998). The initial conditions for this scenario involve a white

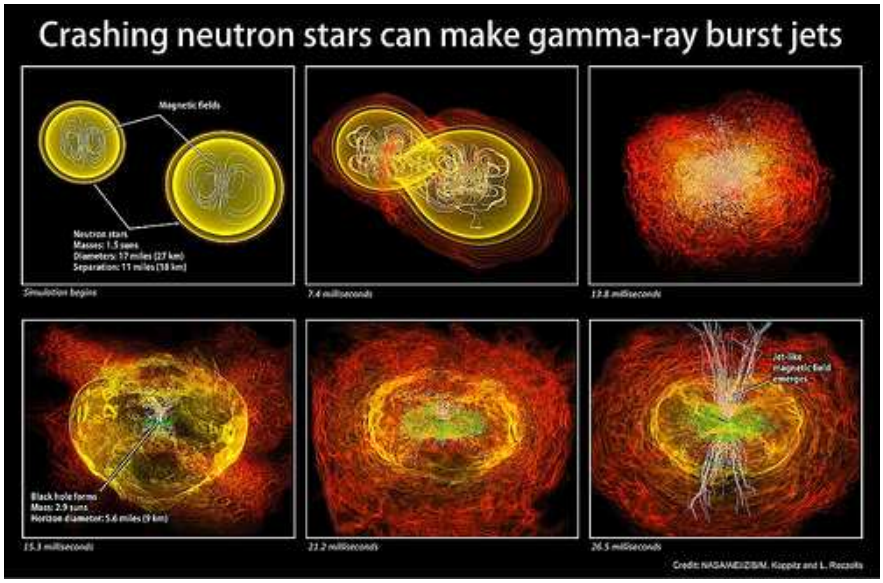

Figure 5.1: Neutron star merger - Representation of a neutron star merger - Credit: NASA/AEI/ZIB/M. Koppitz and L. Rezzolla.

dwarf in a binary system accreting matter from its companion. Once the white dwarf mass reaches the Chandrasekhar limit (Chandrasekhar 1935) it collapses to a neutron star of radius less than the white dwarf (Shapiro & Teukolsky 1983; Woosley & Baron 1992; Usov 1992). With exceptionally strong magnetic fields and high angular velocity (Friedman 1983; Manchester et al. 1981), the neutron star produced as a result of the collapse of white dwarf in a closed binary becomes a pulsar. The rotational kinetic energy produced by the pulsar is sufficiently high to explain the energy estimates of observed GRBs. The rotating magnetic fields of the pulsar produces strong electric fields, which accelerate particles from the surrounding plasma to relativistic energies. These accelerated particles then produce gamma-ray radiation which could take the form of a GRB. Figure 5.2 is a representation of a pulsar.

Dai & Lu (1998) and Zhang & Meszaros (2001) have also invoked a model in which they propose a highly magnetized pulsar or magnetar as the central engine for a GRB. They also argue that such a progenitor can also provide sufficient energy to refresh the forward shock (Zhang et al. 2006) via an "energy injection mechanism". This energy injection manifests as peculiar variations in the light curves of the GRB afterglow. This model will be further discussed in Chapter 6 in the context of a study of GRB 100418A.

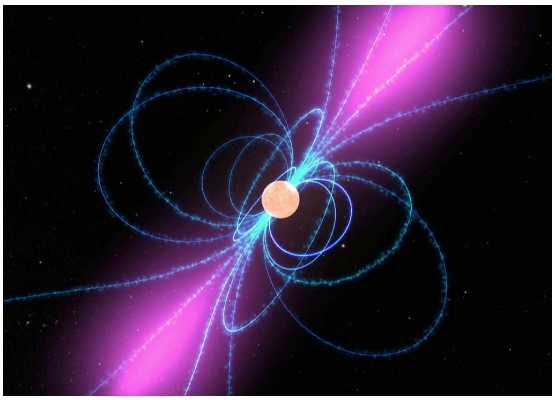

Figure 5.2: A Pulsar - Representation of a pulsar as a GRB progenitor - The blue lines show the magnetic field lines of a pulsar and the beamed electromagnetic radiation is indicated as the purple shading. Credit: Fermi Group/NASA.

5.3.3 Black Hole Accretion

The black-hole accretion model for GRBs bears similarities with the merger models in a sense that it involves an accretion disc. However, it is primarily based on the concept of a "failed" supernova rather than merger of compact objects (Woosley 1993). This model was further refined and developed into the "collapsar model" which will be discussed in section 5.3.4. As a possible GRB scenario, Woosley (1993) has discussed the collapse of a massive star in the "Wolf-Rayet" phase, in which the star starts to lose its mass at a very high rate and its stellar life comes to an end with a supernova explosion (e.g. Filippenko & Sargent 1986). When the core of a Wolf-Rayet star collapses, material accretes around it to form an accretion disc and the star explodes in a *Type Ib* supernova (e.g. Ensman & Woosley 1988; Heger et al. 2003). The compact object with matter accreting on it first transforms into a neutron star and when it has sufficient mass, it collapses to a black hole. Woosley (1993) suggested that the collapse of a massive Wolf-Rayet star to a black hole could produce a GRB when the accretion disc forces a particle flow along the rotation axis. Given the timescale of the whole process, the explanation seems more plausible for long duration GRBs. Figure 5.3 depicts the accreting black hole as a possible progenitor of a GRB.

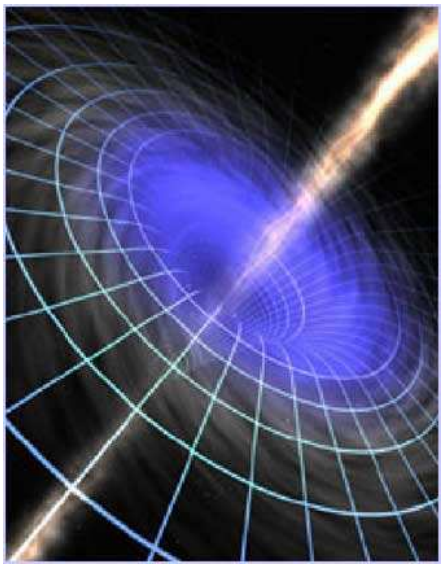

Figure 5.3: Black hole with accretion disc - Representation of a black hole surrounded by an accretion disc as a possible scenario for GRB. The picture shows that relativistic particles are beamed along the rotation axis of an accretion disc formed when a massive star collapses. This energetic outburst could be what manifests itself as a GRB. Credit: NASA.

5.3.4 The Collapsar Model: GRB-Supernova connection

The collapsar model is essentially an extension of the previous models which proposes the core collapse of a massive star producing a supernova and eventually turning into a black hole as the most likely progenitor of a GRB (Woosley 1996; MacFadyen, Woosley & Heger 2001; Woosley & Bloom 2006). The event that strengthened the GRB-supernova connection was GRB 980425, which was found to be associated with an unusually bright supernova SN1998bw (Galama et al. 1998, Kouveliotou et al., 2004, Kulkarni et al., 1998). In this case, the GRB event and supernova occurred at the same time and same location and spectroscopic studies of the GRB provided strong evidence of the link between the supernova and the GRB (Christensen et al. 2008). Developed and proposed in the late 1990s, the collapsar model involves the core collapse of a star in its Wolf-Rayet stage to a neutron star and then the production of a black hole by the collapse of the neutron star (Woosley 1993).

The collapse of the central core launches a shock wave that is powered by the energy radiated by the neutron star, formed as a result of the core collapse in the first

instance. The shock interacts with, and pushes, the outer layers of the star outwards into the circumstellar medium to produce a shell of material (e.g. Woosley & Weaver 1986; Bethe 1990; Woosley, Heger & Weaver 2002). The collapsar model predicts the formation of an accretion disc around the black hole which is produced after the collapse of the neutron star (MacFadyen & Woosley 1999). The mechanism by which the energy associated with the rotation of the black hole or the accretion disc is converted to gamma-ray emission is still not well established but there are suggestions supported by observations that it could be the neutrinos that produce electron-positron pairs and accelerate the particles, launching relativistic outflows or jets that manifest themselves as the GRB (Woosley 1993, Sari, Piran & Halpern 1999; Narayan, Piran & Kumar 2001). Other possibilities are magnetic instabilities in the accretion disc (McKinney 2006, Proga et al. 2003) and the magnetohydrodynamic (MHD) extraction of rotational energy from the black hole (Takahashi et al. 1990; Meszaros, Rees & Wijers 1999), but the energy budget has made the neutrino-based explanation more plausible.

Even after years of theoretical and observational work, none of the proposed GRB models can fully and satisfactorily explain the range of phenomena seen in gamma-ray bursts. The models succeed in partly explaining the mechanisms and help constrain the observational characteristics of the GRBs, but they remain a mystery. Because of their short duration, it has only been possible to study the "afterglow" of the GRB event with some detail at different frequencies. Light curves of the X-ray, optical and radio afterglows have helped astronomers understand to a certain extent the post-burst events, i.e. the production of the "forward shocks" that produce the afterglow, the evolution of the afterglow with time, the energetics involved in the movement of the ejecta, and some characteristics of the emitting region (Frail et al. 1997; Waxman 1997; Panaitescu, Meszaros & Rees 1998; Zhang et al. 2006; Greiner et al. 2009). Due to the extreme nature of GRBs, it has not been possible so far to clearly establish the type of the progenitor of the GRB. The high-energy and short duration gamma-ray light curve of a GRB doesn't reveal much about the true nature of the GRB progenitor. There still are a number of aspects such as the true geometry of the outflow, the transition from prompt gamma-ray emission to X-ray and lower frequency emission, peculiar variations in the multi-frequency light curves, and the cause of a range of durations of the radio afterglow which are yet to be clearly understood. Even the afterglow observations suffer from poor sampling which makes the light curve discontinuous and difficult to establish

the variation in the emission as a function of time. Figure 5.4 is an artist's impression of a supernova explosion producing a beam of gamma-rays.

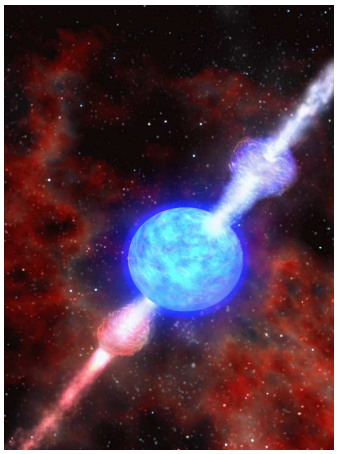

Figure 5.4: The GRB-Supernova connection - Representation of a star exploding into a supernova possibly powering a GRB event. The core collapse of a massive star produces a shock that interacts with outer layers of the exploded star launching a relativistic outflow for which there is some evidence that it is collimated. These beamed jets holds enormous amount of energy resulting in a GRB event - Credit: NRAO.

Recent advances such as the strengthening of the GRB-supernova connection, accurate localisation, support for afterglow models with observations in the case of some GRBs, and multi-wavelength studies of the afterglows of the GRBs have provided improved understanding of some GRBs, but has also made clear that the GRB events can be associated with different types of objects and different astrophysical processes.

5.3.5 GRB afterglow: The fireball model

A GRB event typically lasts only for about 100 seconds. The only way to probe the environment of the GRB and to study the object in the longer-term is to observe and monitor the GRB remnant (afterglow) at longer wavelengths. The GRB afterglow is the delayed counterpart emission following the prompt emission, which is observed in the X-ray, optical and radio bands (Meszaros 1995, Meszaros & Rees 1997; Paczynski & Rhoads 1993). According to the standard core-collapse model, once the progenitor star has undergone the last stages of its evolution, the dense plasma of relativistic material expands outwards and accelerates to relativistic velocities creating a "fireball". As the fireball expands, it cools and produces relativistic forward shocks that sweep up

the surrounding medium (Waxman 1997; Kulkarni et al. 1998; Yost et al. 2003). The shocks interact with the circumburst medium and accelerate relativistic electrons, which then emit the delayed radiation that, unlike the GRB itself, persists on a time scale of days to months. As the fireball expands, the peak of emission shifts to lower frequencies. The GRB afterglow can be detected in X-rays even before the burst comes to an end and, as the fireball expands, the relativistic electrons emit at optical wavelengths. Eventually the counterpart of the X-ray/optical afterglow can be detected at radio frequencies.

There is some evidence that the expanding shell proposed in the fireball model for a GRB is in fact a collimated jet (Frail et al. 2001; Cenko et al. 2010) which appears no different from a spherical expansion when the observer is along the direction of the jet axis (Piran 1995). However, in some cases, light curves from GRB afterglows have shown a peculiar early-time steepening, which points towards a jet-like outflow (Harrison et al. 1999). Evidence for a jet-like behaviour can also be observed if the relativistic ejecta start to expand sideways from the emitting cone of the fireball (Waxman 1997) and a "jet break" is observed in the light curve of the afterglow (Bloom, Frail & Kulkarni 2003; Rhoads 1997, 1999; Meszaros & Rees 1997; Chandra et al. 2010).

The detection and monitoring of GRB afterglows allows astronomers to localise the GRBs more accurately, identify them with their respective host galaxies by determining spectroscopic redshifts, and associate the GRBs with astronomical events such as supernovae (Waxman 1997; Galama et al 1998, Kulkarni et al. 1998, Frail et al. 2003). The radio afterglow of a GRB is of special significance as it is possible to monitor a radio afterglow for a longer period of time (days, months) and it allows estimates of the size, energetics associated with the GRB and some properties of the circumburst environment as well. In the case of the detection of a nearby GRB, it should be possible to observe the afterglow using VLBI, which holds the potential to directly measure the morphology of the source (Taylor et al. 2004; Pihlstrom 2007). Most of the GRB break-throughs over the past 15 years were possible because of the detection of unusual GRBs with exceptionally persistent radio afterglows (more than a year for some).

5.4 Radio studies of GRB afterglows

GRB afterglow research in the radio band greatly benefits from long-term programs to systematically observe GRBs as quickly after the burst as possible in an attempt to detect and monitor the radio afterglow right from the earliest times. Early-time observations will allow us to infer the connection between the prompt emission and the afterglow, which in turn would help understand the transitions and physical processes associated with the GRB under investigation. Following initial detection, there must be frequent observations to have a good sampling of the afterglow as it evolves with time. The observations should cover the entire period of the afterglow evolution in order to closely study the processes that manifest themselves as the variations in the afterglow light curve.

The aforementioned approach can be executed in response to a search program which continuously looks for GRBs with persistent afterglows, providing an opportunity for long-term monitoring. The GRB detection and monitoring program carried out as part of this PhD project was aimed at achieving this. The program ran for approximately two and a half years, 52 GRBs were observed, four were detected and a single GRB stood out as an exceptional source to study further. The next chapter describes the study of this GRB, GRB 100418A.

This program was an attempt to carry out a systematic observational program to study GRB radio afterglows in the Southern Hemisphere. Since the advent of sophisticated Gamma-ray/X-ray satellites such as Swift and Fermi, the GRB detection rate has climbed to almost a GRB every second day. But not all the GRBs provide the opportunity for long-term radio observation programs, as the radio afterglow of a GRB often fades away in a matter of days and, for a sizeable population of GRBs, the radio afterglow is not detected at all.

This GRB program was primarily aimed at searching for one or more such GRBs for which the radio afterglow could be studied over an extended period of time. The ultimate objective was to test afterglow models, such as the "energy injection model", that attempt to explain the variations in the afterglow light curves. In fact, it is not possible to single out GRBs for detailed studies unless there are long-term monitoring programs. Thus the GRB program carried out as part of this PhD project was crucial in the search for a GRB with radio afterglow stretched reasonably in time so as to

be able to sample the trends and transitions providing useful inferences regarding the associated physical processes.

In time, large all-sky surveys with instruments such as ASKAP (Johnston et al. 2007), having a very large field-of-view, will provide the next step in radio studies of GRB afterglows. Most likely, such a survey will detect many GRB afterglows and provide an opportunity for monitoring with high time resolution, which will enable us to follow the orphan afterglow as it evolves. ASKAP will also hold the potential to detect unbeamed GRB afterglows and that may be very important to understand beaming angles.

5.5 GRB Observations

As part of the GRB work carried out within the scope of this PhD project, four proposals were submitted to conduct GRB observations. Out of the four, three proposals were submitted to the ATNF to observe samples of GRBs with the ATCA and the LBA, and one proposal was submitted to the National Radio Astronomy Observatory (NRAO) to conduct VLBI observations of a strong GRB afterglow using the Very Long Baseline Array (VLBA) in the US. The proposals were successful and a total of approximately 450 hours of telescope time were granted over the course of the PhD project. Following is the list of proposals:

- C1802: A southern sky survey to detect and monitor radio afterglows associated with recently detected gamma-ray bursts (GRBs) - ATCA [A. Moin, S. J. Tingay, C. J. Phillips, G. B. Taylor, M. Wieringa, R. Martin]

- C2147: Extreme Gamma-ray bursts (GRBs): constraining energetics and probing central engines - ATCA [A. Moin, D. A. Frail, J-P. Macquart, S. J. Tingay]

- V270: e-VLBI follow-up observations of GRB radio afterglows detected with the ATCA - LBA [A. Moin, S. J. Tingay, C. J. Phillips, G. B. Taylor, M. Wieringa, R. Martin]

- BM347: High Resolution Monitoring of GRB 100418a - VLBA [A. Moin, P. Chandra, S. J. Tingay, D. A. Frail, G. B. Taylor, M. Wieringa, C. J. Phillips]

5.5.1 ATCA Observations

C1802 was the first long-term systematic and coordinated Southern Hemisphere GRB observation and monitoring campaign that ran for about two and a half years as part of this PhD project. This program was aimed to take advantage of the emergence of more sensitive and sophisticated space-based instruments such as SWIFT and Fermi developed to detect Gamma-ray bursts. The observations spanned over five ATCA semesters and the GRBs were observed at the frequencies of 4.8 and 8.4 GHz with a bandwidth of 128 MHz in the pre-CABB era and 5.5 and 9.0 GHz for the observation sessions conducted after CABB came online, with a 16-times higher bandwidth of 2.048 GHz (Chapter 2). C1802 was one of the first projects to utilise the capabilities of CABB. A total of 52 GRBs were observed under this program and radio afterglows associated with four GRBs were clearly detected.

For each C1802 observation session, a sample of 5-6 GRBs was selected from the announcements of GRB Coordinates Network (GCN) Circulars based on a pre-established selection criteria as described below. Table 5.1 lists all of the GRBs observed under C1802. The first column lists the GCN circular numbers for all the GRB and the second column contains the full GRB names. The third column shows the duration of each GRB and the fourth gives the gamma-ray "fluence" (erg cm^{-2}). The fifth column lists which bands the GRB afterglow was detected in, with X = X-rays, O = Optical and R = Radio.

The parameters that formed the selection criteria were the fluence of the GRBs, detection of counterparts in X-ray and/or optical, X-ray flux and the position. GRBs meeting the following criteria were included in the samples to be observed with ATCA.

- Gamma-ray fluence $\geq 10^{-7}$ erg cm^{-2};
- X-ray and/or optical counterpart detection;
- X-ray flux $\geq 10^{-13}$ erg cm^{-2} s^{-1};
- Declination $\leq$ -30° South (with a few exceptions);
- Swift X-ray position accurate within 2 arcseconds.

During each C1802 session, 5-6 GRBs were observed, interleaved with strong nearby phase-reference calibrators and PKS 1934-638 was observed as the primary flux calibrator. The observations were carried out at the frequencies of 4.8 and 8.4 GHz in the pre-CABB era and at 5.5 and 9.0 GHz after CABB came online and the 2.048 GHz CABB bandwidth gave a sensitivity of about 0.01 mJy/beam. Each GRB was observed for about three hours on average. The data were correlated in the standard continuum mode and full Stokes parameters were recorded.

The correlated ATCA data were transferred to a storage location at Curtin University and were then reduced and calibrated using the ATCA data processing software package MIRIAD (Sault, Teuben & Wright 1995). The multi-source uv data files were loaded in MIRIAD using the task ATLOD and split into individual sources using UVSPLIT. The task UVSPEC was used to examine the data and look for any RFI and contaminated channels were flagged using the task UVFLAG. Standard calibration procedures were then employed to calibrate the phases and amplitudes for each dataset. Task MFCAL was used to determine the calibration corrections (antenna gains, delays etc.) and solutions for gains and polarisations were obtained using the task GPCAL. The flux scale for the phase-reference calibrators was then set using the task GPBOOT with PKS 1934-638 and the calibration solutions were copied to the target datasets using the task GPCOPY. The calibration corrections were finally applied to the GRB datasets using the task UVAVER and FITS files were then written out using the task FITS. The FITS data files were then imported in DIFMAP (Shepherd, Pearson & Taylor 1994) for final imaging and model-fitting.

The calibrated FITS files were loaded in DIFMAP using the *observe* command and the visibilities were examined using the tasks *radplot* and *projplot*. They were then inverted to produce a dirty image using the task *mapplot*. Map sizes for most of the images were set to 512 $\times$ 512 using the command *mapsize*. In order to apply the deconvolution operation on the dirty image, the CLEAN algorithm was utilised by running the command *clean* and the final CLEANed image was produced by running *mapplot cln*. The final image allowed us to determine if the afterglow was detected or undetected and the information on flux density/upper limits and rms noise were also obtained from the final image.

At the end of the GRB afterglow detection and monitoring program, there were four GRBs detected out of the 52 observed. The following GRBs were detected:

- GRB 091026 (Peak brightness: 1.72 ± 0.07 mJy/beam @ 5.5 GHz and 0.69 ± 0.20 mJy/beam @ 9.0 GHz (3σ));
- GRB 100418a (Peak brightness: 0.86 ± 0.12 mJy/beam @ 5.5 GHz and 1.39 ± 0.22 mJy/beam @ 9.0 GHz (3σ));
- GRB 100621a (Peak brightness: 0.82 ± 0.10 mJy/beam @ 5.5 GHz and 1.61 ± 0.18 mJy/beam @ 9.0 GHz (3σ));
- GRB 100702a (Peak brightness: 1.22 ± 0.09 mJy/beam @ 5.5 GHz and 0.72 ± 0.15 mJy/beam @ 9.0 GHz (3σ)).

  Figures 5.5 to Figure 5.12 are the radio images of the GRB afterglows detected with the ATCA as part of the detection and monitoring program.

Out of these four GRBs, only GRB 100418A was detected at multiple epochs and was the only GRB to have a radio afterglow spanning months. The X-ray and optical observations of this GRB revealed that it was unusual. Ultimately, GRB 100418A stood out as the most interesting object observed in the GRB detection and monitoring program. Thus, a detailed study was initiated. The work on GRB 100418A is the subject of Chapter 6.

Table 5.1: Gamma-Ray Bursts observed with ATCA under the scope of Southern Hemisphere GRB detection and monitoring program (C1802). In this table, T is the duration of the prompt emission and F is the gamma-ray fluence. The column "Det." lists the bands in which the GRB afterglow was detected with X = X-rays, O = Optical, R = Radio. ΔT is the time difference between the prompt emission and ATCA observation. S_1 and S_2 are the radio flux densities in case of detections and upper limits (3σ) in case of non-detections at 4.8 and 8.4 (Pre-CABB), 5.5 and 9.0 GHz (post-CABB)

GRB	**T (s)**	**F** (erg/cm^2)	**Det.**	**ΔT (hrs)**	S_1 **(mJy)**	S_2 **(mJy)**	**Observation**
080130	22	7.70×10^{-7}	XO	240	< 0.90	< 1.11	Non-CABB
080218B	12	5.10×10^{-7}	X	260	< 0.75	< 0.80	Non-CABB
080229A	60	9.00×10^{-6}	XR	380	< 0.62	< 0.71	Non-CABB
080229B	100	4.30×10^{-6}	X	400	< 0.73	< 0.56	Non-CABB
080303	30	6.60×10^{-7}	XO	410	< 0.63	< 0.76	Non-CABB
080411	70	2.64×10^{-5}	XO	450	< 0.83	< 1.20	Non-CABB
080916C	10	1.90×10^{-4}	XO	760	< 1.12	< 1.34	Non-CABB
081008	100	4.30×10^{-6}	XO	890	< 0.76	< 0.89	Non-CABB

Continued on next page

Table 5.1 – continued from previous page

GRB	T (s)	F (erg/cm^2)	Det.	ΔT	S_1 (mJy)	S_2 (mJy)	Observation
081029	60	2.10×10^{-6}	XO	215	< 0.58	< 0.43	Non-CABB
081104	30	2.00×10^{-6}	XO	450	< 0.97	< 1.3	Non-CABB
081109	40	3.60×10^{-6}	XO	650	< 0.87	< 0.75	Non-CABB
081118	20	1.20×10^{-6}	XO	650	< 0.90	< 0.95	Non-CABB
090117	10	2.70×10^{-7}	XO	860	< 0.98	< 1.18	Non-CABB
090509	40	8.40×10^{-6}	O	70	< 1.38	< 1.40	Non-CABB
090625B	35	1.50×10^{-6}	X	120	< 0.78	<0.96	Non-CABB
090628	20	7.00×10^{-7}	X	310	< 0.30	< 0.44	Non-CABB
090904B	60	2.44×10^{-5}	X	500	< 0.74	< 0.77	Non-CABB
090926A	26	2.47×10^{-4}	XO	100	< 0.15	< 0.20	CABB
091010	62	1.09×10^{-5}	XO	125	< 0.23	< 0.22	CABB
091018	10	1.40×10^{-6}	XO	630	< 0.36	< 0.32	CABB
091026	20	1.80×10^{-6}	XR	120	1.72±0.07	0.69±0.20	CABB
091029	50	2.40×10^{-6}	XO	1200	< 0.42	< 0.53	CABB
091031	35	2.05×10^{-5}	X	1600	< 0.18	< 0.22	CABB
091109A	25	1.60×10^{-6}	XO	250	< 0.24	< 0.36	CABB
091109B	0.4		XO	370	< 0.39	< 0.48	CABB
091117	0.52	3.50×10^{-7}	XO	230	<0.15	< 0.18	CABB
091127	10	9.00×10^{-6}	XO	400	< 0.15	< 0.20	CABB
091230	120	4.00×10^{-6}	X	540	<0.28	< 0.36	CABB
100103A	40	3.00×10^{-5}	X	320	< 0.49	< 0.56	CABB
100117A	0.4	9.30×10^{-8}	XO	200	<0.60	< 0.66	CABB
100119A	25	1.40×10^{-5}	X	350	< 0.56	< 0.48	CABB
100219A	18	3.70×10^{-7}	XO	90	< 0.33	< 0.34	CABB
100218A	31	2.58×10^{-6}	XO	110	< 0.21	< 0.26	CABB
100225A	13	7.60×10^{-6}		80	< 0.37	< 0.36	CABB
100224B	77	1.08×10^{-5}		85	< 0.40	< 0.58	CABB
100316D	100	3.00×10^{-7}	XO	170	< 0.22	< 0.32	CABB
100418A	4	3.40×10^{-7}	XOR	48	0.86±0.12	1.39±0.22	CABB
100423A	100	8.50×10^{-6}	XO	240	< 0.22	< 0.20	CABB
100423B	21	1.22×10^{-5}		720	< 0.36	< 0.27	CABB
100424A	104	1.50×10^{-6}	X	160	< 0.48	< 0.46	CABB
100425A	14	4.70×10^{-7}	XO	180	< 0.68	< 0.70	CABB
100526B	30	4.70×10^{-7}	X	100	< 0.42	< 0.56	CABB
100606A	30	6.40×10^{-6}	X	390	< 0.32	< 0.34	CABB
100615A	60	5.00×10^{-6}	X	340	< 0.28	< 0.35	CABB
100619A	120	4.50×10^{-6}	X	280	< 0.29	< 0.38	CABB
100621A	100	2.10×10^{-5}	XOR	72	0.82±0.10	1.61±0.18	CABB
100625A	0.4	2.30×10^{-7}	X	100	< 0.15	< 0.18	CABB
100628A	0.1	2.50×10^{-8}	X	96	< 0.18	< 0.20	CABB

Continued on next page

Table 5.1 – continued from previous page

GRB	T (s)	F (erg/cm^2)	Det.	ΔT	S_1 (mJy)	S_2 (mJy)	Observation
100702A	0.3	1.20×10^{-7}	XOR	150	1.22±0.09	0.72±0.15	CABB
100701B	28	2.86×10^{-5}	X	160	< 0.22	< 0.33	CABB
100704A	30	6.00×10^{-6}	X	160	< 0.60	< 0.54	CABB
100707A	82	8.77×10^{-5}	XR	180	< 0.36	< 0.28	CABB

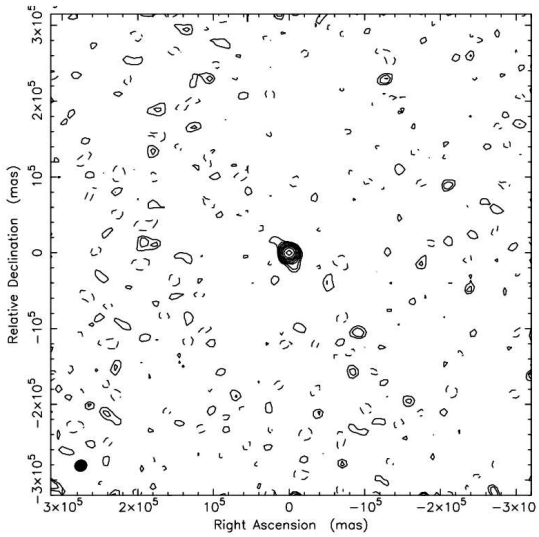

Figure 5.5: GRB 091026 image at 5.5 GHz on October 31, 2009 - Contour levels: -5 5 7.07 9.99 14.13 19.98 28.26 39.96 56.50 79.90 % of peak intensity; Peak brightness: 1.72 ± 0.07 mJy/beam (3σ); Beam size: 8.23 × 7.34 arcsec.

5.5.2 VLBI Observations

As follow-up to the GRB afterglow detection and monitoring program, VLBI observations of two afterglows were carried out. GRB 100621a and GRB 100418a were first detected in the radio band with the ATCA and found to be bright enough to trigger VLBI observations. GRB 100621a was observed with the Australian LBA while GRB 100418a was observed with the VLBA.

The VLBI observations of GRB 100621a were carried out with a single ATCA-Mopra baseline at a frequency of 8.4 GHz by triggering the V270 proposal, to see if the source was detectable. The idea was to bring more telescopes into the array if the

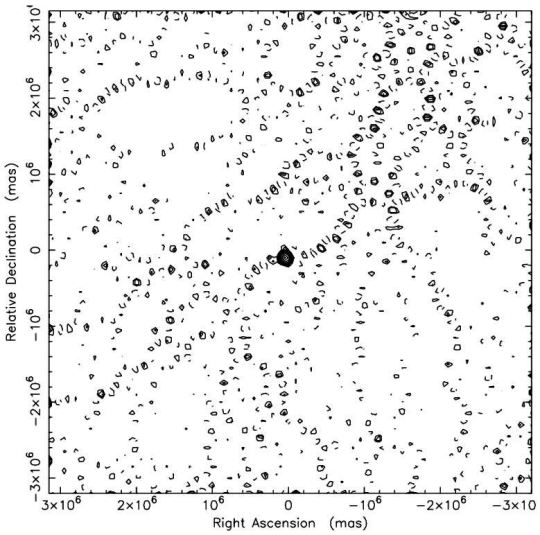

Figure 5.6: GRB 091026 image at 9.0 GHz on October 31, 2009 - Contour levels: -5 5 7.07 9.99 14.13 19.98 28.26 39.96 56.50 79.90 % of peak intenity; Peak brightness: 0.69 ± 0.20 mJy/beam (3σ); Beam size: 1.14 × 1.07 arcsec.

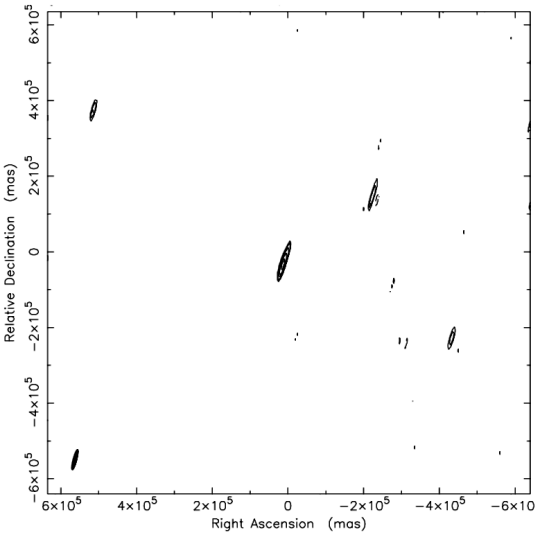

Figure 5.7: GRB 100418a image at 5.5 GHz on April 20, 2010 - Contour levels: -10 10 14.14 19.99 28.27 39.97 56.52 79.92; % of peak intensity; Peak brightness: 0.86 ± 0.12 mJy/beam (3σ); Beam size: 5.53 × 9.82 arcsec.

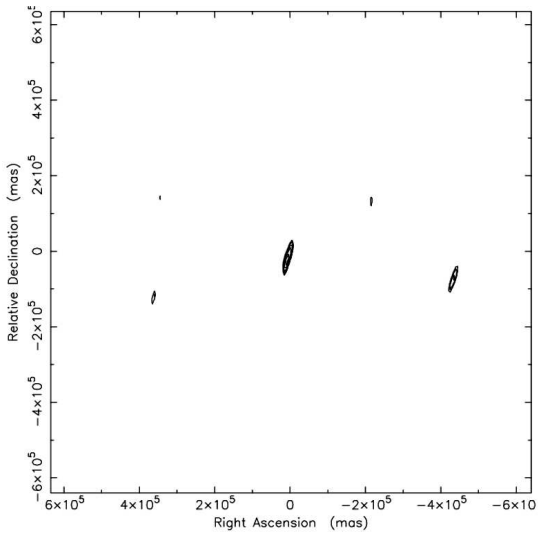

Figure 5.8: GRB 100418a image at 9.0 GHz on April 20, 2010 - Contour levels: -10 10 14.14 19.99 28.27 39.97 56.52 79.92 % of peak intensity; Peak brightness: 1.39 ± 0.22 mJy/beam (3σ); Beam size: 4.34 × 8.65 arcsec.

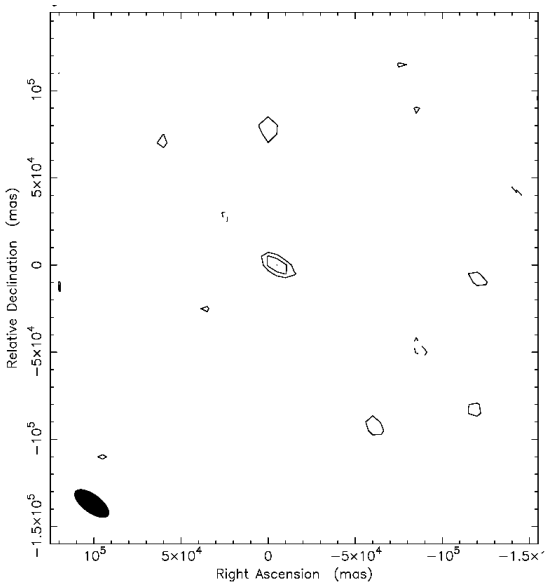

Figure 5.9: GRB 100621a image at 5.5 GHz on June 24, 2010 - Contour levels: -5 5 7.07 9.99 14.13 19.98 28.26 39.96 56.50 79.90 % of peak intensity; Peak brightness: 0.82 ± 0.10 mJy/beam (3σ); Beam size: 5.83 ×1.15 arcsec.

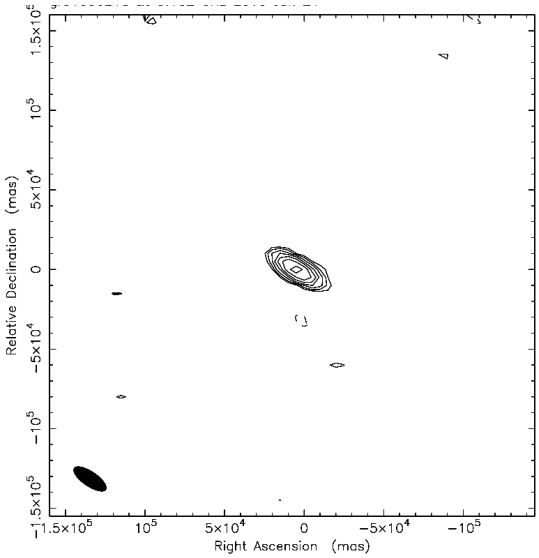

Figure 5.10: GRB 100621a image at 9.0 GHz on June 24, 2010 - Contour levels: -5 5 7.07 9.99 14.13 19.98 28.26 39.96 56.50 79.90 % of peak intensity; Peak brightness: 1.61 ± 0.18 mJy/beam (3σ); Beam size: 3.64 ×0.72 arcsec.

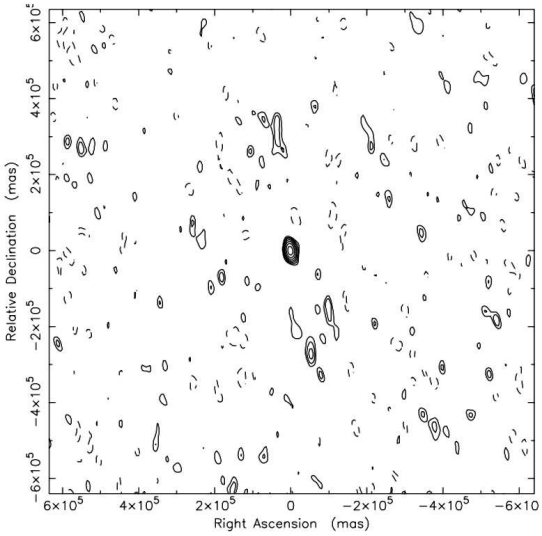

Figure 5.11: GRB 100702a image at 5.5 GHz on July 08, 2010 - Contour levels: -10 10 14.14 19.99 28.27 39.97 56.52 79.92 % of peak intensity; Peak brightness: 1.22 ± 0.09 mJy/beam (3σ); Beam size: 8.69 × 4.44 arcsec.

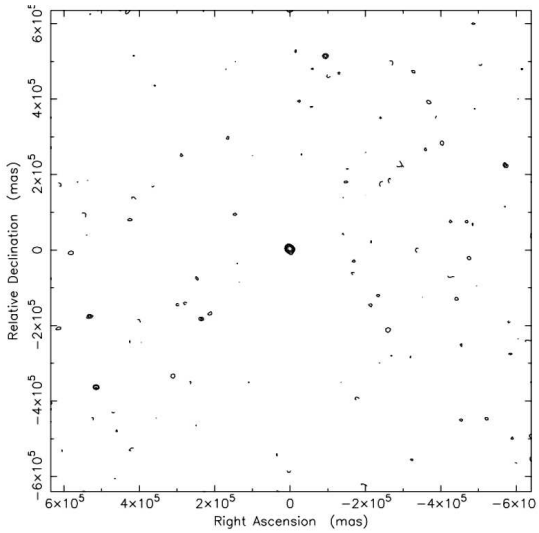

Figure 5.12: GRB 100702a image at 9.0 GHz on July 08, 2010 - Contour levels: -10 10 14.14 19.99 28.27 39.97 56.52 79.92 % of peak intensity; Peak brightness: 0.72 ± 0.15 mJy/beam (3σ); Beam size: 1.72 × 1.50 arcsec.

source was bright enough. However, it was undetected on the single short baseline and the full-array LBA observation was not invoked.

GRB 100418a was observed with the VLBA in a single session at a frequency of 8.4 GHz, in response to the proposal BM347. The observation was conducted 63 days after the burst and the GRB afterglow was clearly detected. Based on the VLBA detection of GRB 100418A, estimates of some parameters were made and some conclusions drawn. The details of that work will appear in Chapter 6.

5.6 ATCA vs EVLA afterglow observations

An extensive GRB afterglow detection and monitoring program has been running at NRAO's VLA/EVLA over the past 15 years. This Northern Hemisphere collaboration has been successful in obtaining key observational results. Well-planned observations and monitoring of the radio afterglows of a number of GRBs have allowed tests of various predictive models against the observed afterglow data. Afterglow models such as the fireball model were found to be plausibly consistent with the observational features of the radio afterglow. The radio observations also allowed estimates of various physical parameters such as the size of the afterglow, the energy associated with the GRB, the

afterglow expansion speed and other source characteristics. Some GRB afterglows were also observed with the ATCA as ToO targets as part of this program and some spectacular southern sky GRB events, such as GRB 980425, were detected. GRB 980425 not only provided better insight into the processes associated with the afterglow, but it also strengthened the GRB-supernova connection.There was thus a need for a long-term program to look for more such sources in the southern sky.

While the northern hemisphere program was so successful in constraining the general properties of this class of objects, the primary objective of this program was to carry out a dedicated search for rare, unusual and interesting classes of GRBs in the southern sky, which can then be continuously monitored and studied in an attempt to understand the underlying mechanisms and the properties of the possible progenitors.

C1802 was a fixed-schedule program at the ATCA in which regular monthly or bi-monthly observation sessions were conducted. Selected samples of potential GRBs, meeting the pre-established criteria, were observed during each session in an attempt to detect the radio afterglows. This approach was deemed feasible due to the advent of new space-borne GRB detectors (Swift, Fermi etc.) with a high rate of detection. The C1802 observation sessions, being fixed in time, didn't always coincide well with the timing of the prompt emission from GRBs. At the end of the observational program, a comparison between the observation strategy and selection criteria of the northern and southern GRB afterglows observation programs was undertaken, in order to study the pros and cons of the strategies adopted for the ATCA (C1802) observations, and to see what modifications could be made in future to improve the ATCA detection rate.

Figure 5.13 is the comparison of the ATCA and EVLA response times for GRB events, the time difference between the prompt gamma-ray emission and the initial radio observation. The plot clearly shows that the EVLA responded much more quickly (within 48 hours in most cases) to the GRB events compared to the ATCA. GRB events require much quicker responses as most radio afterglows fade away in a matter of days. Almost 45% of the GRBs observed by the EVLA were detected, compared to an ATCA post-CABB detection rate of 11% (pre-CABB detection rate was 0%). The ATCA observations of GRBs in the CABB era had a sensitivity comparable to (or better than) the EVLA observations (see Figure 5.16), but a much lower detection rate due to slower response time. A rapid response to the GRB triggers (24 - 48 hrs) can therefore increase the ATCA detection rate.

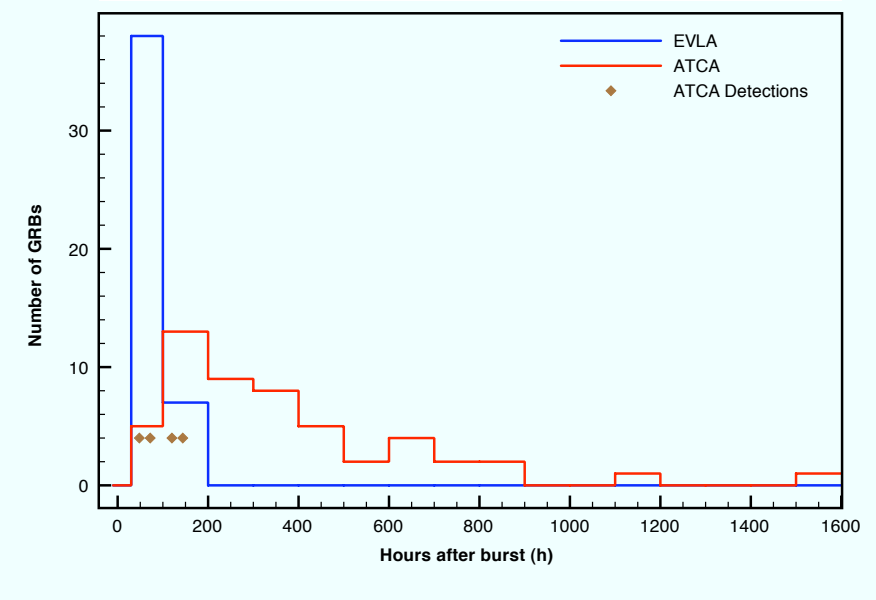

Figure 5.13: ATCA vs EVLA Response times after the prompt emission - The plot compares the response times of EVLA and ATCA GRB observations conducted between 2008 and 2011.

Figure 5.14 compares the gamma-ray fluences (log values) of the GRBs observed by ATCA with those observed with EVLA. The distribution of GRB fluences in the plot shows that 46% of the ATCA observed GRBs had fluence in the range 1.00×10^{-6} - 9.00×10^{-5} ergs cm^{-2} and about 51% of the EVLA observed GRBs had fluences falling in the same range. The fluences of all of the GRBs detected in the radio band by ATCA under C1802 program (see Table 5.1), and most of the GRBs detected by EVLA over the past three years fall in this range. This indicates that for both observational campaigns, GRBs with similar fluence levels were selected for observations and GRB afterglows with fluences belonging to the same range were detected. This reaffirms the general rule that there is not a particular value of GRB fluence that guarantees a detection, but GRBs having fluences that fall in the aforementioned range hold better chances of radio detection. Therefore, in terms of GRB fluence, the current strategy could be carried forward for future detection programs.

The durations of the gamma-ray emission of the GRBs observed by both the ATCA and the EVLA range from about a second to a maximum of 180 seconds, as shown in Figure 5.15. There is not a specific range of GRB durations between the two extremes

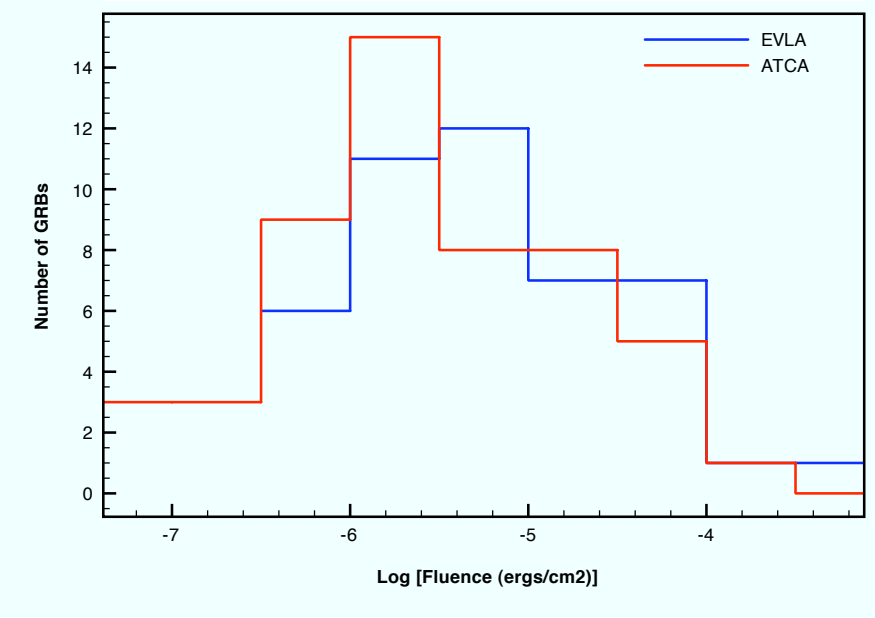

Figure 5.14: GRB Fluence - The plot compares the fluence of GRBs observed by EVLA with the GRBs observed by ATCA.

for which the number of observed or detected GRBs was found to be higher. The GRB afterglows that were selected for observations with the EVLA and the ATCA had varying durations. There is no indication that GRBs with durations falling under a certain range are more likely to be detected.

The enhanced bandwidth of the CABB system has greatly improved the sensitivity that can be obtained for an observation session at ATCA. As can be seen from Figure 5.16, the ATCA GRB observations have much smaller values of RMS noise in the CABB era compared to the pre-CABB era. The RMS values for the GRBs observed with CABB are comparable to the values obtained at the EVLA indicating enhanced sensitivity. All four GRB afterglows detected under the C1802 program were observed with CABB. Since all of them were 3σ detections, smaller values of RMS for the CABB observations facilitated the detections. The GRB observations made with ATCA in the pre-CABB era had much higher RMS values thus much less sensitivity resulting in no detection at all.

The comparison of the ATCA and EVLA observations presented here shows that some refinement in the observation strategy will greatly enhance the detection rate of the GRB radio afterglows. A much quicker response, preferably within 48 hours

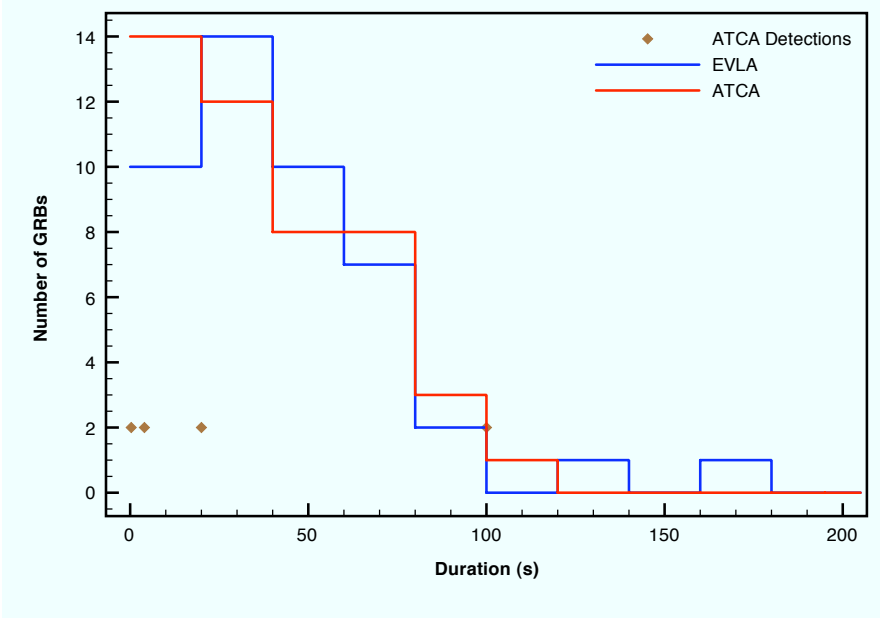

Figure 5.15: GRB Durations - The plot compares the durations of GRBs observed by EVLA with the GRBs observed by ATCA. The brown points indicate the durations of prompt emission of GRBs detected by ATCA.

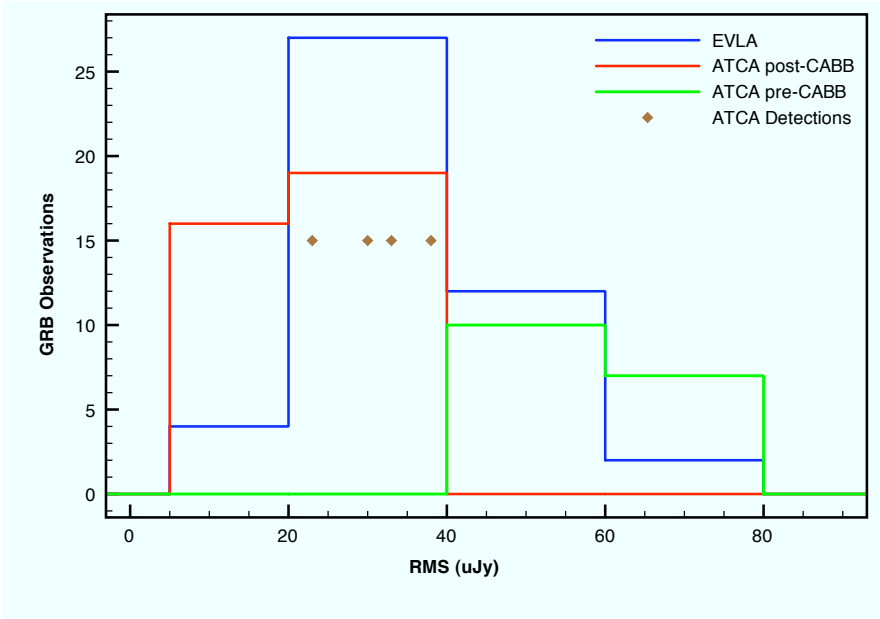

Figure 5.16: GRB rms - The plot compares the RMS noise for the GRBs observed by EVLA with the GRBs observed by ATCA. The brown points are RMS noise values for the GRBs detected with ATCA.

(or even 24), with a high-sensitivity setup might allow the detection of afterglows and monitoring of their evolution as a function of time, which otherwise mostly goes undetected. Rapid response observations and continuous monitoring of a long-lasting GRB afterglow help study the expansion of the fireball and the dynamics of the associated relativistic outflow, enabling to better understand the physics of the GRB phenomenon.

5.7 Summary

Gamma-Ray Bursts are mysterious events and a definitive picture is yet to surface. The best way to study the GRB environment and the series of processes that follow the explosion and the burst is to carry out well-sampled multi-wavelength monitoring of the GRB afterglow. The radio afterglow offers some unique advantages over afterglows in other bands, one of the only ways to obtain a long-term profile of the afterglow, which in turn allows inference to be made regarding the changes and transitions that occur due to the circumburst medium. It also allows estimates of the size of the expanding fireball, the nature of the emission, and the study of the dynamics of outflow.

In order to carefully study the radio afterglow of GRBs, it is critical to find persistent afterglows. Hence, the first dedicated and long-term GRB radio afterglow detection and monitoring program in the Southern Hemisphere was planned and executed as part of this PhD project. The primary objective was to devise a systematic observational campaign, in order to observe GRBs in the southern sky, to search for one or more of those unusual and interesting GRBs which can be further studied.

As an outcome of this campaign, the radio afterglows of four GRBs were detected and one out of the four detected radio afterglows turned out to be the rare and persistent one, fulfilling the purpose for which the campaign was planned and executed. The next chapter reports on the extended study of this object, GRB 100418a.

Near future instruments such as ASKAP hold enormous potential to not only carry out rapid response observations with their multi-beaming capability, and a continuous follow-up of interesting sources, but they will also be used to conduct fast sky surveys to detect the radio afterglow of a GRB right at the onset and to track its evolution in real time.

5. MONITORING OF GAMMA-RAY BURST AFTERGLOWS AT RADIO WAVELENGTHS

Chapter 6

Radio observations of GRB100418a and multi-wavelength analysis: Test of an energy injection model explaining long-lasting GRB afterglow

A. Moin, P. Chandra, G. B. Taylor, S. J. Tingay, D. A. Frail, Z. Wang, C. Reynolds, J. C. A. Miller-Jones, C. J. Phillips, 2012, ApJ, to be submitted.

6.1 Introduction

GRB 100418a was detected by the Swift satellite at 21:10:08 UT, April 18, 2010. The Burst Alert Telescope (BAT) on board the Swift satellite was triggered by the GRB and after the initial trigger, Swift's X-Ray Telescope (XRT) and Ultra-Violet Optical Telescope (UVOT) slewed to the source and detected it in the X-ray and optical bands (Marshall et al. 2010; GCN 10612). After the detection at high energies by space-borne instruments, a number of ground-based telescopes turned to GRB 100418a to carry out detailed studies of the GRB 100418a afterglow. The afterglow of the GRB

exhibited unusual behaviour in the optical and X-ray bands (Marshall et al. 2011), featuring an unusually long "plateau" phase with a very slow change in the light curve. The plateau phases in X-ray and optical bands were similar with different starting and ending times. The X-ray light curve also had a typical steep-decaying component preceding the plateau phase. At the end of the plateau phase, the optical afterglow re-brightened, reaching its peak before transitioning to a steep power-law decay. The X-ray light-curve also had a late steep-decay component, after the shallow plateau phase.

The unusual behaviour of this GRB motivated long-term monitoring of the afterglow across the entire frequency spectrum in an attempt to test previously advanced theories of GRB physics (e.g. Rees & Meszaros 1992; Rees & Meszaros 1998; Panaitescu, Meszaros & Rees 1998; Waxman, Kulkarni & Frail 1998; Dai & Lu 1998; Zhang et al. 2006) to explain the connection between the prompt emission and the afterglow and the peculiar behaviour of afterglows associated with some unusual GRBs.

The radio monitoring of GRB 100418a described in this chapter was used to test the "energy injection" model (Zhang et al. 2006; Rees & Meszaros 1998), a plausible explanation of the physics of long-term afterglows of GRBs. The unique behaviour of the afterglow of this GRB supplies some observational evidence to support the energy-injection model. The availability of X-ray, optical and radio afterglow data help build the whole picture and allows a better understanding of the GRB phenomenon.

In the radio band, GRB 100418a was observed and detected by telescopes such as: the Westerbork Synthesis Radio Telescope (WSRT) in The Netherlands; the Submillimeter Array (SMA) in Mauna Kea, Hawaii; Expanded Very Large Array (EVLA); the Australia Telescope Compact Array (ATCA); and the Very Long Baseline Array (VLBA) in the US. In this chapter, the ATCA and VLBA observations and the analysis of GRB 100418a conducted by the author are presented.

6.2 Gamma-ray, X-ray and optical observations of GRB 100418a

A wide variety of instruments have been used to observe and monitor this unusual GRB, covering almost the entire frequency spectrum from gamma-rays to radio. Following

is a brief description of the results obtained with various instruments, by a number of authors.

6.2.1 Gamma-ray observations

GRB 100418a was initially detected in gamma-rays by the BAT on board the Swift satellite, with a duration of approximately 10s. The fluence of the event was estimated to be $(3.4 \pm 0.5) \times 10^{-7}$ erg cm^{-2}, which is a typical value. Figure 6.1 is the BAT light curve, which shows two peaks of gamma-ray emission. The emission peaks are shown in 5 different energy bands.

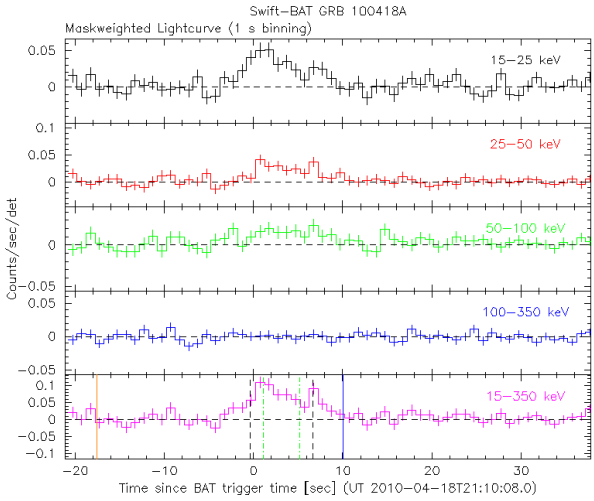

Figure 6.1: BAT light curve - showing GRB 100418a gamma-ray emission peaks in 5 different energy bands. Image credit: GSFC NASA.

Marshall et al. (2011) estimated the isotropic gamma-ray energy release, $E_{\gamma,iso}$, by fitting the BAT spectrum with the Band function (Band et al. 1993), to be 9.9 $\times$ 10^{50} erg. Similarly, the peak luminosity, $L_{\gamma,iso}$, of the GRB was estimated to be 2.1 $\times$ 10^{50} erg s^{-1}. In terms of the estimated $E_{\gamma,iso}$, GRB 100418a does not stand out as an exceptionally energetic event.

Sakamoto et al. (2011) recently presented the second catalog of Swift BAT GRBs containing records of various GRB parameters for 476 GRBs detected between 2004 and 2009. A comparison of the estimated isotropic energy release for GRB 100418a with those of the GRBs catalogued in Sakamoto et al. (2011) indicates that the prompt $E_{\gamma,iso}$

for this GRB is much lower than other GRBs at similar redshifts (0.5 - 0.7). Therefore, the equivalent isotropic energy associated with the prompt gamma-ray emission is not unusually high as might be inferred from the behaviour of the multi-wavelength afterglow, rather it is much lower than the $E_{\gamma,iso}$ of a number GRBs previously investigated (e.g. Butler, Bloom & Poznanski 2010; Butler et al. 2010; Sakamoto et al. 2011) and it easily falls in the category of low $E_{\gamma,iso}$ GRBs. In addition to this, the estimated E_{peak} of 29 keV and the absence of gamma-ray emission above 100 keV also categorises GRB 100418a as a soft burst.

6.2.2 X-ray observations

GRB 100418a was observed in X-rays by the XRT on board Swift satellite. The XRT slewed to the GRB 100418a position at 21:11:27 UT on April 18, 2010, 79.1 seconds after the burst (Palmer et al. 2010, GCN 10612) and the X-ray afterglow was instantly detected. The astrometrically corrected (Goad et al. 2007; Evans et al. 2009) position of GRB 100418a (RA: 17:05:27.18; Dec: +11:27:40.1) was also determined using XRT data (Osborne et al. 2010, GCN 10614). For this GRB, the XRT operated in "Windowed Timing (WT)" and "Photon Counting (PC)" modes (for details see Burrows et al. 2005).

Figure 6.2 is the X-ray light curve for GRB 100418a, plotted using the Swift XRT data. The light curve was obtained using the method given in Evans et al. (2007). The X-ray flux plotted against time after the initial trigger is in the 0.3–10 keV energy band.

The X-ray light curve shows a steep early power-law decay until approximately T_0 + 474 seconds (T_0 = trigger time) with α = -4.23 (Pagani et al. 2010; GCN 10622), where α is the decay index of the afterglow light curve. This value of α is consistent with the segment I of the X-ray afterglow power-law decay model (Zhang et al. 2006) and is typical GRB X-ray afterglow behaviour. After the initial steep decay segment, a transition to a standard shallow-decay would be expected but, after the break, the light curve settles for a "plateau" phase and undergoes a shallow rise instead, with α = 0.23. This unusual phase signifies shallow afterglow brightening and it ends at around T_0 + 66 ks. The plateau phase is followed by a late decay component, with α = -1.37, which matches well with segment III of the X-ray afterglow power-law decay model, presented in the Figure. 1 of Zhang et al. (2006).

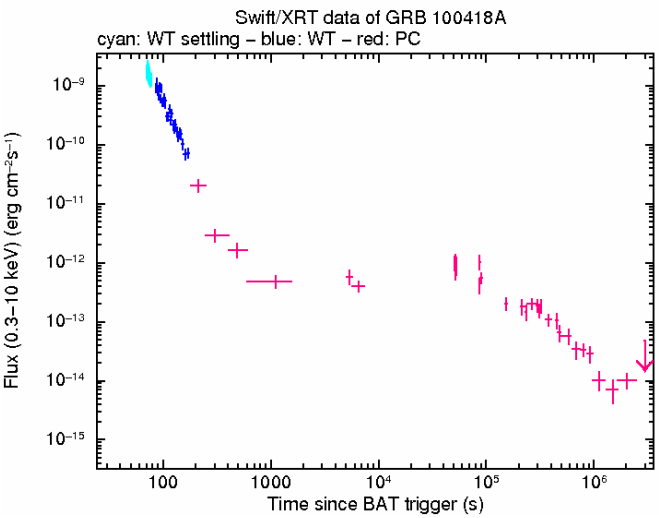

Figure 6.2: XRT light curve - showing the flux of GRB 100418a X-ray afterglow as a function of time. The data in WT mode shown in blue and the data in PC mode shown in red. Image credit: Phil Evans, UK Swift Science Data Centre.

The behaviour displayed by segments I and III (Figure. 1, Zhang et al. 2006) is common in GRB X-ray afterglows but the unexpected plateau phase makes GRB 100418a unusual, demanding further investigation.

6.2.3 Optical observations

The Swift UVOT started to observe the GRB 100418a field 87 seconds after the initial BAT trigger (Marshall et al. 2010, GCN 10612) and detected the optical afterglow. After the UVOT detection, a number of optical telescopes around the world observed GRB 100418a. The optical afterglow was detected in most of the optical filters (v, i, r, u, g, white) and spectroscopic and photometric studies were also carried out (e.g. Filgas et al. 2010, GCN 10617; Updike et al. 2010, GCN 10619; Antonelli et al. 2010; GCN 10620; Cucchiara et al. 2010; GCN 10624; Perley et al. 2010, GCN 10727).

The VLT detected the afterglow 8.37 hours after the burst with a magnitude of 18.1 in R band (Antonelli et al. 2010, GCN 10620). Spectra of the afterglow were obtained using the VLT/X-shooter and Gemini-N spectrographs and the source redshift was determined to be z = 0.6235 (Antonelli et al. 2010, GCN 10620; Cucchiara et al. 2010; GCN 10624). Malesani (2010, GCN 10621) reported the identification of the

host galaxy in the Sloan Digital Sky Survey (SDSS) catalogue at the position of the GRB 100418a afterglow.

The GRB 100418a optical afterglow light curve showed quite an unusual behaviour. It was initially detected as a fading point source (e.g. Filgas et al. 2010, GCN 10617; Malesani et al. 2010, GCN 1063) and it remained in a shallow-decaying "plateau" phase with a decay index α = -0.15 until about T_0 + 7 ks, after which, it started to re-brighten (α = 1.12) and reached its peak at about T_0 + 51 ks followed by a steep power-law decay with α = -0.6, lasting until at least T_0 + 1 Ms. Figure 6.3 is the UVOT light curve of the optical afterglow of GRB 100418a showing the aforementioned behaviour. In this figure, the count rate in the white filter is plotted as a function of time elapsed since onset.

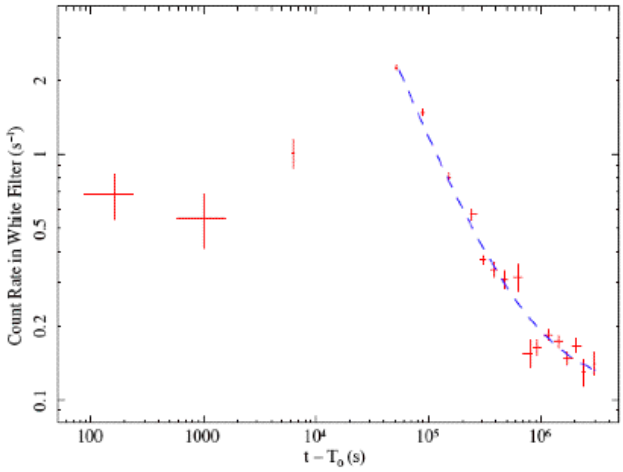

Figure 6.3: UVOT light curve - UVOT light curve for GRB 100418a optical afterglow showing the count rate in White filter plotted against time since the BAT trigger. After a poorly sampled plateau phase, the light curve transitions to a more usual steep decaying phase at T_0 + 51 ks, which is typical GRB afterglow behaviour. Image credit: Marshall et al. 2011.

Roming et al. (2008) present a catalog of 229 Swift UVOT GRB afterglows and they have shown that the optical light curves for most of the GRBs usually have a "well" shape featuring a steep decline starting from the beginning of the observation, which is unlike the complex behaviour of GRB 100418a afterglow described above. Oates et al. (2009) conducted a statistical study of 27 UVOT GRB afterglows confirming the rapid decay of afterglows. For the few exceptions in which the light curves rise up before a

sharp decline, the GRB optical fluxes peak around 500s, whereas in the case of GRB 100418a, the optical flux didn't reach its peak until T_0 + 51 ks. There are reports of a very few other GRB afterglows having a plateau phase (e.g. GRB 060729; Grupe et al. 2007) but their X-ray and optical light curves do not show the same behaviour as GRB 100418a. The unique and unusual nature of the GRB 100418a motivated long-term multiwavelength observations and monitoring to study the behaviour of the afterglow, and to determine if the data support theories postulated to explain the relationship between the prompt emission, the afterglow, and the late-time emission.

6.3 Radio observations of GRB 100418a

As part of the GRB observation and monitoring program carried out in this PhD project, GRB 100418a was observed using the Australia Telescope Compact Array (ATCA) in Australia and the Very Long Baseline Array (VLBA) in the United States. Expanded Very Large Array (EVLA) observations of this source were separately conducted by collaborators at NRAO (Chandra et al. 2010, GCN 10650). This GRB was included in the list of sources to be observed and monitored multiple times with the ATCA due to its unusual nature and persistent afterglow. Given its significant and consistent brightness at radio wavelengths, as seen with the ATCA and the EVLA, the VLBA observation was conducted to observe the GRB afterglow at high angular resolution.

6.3.1 EVLA Observations

GRB 100418a was first detected by the EVLA on 2010 April 21 (Chandra et al. 2010; GCN 10650) at a frequency of 8.46 GHz with a flux density of 0.45 ± 0.02 mJy. After the first EVLA detection, a number of observation sessions were carried out until September 2010, to monitor the GRB 100418a radio afterglow. A separate observation was more recently conducted in 2011 April and it was found that the radio afterglow of GRB 100418a was still detectable even 352 days after the prompt emission.

The flux density of the radio afterglow continued to rise until it reached the peak about 50 days after the prompt emission and the post-peak phase featured a power-law decay. After passing through the rising phase, the flux density decreased at both 4.95

and 8.46 GHz, until the time the afterglow was last observed in April 2011. Figure 6.4 is the EVLA + ATCA light curve for the radio afterglow of GRB 100418a

The size of a GRB radio afterglow source can be crudely estimated as R $\sim$ δtc, where δt is the time range between the prompt emission and the peak of the radio afterglow and c is the speed of light. Looking at the peak in the EVLA light curve, R is estimated to be R $\sim 1.24 \times 10^{17}$ cm. The value obtained using this approximation is consistent with the predictions of the relativistic fireball model for GRB radio afterglows presented by Waxman (1997a, 1997b, 1997c). This model states that the radio emission associated with a GRB comes from a cone of the fireball along the observer's line-of-sight and R is therefore the apparent radius of the cone which is said to be the emitting region.

6.3.2 ATCA Observations

GRB 100418a was observed using the ATCA during three epochs of the GRB observation and monitoring program (ATCA proposal C1802), conducted in 2010 April, May and June. It was significantly detected at all three epochs at 5.5 and 9.0 GHz.

The source was observed with a nearby calibrator for phase referencing and PKS 1934-638 was also observed during the session for primary flux calibration. Data were processed by CABB (see chapter - 2) in the standard continuum mode with a full bandwidth of 2.048 GHz.

The output data files were then loaded into MIRIAD[1] for calibration. Standard MIRIAD calibration routines were used to calibrate the amplitude and the phase of the data and FITS files of the calibrated data were produced. The FITS files containing the calibrated data were then loaded in DIFMAP (Shepherd, Pearson & Taylor 1994) to produce final images of the GRB 100418a afterglow. After imaging the data from each session in DIFMAP, the detected afterglow was fitted with a point-source model using the model-fitting routine with five iterations and the peak flux density for each session was determined. The errors on flux densities are the 3-sigma value of the RMS noise.

After the initial detection, the radio afterglow of GRB 100418a was again detected by the ATCA during a regular GRB observation session (C1802), about 8 days after the initial burst, which was quite unusual as the likelihood of detecting the radio afterglow

[1] http://www.atnf.csiro.au/computing/software/miriad/

of a GRB starts to diminish after about 24 hours of the prompt emission. The GRBs with radio afterglows lasting more than a week are rare. Therefore, it was decided to continue monitoring the radio afterglow of GRB 100418a. The second and third observation sessions were conducted one (2010 May) and two months (2010 June) after the prompt emission respectively and even a number of weeks after the burst, it was possible to detect the radio afterglow with a significant rise in the flux density level as can be seen from Figure 6.4. The early-time rise seen in the ATCA light curve is consistent with the EVLA light curve, which kept rising until it reached its peak after about 50 days since the burst.

There were no further ATCA observations of the GRB 100418a radio afterglow after the third session but the EVLA continued to monitor it. Some drastic short time-scale variations in the flux densities could be due to the diffractive scintillation in the ionized interstellar medium (Frail, Waxman & Kulkarni 2000).

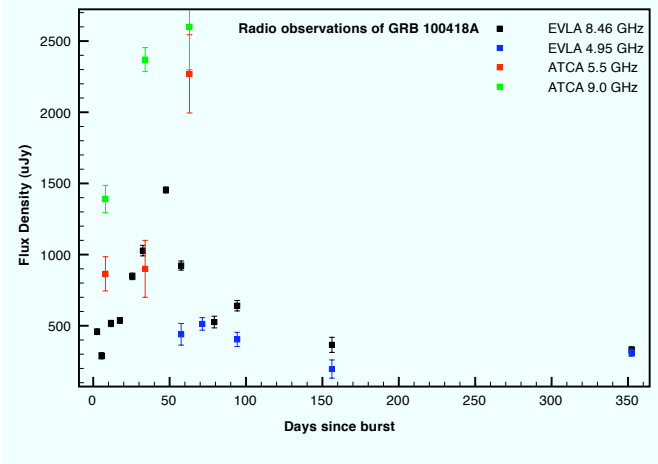

Figure 6.4: GRB 100418a radio light curve - GRB 100418a was detected and monitored by both EVLA and ATCA at 4.95 and 8.46 GHz, 5.5 and 9.0 GHz respectively. This light-curve presents the record of EVLA + ATCA observations of the GRB over the course of 357 days.

Figure 6.5 is the spectral index evolution of the GRB 100418a radio afterglow estimated using both ATCA and EVLA data. The profile clearly shows that the emission came from a compact, optically thick source because the values of the spectral indices never turned negative until the time it was last observed ∼357 days after the prompt emission.

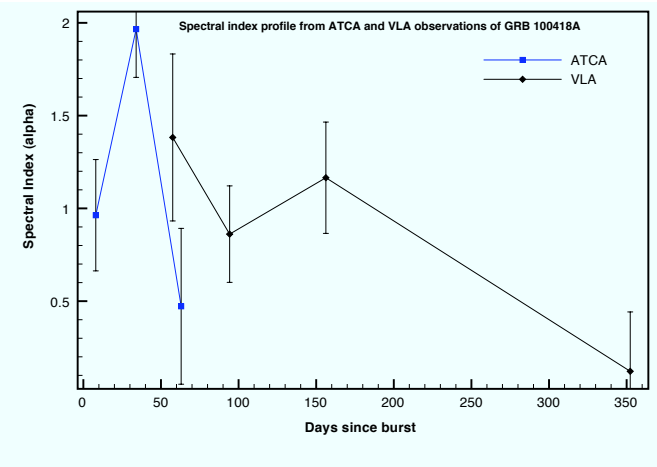

Figure 6.5: GRB 100418a spectral indices - obtained from the ATCA and EVLA observations.

Figure 6.6 to 6.11 are images from the ATCA observations showing the detection of the radio source associated with the GRB at 5.5 and 9.0 GHz respectively.

6.3.3 VLBA Observations

The persistent radio afterglow of GRB 100418a, which was detectable with both the ATCA and the EVLA several weeks after the prompt gamma-ray emission, with a peak flux density of about 1.5 mJy more than 60 days after the burst, provided the motivation to observe this GRB with VLBI. The VLBI observation of GRB 100418a was an attempt to resolve the GRB radio afterglow and to determine the milliarcsecond-scale structure associated with the afterglow. In particular, an estimate of the angular size of the afterglow and possibly the expansion rate would constrain theories of afterglow. Previously, similar studies of a GRB radio afterglow were made via a VLBI campaign carried out for high resolution monitoring of the bright and nearby GRB 030329 (Taylor et al. 2004; Pihlstrom et al. 2007 etc.).

In response to a successful proposal to the VLBA, the GRB 100418a observation session was carried out on June 22, 2010 with NRAO's VLBI stations in Mauna Kea, Owens Valley, Brewster, North Liberty, Hancock, Kitt Peak, Pie Town, Fort Davis, Los Alamos and St. Croix. The source was observed for eight hours with full Stokes parameters at a frequency of 8.4 GHz with a bandwidth of 8×8 MHz. Along with the target source, phase-reference calibrator J1706+1208 and a VLBA fringe finder 3C345

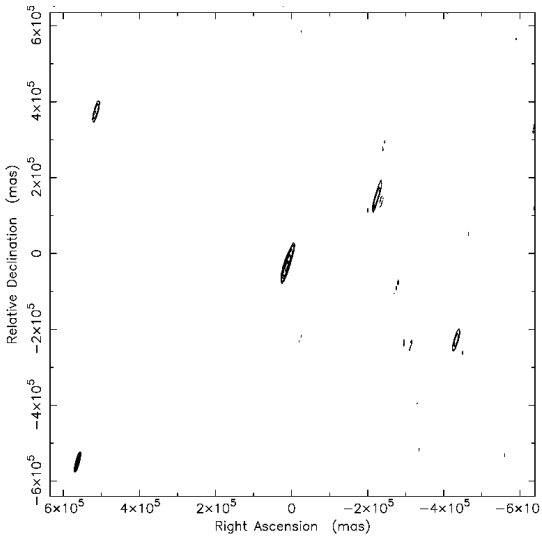

Figure 6.6: GRB 100418a image at 5.5 GHz on April 20, 2010 - Contour levels: -20, 20, 28.3, 40, 56.5, 80 % of peak intensity; Peak brightness = 865 ± 120 μJy/beam (3σ); Beam size: 5.53 × 9.82 arcsec.

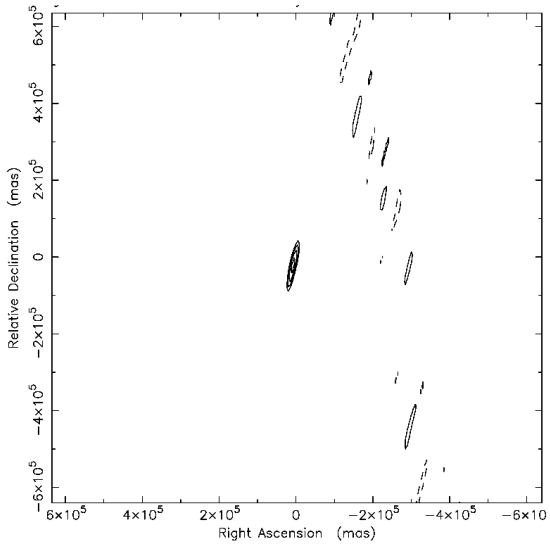

Figure 6.7: GRB 100418a image at 5.5 GHz on May 26, 2010 - Contour levels: -20, 20, 28.3, 40, 56.5, 80 % of peak intensity; Peak brightness = 1390 ± 200 μJy/beam (3σ); Beam size: 4.37 × 8.93 arcsec.

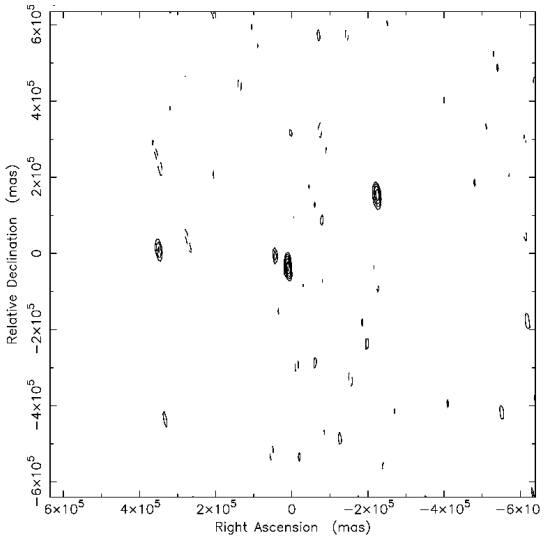

Figure 6.8: GRB 100418a image at 5.5 GHz on June 26, 2010 - Contour levels: -20, 20, 28.3, 40, 56.5, 80 % of peak intensity; Peak brightness = 2200 ± 275 μJy/beam (3σ); Beam size: 5.27 × 1.41 arcsec.

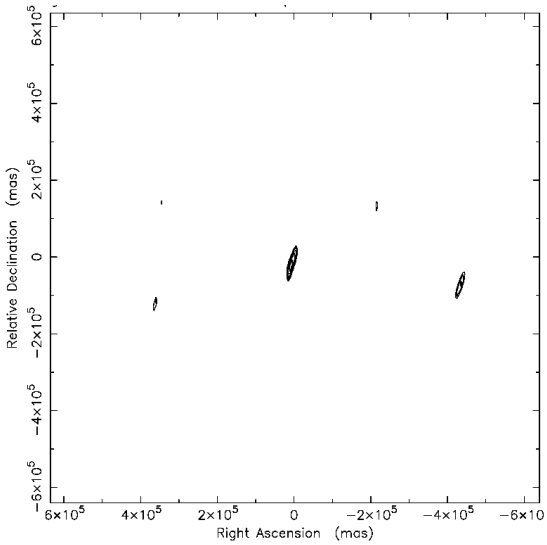

Figure 6.9: GRB 100418a Image at 9.0 GHz on April 20, 2010 - Contour levels: -20, 20, 28.3, 40, 56.5, 80 % of peak intensity; Peak brightness = 1390 ± 96 μJy/beam (3σ); Beam size: 4.24 × 8.65 arcsec.

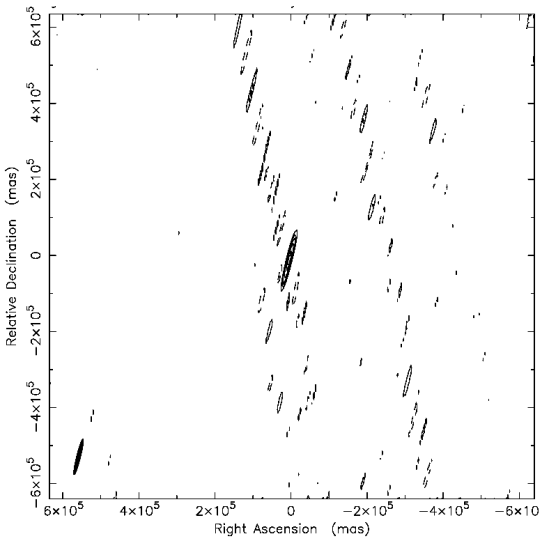

Figure 6.10: GRB 100418a Image at 9.0 GHz on May 26, 2010 - Contour levels: -20, 20, 28.3, 40, 56.5, 80 % of peak intensity; Peak brightness = 2400 ± 24 μJy/beam (3σ); Beam size: 2.82 × 4.38 arcsec.

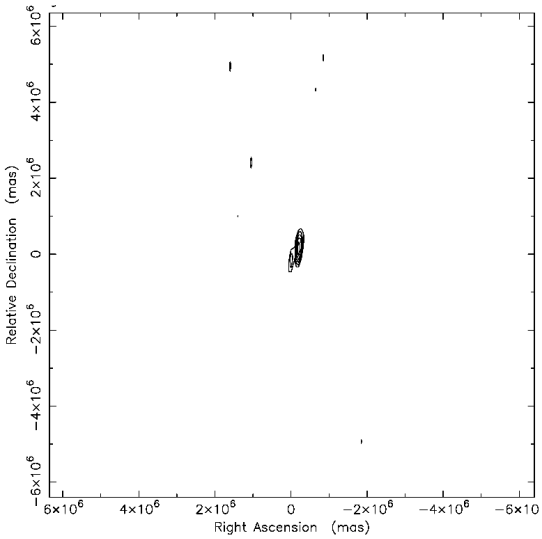

Figure 6.11: GRB 100418a Image at 9.0 GHz on June 26, 2010 - Contour levels: -20, 20, 28.3, 40, 56.5, 80% of peak intensity; Peak brightness = 2700 ±200 μJy/beam (3σ); Beam size: 3.02 × 3.76 arcsec.

were also observed during the observation. The data were correlated with the DiFX correlator in Socorro (Deller et al. 2007, Deller et al. 2011) and the correlated data were downloaded to the CUPPA cluster at Curtin University for data reduction and imaging.

The correlated data were reduced and processed in AIPS as a first step to perform phase and amplitude calibration. Single-source FITS files containing calibrated data were produced. These FITS files were then loaded into DIFMAP for preliminary model-fitting and imaging. A cell size of 0.1 $\times$ 0.1 milliarcsecond was used and the image was produced with natural weighting. The outcome of the VLBI observations and data analysis revealed an unresolved radio source associated with GRB 100418a having a correlated flux density of 0.89 $\pm$ 0.15 mJy, where the error is the 3-sigma RMS noise.

The source was unresolved at the beam size for the VLBA observation, which was 1.99 $\times$ 0.919 mas. A rough upper limit of $<$ 0.33 mas (1-sigma) on the source size was obtained by performing model-fitting in both uv and image plane using elliptical gaussian models in AIPS. The upper limit rules out that there was any structure larger than the limit, at flux densities above the detection threshold at the time of VLBA observations of the afterglow at 8.4 GHz. Based on the size upper limit, the maximum physical size of $<$ 1.375 $\times$ 10^{18} cm and the apparent expansion speed $<$ 8c was also determined. The VLBI observations of GRB 100418a were conducted about 62 days after the prompt emission and the source was found out to be still unresolved, so the derived upper limit on the apparent expansion speed was a long-term average assuming uniform expansion (mildly relativistic) and it does not conflict with the possible early relativistic expansion.

The lower limit on the brightness temperature of the radio emission region is estimated as $T_b > 2.95 \times 10^9$ K. The value was determined using the mathematical formulation for the brightness temperature of a radio source given in Taylor, Carilli & Perley (2008). According to the Planck function with a Rayleigh-Jeans approximation, this lower limit on the brightness temperature ($>10^7$ K, having peak intensity at very high frequencies), indicates that the GRB radio afterglow was optically thick at a frequency of 8.4 GHz at the time of the VLBI observation, which is consistent with the outcome of ATCA/EVLA data analysis. The most likely emission mechanism is synchrotron emission resulting from the excitation of electrons during the interaction of the forward shock with the circumburst medium.

The GRB 100418a radio afterglow position obtained from the VLBA observation is 17:05:27.092 ± 0.005, +11:27:42.24 ± 0.01 (Calibrator position: 17:06:20.4974, +12:08:59.794 with an uncertainty of 0.5 mas; http://www.astrogeo.org). The errors were estimated on the basis of the beamsize and signal-to-noise ratio (SNR) considerations. A systematic uncertainty of 0.06 mas was estimated in both coordinates based on the calibrator-target separation (Pradel et al. 2006). The VLBI position is consistent with the position of the optical counterpart detected by GROND with an error circle of 0.5 arcsec (Klose et al. 2010; GCN 10616), as well as the position of the radio counterpart detected by the ATCA and EVLA.

Figure 6.12 is the VLBI image of the radio afterglow of GRB 100418a at 8.4 GHz. It is interesting to note that the VLBA flux density matched almost exactly with the flux density obtained from the EVLA observation on the same day. It indicates that there was no missing flux in the VLBA data ruling out that there could be any structure associated with the afterglow at the time of VLBA observation that was resolved out by the long baselines of the VLBA.

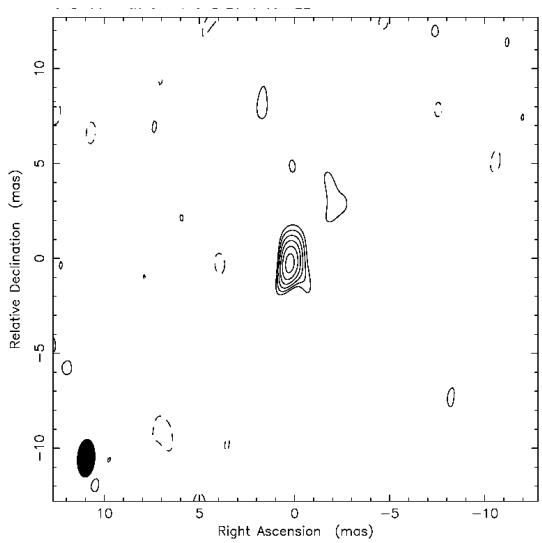

Figure 6.12: GRB 100418a VLBI image - Observations at 8.4 GHz on June 22, 2010. Contour levels: -10, 10, 20, 40, 80 % of peak intensity; Peak flux density = 890 ± 150 μJy; Beam size: 1.99 × 0.919 mas; Position angle -3.7.

6.4 Analysis and Interpretation of multi-instrument observations of GRB 100418a

At the end of the long-term Southern Hemisphere GRB detection program, GRB 100418a stood out as a potentially interesting source, which was studied in detail to learn more about the GRB and its surroundings, test some of the predictions regarding the underlying emission mechanisms and attempt to acquire a better understanding of the GRB phenomenon. GRB 100418a was ordinary in terms of the estimated energy release and the luminosity, but what made it an extraordinary GRB was the unusual afterglow emission behaviour, the late-time rise of the X-ray, optical and radio afterglow light curves and then the subsequent decay at all wavelengths.

As can be seen from both XRT and UVOT light curves (Figure 6.2 & 6.3), after a brief period of steep decline in the X-ray and optical afterglow, there was an unusual "plateau phase" which started about 87 seconds after the burst in the optical band and about 600 seconds after in the X-ray band (Marshall et al. 2011). During this phase there was a shallower rise in the light curves and after about 51 ks in the optical band and about 50 - 90 ks in the X-ray band, the afterglow entered a steeper and more normal power-law decay again.

Zhang et al. (2006) proposed a model called the "energy injection model" to explain this kind of behaviour. This model was invoked by Marshall et al. (2011) to answer questions concerning the mechanisms which could explain the unusual behaviour of the GRB 100418a afterglow.

Before attempting to explain the behaviour of GRB 100418a afterglow with the help of the energy injection model, it is important to put the observational signatures of the GRB 100418a afterglow in the context of the overall GRB phenomenon, and the standard blast wave model (Rees & Meszaros 1992; Meszaros & Rees 1993, 1997; Waxman 1997; Wijers, Rees, & Meszaros 1997) still serves as the most plausible physical framework, since the background physics proposed by this model has been repeatedly found to be in good agreement with the GRB observations. The blast wave, or cosmological fireball model, proposes that a compact central engine undergoes a massive explosion producing a relativistic outflow releasing an enormous amount of energy (of the order 10^{52} ergs). The outflow powers "internal shocks" (e.g. Rees & Meszaros 1994) having different Lorentz factors. Collisions between these internal shocks are thought

to produce the GRB prompt emission. Following the internal shocks, a blast wave, also known as a forward shock or external shock, powered by the expanding ejecta, is driven into the circumburst medium, which is believed to produce the afterglow that is then observed at lower frequencies. The forward shock accelerates the electrons in the circumburst medium to relativistic speeds and they emit synchrotron radiation as they move in the surrounding magnetic field, which can then be detected and monitored for long-term GRB studies (Meszaros & Rees 1997a; Kulkarni et al. 1998; Sari, Piran & Narayan 1998; Waxman 1998; Frail et al. 2000 and many references therein).

Studies have indicated that the various GRB afterglow phases seen in the light curves represent the transitions which the decelerating ejecta and the expanding blast wave might be going through. In other words, the variations in the afterglow light curves can help infer the state of the emitting region. Figure 6.13 shows the five possible components that the light curve of a GRB X-ray afterglow can have (Zhang et al. 2006). The X-ray light curve of GRB 100418a exhibits three distinct phases, out of which the first and third phases match well with the segment I and segment III respectively of Figure 6.13 and are considered as normal X-ray behaviour for a GRB (Figure 6.2).

The rapid early decay of the GRB 100418a light curves is common amongst most of the GRBs and is attributed to the "GRB tail-emission", that is the steeply declining prompt emission that comes from the internal shocks immediately after the burst (Dermer 2004; Liang et al. 2006; Zhang et al. 2006). In general, the transition from declining prompt emission to early X-ray emission manifests itself as the transition from a sharp decline to a shallow decline in the afterglow light curve (Tagliaferri et al. 2005).

The second component in the optical and X-ray light curves is the unusual plateau phase with a very shallow rise. This is a rare feature in terms of the duration and behaviour and it looks like the manifestation of some sort of a continuous post-burst activity extending the afterglow to a longer time span. This behaviour has only been seen in very few GRB X-ray afterglows (e.g. GRB 060729; Grupe et al. 2007).

Coming back to the energy injection model, which holds the potential to explain the GRB 100418a behaviour, the model states that if the external (forward) shock that produces the GRB afterglow is continuously fed with energy after the initial supply, the forward shock keeps getting refreshed to produce a multiwavelength afterglow for a

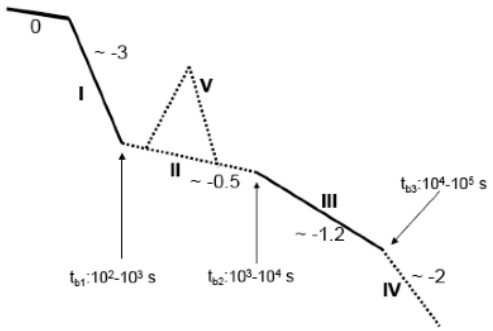

Figure 6.13: GRB X-ray light-curve components - Zhang et al. 2006 presented a generic cartoon of the X-ray afterglow light curve of a GRB, which shows various possible components of the light curve representing the phases and transitions of the X-ray afterglow.

longer period of time. According to the model, this continuous energy injection which is powered by some form of continued activity manifests itself as the very shallow plateau phase in the afterglow light curve, which is what is seen in the case of GRB 100418a.

The observational signature seen in the GRB 100418a afterglow light curves may be considered as some evidence supporting the energy injection theory which suggests that the forward shocks, that produce the GRB afterglow, keep getting a continuous supply of energy through some mechanism.

The total isotropic gamma-ray kinetic energy in case of GRB 100418a afterglow that powered the forward shock to continuously produce the afterglow is estimated by Marshall et al. (2011) as $E_{k,iso,f} \geq 10^{53}$ ergs given $t_p \sim$ 50-90 ks and $t_i \sim$ 600s, where t_i is the time when the plateau phase starts, and t_p is the time when the afterglow reached its peak before the transition to a steep decay phase. This energy is 100 times the initial isotropic energy and is thought to be continuously injected into the forward shock, which then produced long-term, slowly varying afterglow (Dai & Lu 1998; Zhang & Meszaros 2001; Zhang et al. 2006). The energy budget is thus consistent with the energy injection model and plausibly explains the behaviour exhibited by the afterglow of GRB 100418a.

Investigators have outlined the following mechanisms which can give possible explanations for the energy injection model.

- Ejecta with a range of Lorentz factors, with slower ejecta catching up with the forward shock at late times (Rees & Mezaros 1998; Zhang et al. 2006).
- Continued activity of central engine producing Poynting flux dominated flow (Dai & Lu 1998; Zhang et al. 2006).

Rees & Meszaros (1998) presented a detailed formulation of a plausible mechanism to support the energy injection model and to explain the slowly varying afterglow in which they suggest the possibility of more than one spherical shells of material moving forward with different Lorentz factors. These concentric shells catch up with the forward shock at different times so the continuous striking of the forward shock by these shells keep refreshing the shock which gives rise to a longer-lasting and slowly varying afterglow. This model can be described as a relation between the ejected mass M_{grb} and the range of Lorentz factors of the mass, expressed as:

$$M_{grb} \propto \gamma^{-s} \text{.....(1)}$$

where s is the mass outflow index and the Lorentz factor is γ.

The GRB 100418a VLBI observation carried out as part of this PhD project led us to test this model by determining the upper limit on the long term average of Lorentz factor of the ejecta $\gamma < 7$, and an upper limit on the apparent expansion speed of < 8c. The upper limit on the expansion speed was determined using the upper limit on the source size obtained from the VLBA data and estimating the value of angular diameter distance (Raine & Thomas 2001) at the redshift (z = 0.62) of GRB 100418a. Using the formulation (Sedov-von Neumann-Taylor solutions) presented in Frail, Waxman & Kulkarni (2000), the equivalent isotropic energy E_a associated with the radio afterglow can be given as:

$$E_a \approx 4.4 \times 10^{50}\ \eta_1^{-2/17}\ \nu_*^{-0.56}\ a_*^{35/17} b_*^{15/17} d_*^{70/17}\ \text{ergs.....(2)}$$

where a_*, b_*, d_*, η_1, ν_* are the parameters which define the afterglow model developed by Frail, Waxman & Kulkarni (2000) and are related to the fireball expanding at a subrelativistic velocity. The details of this model, parameters and the assumptions

can be found in Frail, Waxman & Kulkarni (2000). Given the constraints (e.g. upper limits on physical size and Lorentz factor) obtained from the VLBI observations and some model-based terms, the values of the parameters in equation (2) were calculated using the expressions given in the appendix of Frail, Waxman & Kulkarni (2000). Those values were then plugged in equation (2) and the approximate value of the afterglow (fireball) energy came out to be $E_a \approx 6.0 \times 10^{51}$ ergs.

The ejected mass M_{grb} corresponding to the afterglow energy release can be estimated using Einstein's equation relating relativistic mass and energy (e.g. Bloom 2011):

$$M_{grb} \approx E_a \ / \ c^2(\gamma - 1) \text{ kg}.....(3)$$

An approximate value of the mass corresponding to this energy release was determined as $M_{grb} \approx 0.55 \times 10^{-3} M_{\odot}$, where $M_{\odot}$ is the solar mass.

The upper limits on γ and M_{grb} provide a window within which the range of Lorentz factor model (Rees & Meszaros 1998) could be valid. Based on the constraints on γ and M_{grb} obtained from the VLBA observations, it can be concluded that the shells of material were not moving at Lorentz factors > 7. The VLBA Lorentz factor limit ($\gamma < 7$) is model-independent since it is a direct observation. The model, relating the ejected mass and Lorentz factor, when tested against the observations showed that 62 days after the GRB 100418a prompt emission, the mass outflow and the energy release were dominated by comparatively slow moving ejecta having lower values of γ, possibly powered by the continued activity of the central engine producing unusual and long-lasting afterglow. Therefore, in case of GRB100418a , the model invoking the mechanism of energy injection in which shells of material ejected at a wide range of Lorentz factors cause the longevity of the afterglow can only be valid for $\gamma < 7$ and it may well be possible that continued supply of energy and in turn the long-lasting afterglow was due to the contribution of extended activity of the central engine.

In the case of continued activity of the central engine, the theory suggests that there could be at least some long-duration GRBs, which are produced when a massive progenitor collapses into a neutron star or a highly magnetized pulsar or a black hole continuously accreting matter. For instance, in the case of the birth of a pulsar or magnetar, the relativistic outflow produces internal shocks closer to the central engine which could produce the prompt emission, with the energy transported to a distance

feeding the external shocks which produce the GRB afterglow. The central engine may then start to spin-down and lose its energy by magnetic dipole radiation. In the presence of a strong electro-magnetic field, the energy is transported via a relativistic magnetohydrodynamic wind as Poynting flux energy which keeps refreshing the external (forward) shock, due to which it decelerates less slowly in the circumburst medium, resulting in continued emission of afterglow radiation (Duncan & Thompson 1992; Thompson 1994; Zhang & Meszaros 2001; Zhang et al. 2006).

The radio afterglow light curves of GRB 100418a can also be discussed against the back drop of the fireball model (Waxman 1997, Frail et al. 1997) and the energy injection model (Zhang et al. 2006; Marshall et al. 2011). According to the fireball model, a relativistic decelerating shell drives a forward shock into the circumburst medium. The interaction of the medium and the shock accelerates the relativistic electrons which then produces radio afterglow through synchrotron emission (Waxman 1997b). In the case of GRB 100418a, the continued injection of energy into the forward shock, the effect which translated into the plateau phase in X-ray and optical afterglows, can also explain the long-term radio emission. The forward shock may have been continuously fed with energy from the activity of the central engine, heating up the gas in the surrounding medium and accelerating electrons to relativistic velocities in an optically thick region. Therefore, the afterglow kept rising until it reached its peak. With the expansion and deceleration of the emitting sphere, the radio afterglow started fading slowly. Unlike many other GRBs, in which the afterglow fades away in about 10 days, it is suggested that in some GRBs, the energy injection mechanism can be the underlying process producing a long-term afterglow.

The models based on the continued activity of the central engine, such as the pulsar model can be further explored by, for instance, the comparison between the pulsar rotational energy and the GRB energy and the similarities between the pulsar environment and the circumburst medium (e.g. Dai & Lu 1998) with the aid of regular observational campaigns.

In addition to the observed results, a simple mathematical formulation of the standard blastwave model for GRB afterglows (Granot et al. 2003; Taylor et al. 2004; Pihlstrom et al. 2007) was used to predict the theoretical upper limit, based on a number of cosmological assumptions, on the angular size of the afterglow on the day it was observed with the VLBA and it came out to be a very small number compared

to the beam size (<0.04 mas). This upper limit is, however, much smaller than what was estimated using the data from the observations (<0.33 mas) but is consistent with the conclusion that the afterglow was unresolved even after more than 60 days of the prompt emission indicating that the forward shock or the shell of material wasn't expanding fast enough (i.e. slow moving ejecta) that it could be resolved on 62th day. Although the radio source associated with the GRB was unresolved by VLBA, the estimates of upper limits on the source size and expansion speed are not in conflict with the energy injection model, invoking a plausible underlying mechanism such as the activity of central engine, which proposes that long-term GRB 100418a afterglow was due to the continuous supply of energy to the forward shock as it sweeps the circumburst medium.

6.5 Summary

GRB 100418a turned out to be an unusual GRB in terms of the duration of its afterglow and the light-curve profile. The afterglow light-curves showed the rare "plateau phase" which is thought to be a signature of the physical process associated with the longevity of the afterglow. A long-term radio observational campaign was carried out with the EVLA, ATCA and VLBA to monitor the afterglow in the radio band. Based on the results obtained from the radio observations and analysis, a hypothesis of the energy injection model was tested which proposes that the long-lasting afterglow is due to the fact that there are concentric shells of material that move with different Lorentz factors and the slower shells keep catching up with the forward shock to continuously power the afterglow.

In order to test the aforementioned model, constraints on the Lorentz factor and the GRB afterglow mass were obtained from the VLBA data. It was found that the upper limits support the notion that a range of Lorentz factors might have continuously supplied energy to the forward shock to produce long-lasting afterglow for $1 < \gamma < 7$. It is inferred that it is the slow-moving ejecta with lower values of γ which must have contributed to the continuous energy injection to the forward shock, with additional contribution from some other mechanism e.g. the continued activity of the central engine, which gave rise to long-term afterglow in the case of GRB 100418a. Thus, observed results and analysis of VLBA observations of GRB 100418a only support the

range of Lorentz factor model for $\gamma < 7$ for energy injection to produce a prolonged afterglow.

6. RADIO OBSERVATIONS OF GRB100418A AND MULTI-WAVELENGTH ANALYSIS: TEST OF AN ENERGY INJECTION MODEL EXPLAINING LONG-LASTING GRB AFTERGLOW

Chapter 7

Conclusions

7.1 Recapitulation

Detection, observation and long-term monitoring of transient sources has become a hot topic in astronomy. Transient events last for only a brief period of time and they are thought to be associated with very high energy phenomena and extreme processes, unlike objects with persistent and stable emission. The detailed and timely study of transients opens up windows of opportunity to probe the environments and processes that might hold the key to some of the most fundamental problems in astrophysics. Along with other frequency bands, the study of transients in the radio band is of critical importance in order to understand the nature, characteristics and behaviour of transient sources better. This PhD project was designed to conduct detailed observational studies of two types of transient radio sources: a) Galactic X-ray binary systems b) Gamma-ray Burst afterglows.

The study of X-ray binaries in this thesis concentrated on Circinus X-1. Observations of Circinus X-1 were carried out with a unique observational campaign employing the new e-VLBI capability of the LBA. Circinus X-1 is a peculiar Galactic X-binary system with a neutron star orbiting a massive star with a 16.6 day orbit. The radio behaviour of the system was closely studied for the first time by monitoring it throughout its entire binary orbit, making use of the LBA network in e-VLBI mode. Subsequently, high-resolution Target-of-Opportunity VLBI observations were also conducted to study the evolution of the radio source associated with the system, resolving the milliarcsecond jet for the first time.

As part of the GRB stream, a Southern Hemisphere GRB detection and monitoring program was carried out. The program ran for nearly three years and the primary objective was to look for GRBs with relatively long-lasting radio afterglows and characteristics which could shed some light on the underlying physics of GRBs, in order to test previously proposed models with observations. Secondary objectives were to cover the southern sky and follow up interesting GRBs with a systematic observational program and to build a statistical record of radio observations of southern GRBs.

7.2 Circinus X-1 study

A comprehensive and coordinated e-VLBI/VLBI campaign was carried out between 2009 - 2010 to observe Circinus X-1 at about a dozen points along its orbit so as to adequately sample it to monitor the radio behaviour of the system as a function of its orbital phase (Chapter 3). The Circinus X-1 e-VLBI program, involving e-VLBI sessions every second day to cover the entire 16.6 day orbit of the system, was an unprecedented initiative and the LBA was never operated in this way before. The campaign turned out to be very successful allowing us to study the radio behaviour of Circinus X-1 when it was in a quiescent state. As a key outcome of the program, it was found that the system only produced radio emission close to the periastron passage and there was no compact radio component associated with system emitting beyond the vicinity of the periastron passage. No evidence for the previously hypothesized (Phillips et al. 2007) non-variable, quiescent and continuously emitting component was found.

In May 2010, Circinus X-1 was found to have returned to a high-flaring state. Enhanced X-ray activity was observed by X-ray telescopes and type I X-ray bursts were detected confirming the neutron star nature of the compact object (ATel 2608, ATel 2643, ATel 2651, ATel 2653). In response to the X-ray activity, follow-up radio observations were carried at HartRAO (Nicolson, private communication) and the measured flux density (500mJy) was a factor of 10 higher than the maximum intensity measured over the past few years. Based on the trigger from HartRAO, we planned and conducted ATCA observations (ATel 2699) of the system on June 24, 2010, when it was close to the periastron passage. The ATCA observations last 12 hours and revealed a highly variable and bright radio source, peaking at 170 $\pm$ 20 mJy at 5 GHz and 230 $\pm$

20 mJy at 8 GHz (ATel 2699). This is the strongest Cir X-1 radio flux density detected using ATCA in 15 years. The radio emission was even an order of magnitude stronger than when ATCA observations in 1998-2000 appeared to reveal an ultrarelativistic flow (Fender et al. 2004). In an attempt to detect and monitor any structure associated with the system, VLBI ToO observations of Cir X-1 were invoked using the LBA with the ATCA, Mopra, Hobart and Ceduna telescopes (Chapter 4). As a result of these observations, we were able to resolve symmetric milliarcsecond-scale jets (∼20mas) in Circinus X-1 for the first time. It was found that the orientation of the jets was consistent with the arcsecond-scale jets previously detected with the ATCA. The symmetry and the estimates of proper motion also indicated that the jets were mildly relativistic weakening the support for the ultra-relativistic flow proposed by Fender et al. (2004).

7.3 The GRB afterglow study

A total of 52 GRBs were observed with ATCA under a Southern Hemisphere GRB detection and monitoring program as part of this PhD project in an attempt to a) search for peculiar and long-lasting GRB afterglows, which could be monitored and studied for a longer period of time and b) build a record of southern GRBs complementing the Northern Hemisphere GRB program and to carry out a statistical analysis based on various parameters to evaluate and compare the strategies for GRB campaigns (Chapter 5). The emergence of CABB in April 2009 gave a significant boost to the program and enhanced the possibility of detection. Out of the entire GRB sample observed over almost two-and-a-half years, four GRBs were detected at 5.5 and 9.0 GHz and one out of those four turned out to be a GRB with an unusual and long-lasting afterglow. GRB 100418a was detected at multiple sessions and an extended study of this GRB was carried out using the ATCA, EVLA and VLBA (Chapter 6).

In order to study the behaviour of GRB 100418a in detail, long-term multi-instrument observations in Gamma-ray, X-ray, optical and radio bands were conducted. The radio monitoring was carried out with EVLA, ATCA and VLBA. The X-ray and optical light curves showed an unusual, slowly-varying plateau phase and the radio afterglow also had a rising component until about ∼62 days after the prompt emission. The longevity and peculiarity of the GRB 100418a afterglow put it in the category of afterglows which

are thought to be powered by a continuous energy injection mechanism in which the energy is supplied to the forward shock producing a long-lasting afterglow.

The radio monitoring campaign and the subsequent VLBA observations were aimed at testing one of the energy injection mechanisms, thought to provide a plausible explanation for the energy injection model, stating that the continuous supply of energy to produce the persistent afterglow comes from concentric shells of ejected material having a range of Lorentz factors. Delayed shells of material strike the forward shock at late times, refreshing it to produce a longer-lasting afterglow. To test this hypothesis, high-angular resolution VLBA observations of the afterglow were conducted in response to the continued radio detection with the EVLA and ATCA and rising afterglow light-curve, by estimating parameters such as the expansion speed and the associated energy and mass of the ejecta. The afterglow was detected as an unresolved compact source and no jet-like structure was found to be associated with it. The VLBA data provided constraints on the Lorentz factor γ and the mass M_{grb} of the ejecta, with which the model involving the range of Lorentz factors was tested. It was concluded that the model was true for $\gamma < 7$ and comparatively slow moving ejecta with low γ satisfies the constraints obtained from the observations. Therefore, in the case of GRB 100418a, there is a likelihood that the observed prolonged afterglow could be due to the energy injection fueled by the continued activity of the progenitor with slow-moving ejecta.

7.4 Future possibilities

The extensive transient detection and monitoring programs executed as part of this PhD project can be extended with some adjustment and modification in order to detect a greater number of sources with a wide range of observational signatures.

The advent of next generation instruments such as ASKAP, MWA, MeerKAT, LOFAR and eventually SKA will revolutionise the way transient astronomy will be done. These instruments, with wide fields-of-view and unprecedented sensitivity will conduct all sky surveys, observing the full sky quickly, dramatically increasing the detection rate of transients. Making the use of multi-beaming capabilities, the most interesting sources could be constantly monitored from very early times to times when the emission fades, giving an exceptional temporal coverage of events. Automated data

processing pipelines will produce final data products instantly, so that the behaviour of every interesting transient can be studied in near real-time.

In addition to this, the extension of current VLBI arrays and the integration of the next generation telescopes in regional and global VLBI networks will enable very high angular resolution observations of these transients to study the morphology of the transient sources and make much more accurate estimates of their dynamics.

This is indeed a great time for transient radio astronomy as new technologies are being developed around the globe to do innovative experiments, new instruments with enhanced capabilities are being designed and built and many new collaborations are being established to carry out large observational programs that expand the horizons of astronomical research. My future pursuit would be to get associated with the extended versions of transient detection and monitoring programs such as these conducted under the scope of this PhD project so as to broaden my experience, gain in-depth knowledge and build a decent career in this intriguing and exciting branch of astronomy. These programs will only get bigger allowing more frequent, more sensitive, and more effective long-term observational campaigns conducted to study these objects better and to help solve a number of puzzling and intriguing mysteries in astrophysics.

Bibliography

[Atwood et al. 2009] Atwood, W. B. et al. 2009, ApJ, 697, Issue 2, 1071-1102

[Band et al. 1993] Band, D. et al. 1993, ApJ, 413, 281

[Barthelmy et al. 2005a] Barthelmy, S. D. et al. 2005a, Nature, 438, Issue 7070, 994-996

[Barthelmy et al. 2005b] Barthelmy, S. D. et al. 2005b, Space Science Reviews, 120, Issue 3-4, 143-164

[Batchelor et al. 1976] Batchelor, R. A. et al. 1976, Pisma v Astronomicheskii Zhurnal, 2, 1976, 467-473.

[Belczynski, Bulik & Kluzniak 2002] Belczynski, K., Bulik, T., Kluzniak, W. 2002, AJ, 567, Issue 1, L63-L66

[Belczynski, Bulik & Ruiter 2005] Belczynski, K.; Bulik, T. & Ruiter, A. J. 2005, AJ, 629, Issue 2, 915-921

[Belczynski et al. 2006] Belczynski, K. et al. 2006, AJ , 648, Issue 2, 1110-1116

[Berger et al. 2003] Berger, E. et al. 2003, Nature, 426, Issue 6963, 154-157

[Bethe 1990] Bethe, H. A. 1990, Reviews of Modern Physics, 62, Issue 4, 801-866

[Blandford & Konigl 1979] Blandford R. D., & Konigl, A. 1979, ApJ, 232, 34

[Bloom et al. 1999] Bloom, J. S. et al. 1999, Nature, 401, Issue 6752, 453-456

[Bloom, Frail & Kulkarni 2003] Bloom, J. S., Frail, D. A., & Kulkarni, S. R. 2003, ApJ, 594, Issue 2, 674-683

BIBLIOGRAPHY

[Bloom 2011] Bloom, J. S. 2011, "What are Gamma-Ray Bursts", Princeton University Press, Princeton, New Jersey 2011, 280

[Brandt & Schulz 2000] Brandt, W. N. & Schulz N. S., 2000, ApJ, 544, L123

[Brandt et al. 1996] Brandt, W. N., et al. 1996, MNRAS, 283, 1071

[Briggs 1995] Briggs, M. S. 1995, Astrophysics and Space Science, 31, Issue 1-2, 3-10

[Burgay et al. 2003] Burgay, M. et al. 2003, Nature, 426, Issue 6966, 531-533

[Burrows et al. 2005] Burrows, D. N. et al. 2005, Space Science Reviews, 120, Issue 3-4, 165-195

[Butler et al. 2007] Butler, N. R. et al. 2007, ApJ, 671, Issue 1, 656-677

[Butler, Bloom & Poznanski 2010] Butler, N. R., Bloom, J. S. & Poznanski, D. 2010, ApJ, 711, Issue 1, 495-516

[Calvelo et al. 2010] Calvelo D. E. et al. 2010, The Astronomer's Telegram, 2699

[Campana et al. 2006] Campana, S. et al. 2006, Nature, 442, Issue 7106, 1008-1010

[Camilo et al. 2008] Camilo, F. et al. 2008, ApJ, 679, Issue 1, 681-686

[Cenko et al. 2010] Cenko, S. B. et al. 2010, ApJ, 711, Issue 2, 641-654

[Chandra et al. 2008] Chandra, P. et al. 2008, ApJL, 683, Issue 2, 924-942

[Chandrasekhar 1935] Chandrasekhar, S. 1935, MNRAS, 95, 207-225

[Chevalier & Li 1999] Chevalier, R. A. & Li, Z-Y 1999, ApJ, 520, Issue 1, L29-L32

[Christensen et al. 2008] Christensen, L. et al. 2008, A & A, 490, Issue 1, 2008, 45-59

[Clark 1980] Clark, B. G., 1980, A & A, 89, no. 3, 377, 378

[Cohen et al. 1969] Cohen, M. H. et al. 1969, ApJ, 158, L83

[Corbel et al. 2002] Corbel, S. et al. 2002, Science, 298, Issue 5591, 196-199

[Costa et al. 1997] Costa, E. et al. 1997, Nature, 387, Issue 6635, 783-785

[Dai & Lu 1998] Dai & Lu 1998, A & A, 333, L87-L90

[Deller et al. 2007] Deller, A. T. et al., 2007, PASP, 119, 318

[Deller et al. 2011] Deller A. T. et al., 2011, PASP, 123, issue 901, 275-287

[Dermer 2004] Dermer, C. D. 2004, ApJ, 614, Issue 1, pp. 284-292

[Dermer & Atoyan 2006] Dermer, C. D. & Atoyan, A. 2006, ApJ, 643, Issue 1, L13-L16

[Dhawan, Mirabel & Rodriguez 2000] Dhawan, V., Mirabel, I. F., Rodriguez, L. F. 2000, ApJ, 543, 373

[Duncan & Thompson 1992] Duncan, R. C. & Thompson, C. 1992, ApJ, Part 2 - Letters, 392, no. 1, June L9-L13

[Eichler et al. 1989 1989] Eichler, D. et al. 1989, Nature, 340, 126-128

[Ensman & Woosley 1988] Ensman, L. M. & Woosley, S. E. 1988, ApJ, Part 1, 333, Oct. 15, 1988, 754-776

[Evans et al. 2007] Evans, P. A. et al. (2007), A & A, 469, Issue 1, 379-385

[Fender et al. 1998] Fender, R. P. et al., 1998, ApJ, 506, L21

[Fender et al. 2004] Fender, R. P. et al., 2004, Nature, 427, 222

[Fender, Belloni & Gallo 2004] Fender, R. P., Belloni, T. M. & Gallo, E. 2004, MNRAS, 355, Issue 4, 1105-1118

[Fender, Tzioumis & Tudose 2005] Fender, R. P., Tzioumis, A. K., Tudose, V., 2005, The Astronomer's Telegram, 563

[Filippenko & Sargent 1986] Filippenko, A. V. & Sargent, W. L. W. 1986, AJ, 91, 691-696

[Fomalont, Geldzahler & Bradshaw 2001a] Fomalont, E. B., Geldzahler, B. J., Bradshaw, C. F., 2001a, ApJ, 553, L27

[Fomalont, Geldzahler & Bradshaw 2001b] Fomalont, E. B., Geldzahler, B. J., & Bradshaw, C. F. 2001b, ApJ, 558, Issue 1, 283-301

BIBLIOGRAPHY

[Frail et al. 1997] Frail, D.A. et al. 1997, Nature, 389, Issue 6648, 261-263

[Frail, Waxman & Kulkarni 2000] Frail, D. A., Waxman, E., & Kulkarni, S. R. 2000, ApJ, 537, Issue 1, 191-204

[Frail et al. 2000] Frail, D. A. et al. 2000, ApJ, 538, Issue 2, L129-L132.

[Frail et al. 2001] Frail, S. R. et al. 2001, ApJ, 562, Issue 1, L55-L58

[Frail et al. 2003] Frail, D. A. et al. 2003, AJ, 125, Issue 5, 2299-2306

[Friedman 1983] Friedman, J. L. 1983, Physical Review Letters, 51, 11-14

[Fryer et al. 1999] Fryer, C. L. et al. 1999, ApJ, 520, Issue 2, 650-660

[Galama et al. 1998] Galama, T. J. et al. 1998, Nature, 395, Issue 6703, 670-672

[Gallo et al. 2004] Gallo, E. et al. 2004; MNRAS, 347, Issue 3, L52-L56

[Goodman 1986] Goodman, J. 1986, ApJL, 308, L47-L50

[Goodman, Dar & Nussinov 1987] Goodman, J., Dar, A. & Nussinov, S. 1987, AJ, 314, L7-L10

[Giroletti et al. 2011] Giroletti, M. et al. 2011, A & A, 528, L11

[Granot et al. 2003] Granot, J. et al. 2003, Nature, 426, Issue 6963, . 138-139

[Greiner et al. 2009] Greiner, J. et al. 2009, A & A, 498, Issue 1, 2009, 89-94

[Griesen 2003] Greisen, E.W. 2003, ASSL, 285, 109

[Grupe et al. 2007] Grupe, D. et al. 2007, The Astrophysical Journal, 662, Issue 1, 443-458

[Gulyaev & Natusch 2008] Gulyaev, G. & Natusch, T. 2008, "New Zealand 12-m VLBI Station for Geodesy and Astronomy". IVS 2008 Annual Report, 2008

[Han & Hjellming 1992] Han, X., & Hjellming, R. M. 1992, AJ, 400, no. 1, 304-314

[Haynes et al. 1978] Haynes R. F. et al. 1978, MNRAS, 185, 661

[Haynes, Lerche & Murdin 1980] Haynes R. F., Lerche I., & Murdin P. 1980, A&A, 87, 299

[Harrison et al. 1999] Harrison, F. A. et al. 1999, ApJ, 523, Issue 2, L121-L124

[Heger et al. 2003] Heger, A. et al. 2003, ApJ, 591, Issue 1, 288-300

[Heinz et al. 2007] Heinz, S. et al. 2007, ApJ, 663, L93

[Hirabayashi et al. 2000] Hirabayashi, H. et al. 2000, PASJ, 52, 997-1014

[Hjellming & Johnston 1988] Hjellming R. M. & Johnston K. J., 1988, ApJ, 328, 600

[Hjellming et al. 1998] Hjellming, R. M. et al. 1998, Bulletin of the AAS, 30, 1405

[Homan et al. 2009] Homan, J. et al. 2009, ApJ, 706, Issue 2, 1253-1268

[Homan et al. 2010] Homan, J. et al., 2010, ApJ, 719, 201

[Hogbom 1974] Hogbom, J. A., 1974, A & A Supplement, 15, 417

[Iaria et al. 2005] Iaria, R. et al. 2005, ApJ, 619, 503

[Jauncey et al. 1994] Jauncey, D. L. et al. 1994, IAU Symposium No. 158: Very high angular resolution imaging, p. 131 - 134

[Jauncey et al. 1995] Jauncey, D. L. et al. 1995, Proceedings of the National Academy of Sciences of the United States of America, 92, Issue 25, 11368-11370

[Jin et al. 2007] Jin, C. C. et al. 2007, ApJ, 656, Issue 2, L57-L60

[Johnston et al. 2007] Johnston, S. et al. 2007, PASA, 24, Issue 4, 174-188

[Johnston et al. 2008] Johnston, S. et al. 2008, Experimental Astronomy, 22, Issue 3, 151-273

[Jones, Terzian & Sramek 1981] Jones, D. L., Terzian, Y. & Sramek, R. A. 1981, ApJ, Part 1, 246, 28-37

[Jonker & Nelemans 2004] Jonker P. G., & Nelemans G., 2004, MNRAS, 354, 355

[Jonker et al. 2007] Jonker, P.G., Nelemans, G. & Bassa, C.G. 2007, MNRAS, 374, 999

BIBLIOGRAPHY

[Kaluzienski et al. 1976] Kaluzienski, L.J., Holt, S.S., Boldt, E.A. & Serlemitsos, P.J. 1976, ApJ, 208, L71

[Kettenis et al. 2006] Kettenis, M. et al. 2006, ASPC, 351, 497

[Kim et al. 1998] Kim, S. et al. 1998, ApJ, 503,674

[Klebesadel et al. 1973] Klebesadel, R. W. et al. 1973, ApJ, 182, L85

[Kouveliotou et al. 2004] Kouveliotou, C. et al. 2004, ApJ, 608, Issue 2, 872-882.

[Koyama et al. 2002] Koyama, K. et al. 2002, Proceedings of the 4th eVLBI workshop, Sydney, Australia.

[Kulkarni et al. 1998a] Kulkarni, S. R. et al. 1998, Nature, 393, Issue 6680, 35-39

[Kulkarni et al. 1998b] Kulkarni, S. R. et al. 1998, Nature, 395, Issue 6703, 663-669

[Laing 1996] Laing, R. A., 1996, ed. Hardee, P., Bridle, A. H., Zensus J. A., ASP Conf. Ser. Vol 100, Energy transport in radio galaxies and quasars. ASP, San Francisco, 241

[Lamb, Pethick & Pines 1973] Lamb, F. K., Pethick, C. J. & Pines, D. 1973, ApJ, 184, 271-290

[Lapsley & Whitney 2004] Lapsley, D. & Whitney, A. 2004, Proceedings of the 7th Symposium of the European VLBI Network, Toledo, Spain, October 12-15 2004. ed. R. Bachiller, F. Colomer, J.-F.; Desmurs, and P. de Vicente, 291-292

[Lazzati & Perna 2009] Lazzati, D. & Perna, R. 2009, ASSL, 359, ISBN 978-1-4020-9263-3, p245

[Liang et al. 2006] Liang, E. W. et al. 2006, ApJ, 646, Issue 1, 351-357

[Linares et al. 2010] Linares, M. et al., 2010, ApJ, 719, L84

[Livio & Waxman 2000] Livio, M. & Waxman, E. 2000, ApJ, 538, Issue 1, 187-191

[Lobanov et al. 2006] Lobanov, A. P. et al. 2006, PASJ, 58, No.2, 253-259

[Lorimer et al. 2007] Lorimer, D. R. et al. 2007, Science, 318, Issue 5851, 777

[Ly, Walker & Junor 2007] Ly, C., Walker, C. R. & Junor, W. 2007, ApJ, 660, Issue 1, 200-205

[MacFadyen & Woosley 1999] MacFadyen, A. I. & Woosley, S. E. 1999, ApJ, 524, Issue 1, 262-289

[MacFadyen, Woosley & Heger 2001] MacFadyen, A. I., Woosley, S. E. & Heger, A. 2001, ApJ, 550, Issue 1, 410-425

[Manchester et al. 1981] Manchester, R. N. et al. 1981, AJ, 86, 1953-1973

[Marshall et al. 2011] Marshall, F. E. et al. 2011, ApJ, 727, Issue 2, article id. 132

[Massardi et al. 2011] Massardi, M. et al. 2011, MNRAS, 412, Issue 1, pp. 318-330

[McClintock & Remillard 2003] McClintock, J. E. & Remillard, R. 2003, arXiv:astro-ph/0306213

[McKinney 2006] McKinney, J. C. 2006, MNRAS, 368, Issue 4, 1561-1582

[Meegan et al. 1992] Meegan, C. A. et al. 1992, Nature, 355, 143-145

[Meegan et al. 2009] Meegan, C. A. et al. 2009, ApJ, 702, Issue 1, 791-804

[Meier 2003] Meier D. L., 2003, New Astronomy Reviews, 47, 667

[Meszaros 1995] Meszaros, P. 1995, 7th Texas Symposium on Relativistic Astrophysics and Cosmology, Ed. Hans Bhringer, Gregor E. Morfill, and Joachim E. Trmper. Annals of the New York Academy of Sciences, 759, 440

[Meszaros & Rees 1993] Meszaros, P. & Rees, M. J. 1993, ApJ, Part 1, 405, 278-284

[Meszaros & Rees 1997a] Meszaros, P. & Rees, M. J. 1997, ApJ, 476, 232

[Meszaros & Rees 1997b] Meszaros, P. & Rees, M. J 1997b, ApJL, 482, L29

[Meszaros, Rees & Wijers 1999] Meszaros, P., Rees, M. J. & Wijers, R. A. M. J. 1999, New Astronomy, 4, 303-312.

[Migliari & Fender 2006] Migliari, S. & Fender, R. P. 2006, MNRAS, 366, Issue 1, pp. 79-91

BIBLIOGRAPHY

[Miller-Jones et al. 2010] Miller-Jones, J. C. A. et al. 2010, ApJL, 716, Issue 2, L109-L114

[Miller-Jones et al. 2011] Miller-Jones, J. C. A. et al. 2011, MNRAS, submitted

[Mirabel & Rodríguez 1994] Mirabel I. F., Rodriguez, L.F., 1994, Nature, 371, 46

[Mirabel & Rodriguez 1999] Mirabel, I. F. & Rodriguez, L. F. 1999, Ann. Rev. of A & A, 37, 409-443

[Mitrofanov 1990] Mitrofanov 1990, Astrophysics and Space Science, 165, 137-145

[Moin et al. 2011] Moin, A. et al. 2011, MNRAS, 414, Issue 4, 3551-3556

[Mori et al. 2009] Mori et al, 2009, Transactions of the Japanese Society for Artificial Intelligence, Aerospace Technology Japan, Volume 8, 425-431

[Murdin et al. 1980] Murdin, P. et al., 1980, A&A, 87, 292

[Nakajima et al. 2010] Nakajima, M. et al., 2010, The Astronomers Telegram, 2608

[Narayan, Paczynski & Piran 1992] Narayan, R., Paczynski, B. & Piran, T. 1992, ApJL, 395, L83-L86

[Narayan, Piran & Kumar 2001] Narayan, R., Piran, T. & Kumar, P. 2001, ApJ, 557, Issue 2, pp. 949-957

[Narayan, Piran & Shemi 1991] Narayan, R., Piran, T. & Shemi, A. 1991, ApJL, 379, L17-L20

[Nicolson 2007] Nicolson, G.D. 2007, ATel, 985

[Norris et al. 1993] Norris, R. P. et al. 1993, ApJ, 412, 222-232

[Oates et al. 2009] Oates, S. R. et al. (2009), MNRAS, 395, Issue 1, 490-503

[Oosterbroek et al. 1995] osterbroek, T. et al. 1995, A&A, 297, 141

[Paczynski 1986] Paczynski, B. 1986, ApJL, 308, L43-L46

[Paczynski 1991] Paczynski, B. 1991, Acta Astronomica, 41, no. 4, 257-267

[Paczynski 1995] Paczynski, B. 1995, PASP, 107, 1167

[Paczynski & Rhoads 1993] Paczynski. B. & Rhoads, J. E. 1993, Astrophysical Journal Letters v.418, L5

[Panaitescu, Meszaros & Rees 1998] Panaitescu, A., Meszaros, P. & Rees, M. J. 1998, ApJ, 503, 314

[Panaitescu & Kumar 2002] Panaitescu, A. & Kumar, P. 2002, ApJ, 571, Issue 2, 779-789

[Paragi et al. 2005] Paragi, Z. et al. 2005, Memorie della Societa Astronomica Italiana, 76,570

[Perez-Torres et al. 2009] Perez-Torres, M. A. et al. 2009, Proceedings of the 8th International e-VLBI Workshop. 22-26 June 2009. Madrid, Spain, 68

[Petrov et al. 2011] Petrov, L. et al. 2011, PASA, 28, Issue 2, 107-116

[Petrillo & Dietz 2012] Petrillo, C. E. & Dietz, A. et al. 2012, arXiv:1202.0804v2

[Phillips et al. 2007] Phillips, C.J. et al., 2007, MNRAS, 380, L11

[Pihlstrom et al. 2007] Pihlstrom, Y. M. et al. 2007, ApJ, 664, Issue 1, 411-415

[Piran 1992] Piran, T. 1992, ApJL, 389, L45-L48

[Piran 2004] Piran, T. 2004, Reviews of Modern Physics, 76, Issue 4, 1143-1210

[Piran 2005] Piran, T. 1995, arXiv:astro-ph/9507114

[Piro, Scarsi & Butler 1995] Piro, L., Scarsi, L., & Butler, R. C. 1995, Proc. SPIE 2517, 169-181

[Portegies Zwart & Yungelson 1998] Portegies Zwart, S. F., Yungelson, L. R. 1998, A&A, 332, 173-188

[Preston et al. 1983] Preston, R.A. et al., 1983, ApJ, 268, L23

[Preston et al. 1984] Preston, R. A. et al. 1984, VLBI and Compact Radio Sources. Symposium no. 110, Bologna, Italy, June 27-July 1, 1983. Ed. R. Fanti, K. Kellermann, and G. Setti. 67

BIBLIOGRAPHY

[Preston et al. 1993] Preston et al. 1993, Sub-arcsecond Radio Astronomy, Proceedings of the Nuffield Radio Astronomy Laboratories conference, Manchester, July 20-24, 1992. ed. R.J. Davis and R. S. Booth, Cambridge University Press, 428

[Price et al. 2002] Price, P. A. et al. 2002, ApJ, 572, Issue 1, L51-L55

[Proga et al. 2003] Proga, D. et al. 2003, ApJ, 599, Issue 1, L5-L8

[Rees & Meszaros 1992] Rees, M. J. & Meszaros, P. 1992, MNRAS, 258, no. 2, 41P-43P

[Rees & Meszaros 1994] Rees, M. J. & Meszaros, P. 1994, ApJ, 430, no. 2, L93-L96

[Rees & Meszaros 1998 1998] Rees, M. J. & Meszaros, P. 1998, ApJL, 496, L1

[Rhoads 1997] Rhoads, J. E. 1997, ApJL, 487, L1

[Rhoads 1999] Rhoads, J. E. 1999; ApJ, 525, Issue 2, 737-749

[Roming et al. 2005] Roming, P. W. A. et al. 2005, Space Science Reviews, 120, Issue 3-4, 95-142

[Roming et al. 2008] Roming, P. W. A. et al. 2008, Nanjing GRB Conf. AIP Conference Proceedings, 1065, 81-84

[Romney 1999] Romney 1999, Synthesis Imaging in Radio Astronomy II, A Collection of Lectures from the Sixth NRAO/NMIMT Synthesis Imaging Summer School. ed. G. B. Taylor, C. L. Carilli, and R. A. Perley. ASP Conference Series, 180, 57

[Sakamoto et al. 2011] Sakamoto, T. et al. 2011, ApJS 195, Issue 1, article id.2

[Sari, Piran & Halpern 1999] Sari, R., Piran, T. & Halpern, J. P. 1999, ApJ, 519, Issue 1, L17-L20

[Sari, Piran & Narayan 1998] Sari, R., Piran, T. & Narayan, R. 1998, ApJL, 497, L17

[Sault, Teuben & Wright 1995] Sault, R. J., Teuben, P. J. & Wright, M. C. H. 1995, Astronomical Data Analysis Software and Systems IV, ASP Conference Series, 77, ed. R.A. Shaw, H.E. Payne, and J.J.E. Hayes, 433

[Sekido et al. 2008] Sekido, M. et al. 2008, Earth, Planets and Space, 60, p. 865-870

[Sell et al. 2010] Sell P. H. et al., 2010, ApJ, 719, L194

[Shapiro & Teukolsky 1983] Shapiro, S. L. & Teukolsky, S. A. 1983, "Black Holes, White Dwarfs and Neutron stars: The physics of compact objects", New York, Wiley-Interscience, 1983, 663

[Shepherd, Pearson & Taylor 1994] Shepherd, M.C., Pearson, T.J. & Taylor, G.B. 1994, BAAS, 26, 987

[Shirey et al. 1997] Shirey et al. 1997, AAS, 29, 1369

[Shirey, Levine & Bradt 1999] Shirey R. E., Levine A. M. & Bradt H. V. 1999, ApJ, 524, 1048

[Sol, Pelletier & Asseo 1989] Sol H., Pelletier G. & Asseo E. 1989, MNRAS, 237, 411

[Soleri et al. 2009a] Soleri P. et al. 2009, MNRAS, 397, L1

[Soleri et al. 2009b] Soleri P. et al. 2009b, MNRAS, 399, 453

[Staveley-Smith et al. 2002] Staveley-Smith et al. 2002, Seeing Through the Dust: The Detection of HI and the Exploration of the ISM in Galaxies, ASP Conference Proceedings, 276. ed. A. R. Taylor, T. L. Landecker, and A. G. Willis., 391

[Stewart et al. 1993] Stewart R. T. et al. 1993, MNRAS, 261, 593

[Stirling et al. 2001] Stirling A. M. et al. 2001, MNRAS, 327, 1273

[Schwab 1984b] Schwab, F. R. 1984b, AJ, 89, 1076-1081

[Tagliaferri et al. 2005] Tagliaferri, G. et al. 2005, Nature, 436, Issue 7053, 985-988

[Takahashi et al. 1990] Takahashi, M. et al. 1990, ApJ, 363, 206-217

[Taylor & Weisberg 1989] Taylor, J. H. & Weisberg, J. M. 1989, AJ, 345, 434-450

[Taylor et al. 2004] Taylor, G. B. et al. 2004, ApJ, 609, Issue 1, L1-L4

[Taylor, Carilli & Perley 2008] Taylor, Carilli & Perley 2008, Synthesis imaging in Radio Astronomy, 180, ASP Conference Series

[Thompson 1994] Thompson, C. 1994, MNRAS, 270, 480

BIBLIOGRAPHY

[Thompson, Moran & Swenson 2002] Thompson, A. R., Moran, J. M. & Swenson, G. W. 2002, Interferometry and Synthesis in Radio Astronomy, 2nd ed. Wiley-Interscience publication, New York.

[Tingay et al. 1995] Tingay, S. J. et al. 1995, Nature, 374, Issue 6518, 141-143

[Tingay et al. 1998] Tingay, S. J. et al. 1998, ApJ, 115, Issue 3, 960-974

[Toma et al. 2007] Toma, K. et al. 2007, ApJ, 659, Issue 2, 1420-1430

[Troja et al. 2008] Troja, E. et al. 2008, MNRAS, 385, Issue 1, L10-L14

[Troja, Rosswog & Gehrels 2010] Troja, E., Rosswog, S. & Gehrels, N., 2010, ApJ, 723, 1711

[Tudose et al. 2006] Tudose, V. et al. 2006, MNRAS, 372, 417

[Tudose et al. 2008] Tudose, V. et al. 2008, MNRAS, 390, 447

[Tzioumis et al. 1997] Tzioumis, A. K. 1997, Vistas in Astronomy, 41, Issue 2, 311-315

[Tzioumis et al. 2002] Tzioumis, A. K. et al. 2002, A & A, 392, 841-850

[Tzioumis et al. 2010] Tzioumis, A. K. et al. 2010, AJ, 140, Issue 5, 1506-1510

[Usov 1992] Usov, V. V. 1992, Nature, 357, 472-474

[van der Horst, Wijers & Rol 2005] van Der Horst, A. J., Wijers, R. A. M. J. & Rol, E. 2005, Il Nuovo Cimento C, 28, Issue 3, 467

[van der Horst et al. 2008] van der Horst, A. J. et al. 2008, A & A, 480, Issue 1, 35-43

[van der Laan 1966] van der Laan, H. 1966, Nature, 211, 1131

[Waxman 1997a] Waxman, E. 1997a, ApJL, 485, L5

[Waxman 1997b] Waxman, E. 1997b, ApJL, 489, L33

[Waxman 1997c] Waxman, E. 1997c, ApJL, 491, L19

[Waxman, Kulkarni & Frail 1998] Waxman, E., Kulkarni, S. R. & Frail, D. A. 1998, ApJ, 497, 288

[Waxman, Meszaros & Campana 2007] Waxman, E., Meszaros, P. & Campana, S. 2007, ApJ, 667, Issue 1, 351-357

[Whitney et al. 2003] Whitney et al. 2003, New technologies in VLBI, Proceedings of a symposium of the International VLBI Service for Geodesy and Astrometry, Gyeong-ju, Korea, 5-8 November 2002. Ed. Y.C. Minh. ASP Conference Series, 306, 217

[Whitney, Lapsley & Doeleman 2003] Whitney, Lapsley & Doeleman 2003, AAS Meeting 203; Bulletin of the AAS, 35, 1209

[Wijers, Rees & Meszaros 1997a] Wijers, R. A. M. J., Rees, & Meszaros, P. 1997, MNRAS, 288, Issue 4, L51-L56

[Wijers, Rees & Meszaros 1997b] Wijers, R. A. M. J., Rees, M. J. & Meszaros, P. 1997, ApJ, 476, 232

[Wilson et al. 2011] Wilson, W. E. et al. 2011, arXiv:1105.3532, MNRAS, accepted

[Woosley 1993] Woosley, S. E. 1993, ApJ, 405, 273-277.

[Woosley 1996] Woosley, S. E. 1996, Gamma-ray bursts: 3rd Huntsville symposium. AIP Conference Proceedings, Volume 384, 709-718

[Woosley & Baron 1992] Woosley, S. E. & Baron, E. 1992, ApJ, 391, 228-235

[Woosley & Bloom 2006] Woosley, S. E. & Bloom, J. S. 2006, Ann. Rev. of A & A, 44, Issue 1, 507-556

[Woosley, Heger & Weaver 2002] Woosley, Heger, A. & Weaver, T. A. 2002, Reviews of Modern Physics, vol. 74, Issue 4, pp. 1015-1071

[Woosley & Weaver 1986] Woosley, S. E. & Weaver, T. A. 1986, Ann Rev A & A, 24, 205-253

[Yost et al. 2003] Yost, S. A. et al. 2003, ApJ, 597, Issue 1, 459-473

[Zhang & Meszaros 2001] Zhang, B. & Meszaros, P. 2001, ApJ, 552, Issue 1, L35-L38

[Zhang et al. 2006] Zhang, B. et al. 2006, The ApJ, 642, Issue 1, 354-370

BIBLIOGRAPHY

[Zheng, Zhang & Shu 2005] Zheng, W-M., Zhang, X-Z., & Shu, F-C. 2005, Progress in Astronomy, Vol. 23, No. 3, 272 - 286